Cascading effects of transverse failure of a transmission tower

by

Syed Fiza Edroos

May 2018

Department of Civil Engineering and Applied Mechanics

McGill University,

Montreal

A Thesis submitted to the Faculty of Graduate Studies and Research in partial fulfillment of the requirements of the degree of Master of Engineering

Abstract

Cascades are a major cause for widespread damages in overhead lines which pose a grave challenge to reinstate serviceability in the power supply network. The inconvenience due to power outages caused to the efficient functioning of human activities as a whole is a major cause for concern for utilities and governments across the globe. Nevertheless, considerable research has been conducted into identifying and mitigating certain longitudinal overhead transmission line cascades. Transverse cascades of transmission lines have rarely been dealt with until recently.

The primary objective of this computational study is to understand the effects of the transverse failure of a flexible transmission line support on its adjacent supports and spans. Tubular supports numerically modelled for the study conform to a design used by Hydro Quebec for double-circuit 230 kV lines. The components of the overhead line system modelled include the towers, insulators, conducting and shield wire spans. Two-node Hermitian beam elements with a pipe cross-section have been used to model the elements of the support. The spans and insulator strings are modelled as tensile-only truss elements, while all cable elements include initial strains. A non-linear material model has been utilized for the elements of the supports to enable the simulation of inelastic response and progressive tower failures.

The investigation involves imposing transverse displacements on a tower to study its effects on adjacent spans and supports. Commercial software ADINA is used to simulate non-linear dynamic response of the system to the failures. The influence of rigidity of the tower on the response of the system is also studied. The unbalanced loading on the adjacent supports due to the failures are summarized and the conditions that may lead to rupture of spans are identified. Under bare conditions, localized failures within a tubular support will not lead to conductor or shield wire rupture translating into a cascade. The tension in the spans increases as the location of failure within the support moves lower from the apex. But, for a stiffer support, the outcome is contrary. In this study, the design of the supports adopted by Hydro Quebec were modified to stiffen it to an extent that localized failures within the support caused ground wire rupture.

Sommaire

Les cascades de pylônes sont une cause majeure de dommages sur les lignes de transport d'électricité et posent un grand défi à la restauration du service dans le réseau. Les pannes de courant perturbent les activités humaines de toute nature et sont une préoccupation importante pour les compagnies de services publics et les gouvernements partout dans le monde. Beaucoup de travaux de recherche ont été consacrés à l'identification et la mitigation de certains types de cascades de lignes dites longitudinales, alors que l'étude des cascades transversales n'est que très récente.

L'objectif premier de cette étude computationnelle est d'éclairer la compréhension des effets mécaniques causés par la ruine transversale d'un support de ligne tubulaire flexible sur les supports et portées adjacents. Les supports tubulaires modélisés dans cette étude sont conformes à une conception d'Hydro Québec utilisée sur lignes doubles ternes à 230 kV. Les composants de lignes inclus dans le modèle numérique sont les supports, les files d'isolateurs en suspension, et les conducteurs et câbles de garde. Les supports sont modélisés à l'aide d'éléments de poutre hermitienne avec section tubulaire circulaire. Les câbles sont modélisés par une série d'éléments barres avec pré-tension initiale, ne pouvant pas reprendre de d'effort de compression. Les tiges d'isolateurs sont des éléments barres sans pré-tension initiale, reprenant seulement des efforts de traction. Le matériau des supports tubulaires est du type non-linéaire inélastique afin de pouvoir modéliser l'endommagement progressif et la rupture.

L'étude implique l'imposition d'un déplacement transversal contrôlé du support sacrifié afin d'étudier les effets mécaniques sur les supports et dans les câbles adjacents au bris. Les simulations numériques de la réponse non-linéaire dynamique du système utilisent le logiciel commercial ADINA. L'étude examine également l'effet de la rigidité relative des supports sur la réponse de l'ensemble du système. Les résultats sont présentés sous forme d'un résumé des efforts débalancés sur les supports adjacents aux bris (en bout de consoles et en tête du mât), et les conditions susceptibles de mener à la rupture des composants sont identifiées. Les résultats des simulations numériques indiquent que sous des conditions de charges normales (sans vent et sans accumulation de verglas) la rupture d'un support tubulaire ne cause pas de rupture de câbles, lesquelles sont susceptibles de causer une cascade longitudinale. Les charges de

débalancement et les tractions dans les conducteurs et câbles de garde adjacents au bris augmentent à mesure que le point de bris du support flexible sacrifié bouge vers la base. L'effet contraire est observé lorsque le pylône sacrifié est modélisé comme étant plus rigide, entrainant la rupture du câble de garde dans sa chute transversale.

Acknowledgements

Words can barely express my happiness and gratitude to the Almighty Allah for this amazing opportunity of self-discovery and progress accorded to me here, in Canada, amongst a progressive and welcoming society. I am thankful to all at McGill University for designing an effective approach towards education that allows its students to grow into well-informed and dependable professionals.

Professor Ghyslaine McClure, my supervisor, I can only be grateful for your time, understanding, persistence and vision that has moulded me as an individual and a student. I deeply value this bond that we share and hope to cherish it for the rest of my life.

Professor Sébastien Langlois, I extend my warm gratitude for always helping me out and standing by me in the toughest of times inspiring me to overcome each obstacle I faced through our detailed discussions. I would also like to thank Dr. Saeed Mirza, who always had an answer to all my queries and filled me with immense enthusiasm. Dr. Hani Mitri, whose invaluable advice in Finite element analysis made a major contribution to the progress of my thesis.

My Abba, Capt. Syed Zia Ul Islam Edroos & Ammi, Mrs. Shaista Edroos, I owe my life to you. I hope to be a reason of joy to you both and I love you. Your self-less love and unending sacrifices have only benefitted my life. You are pretty much the only reason, I want to succeed in life. My amazing sisters, Dr. Syed Shazia Edroos and Syed Zoya Edroos, you are my pillars of strength. Life is amazing and complete with the two of you.

Dr. Kahina Saad Saoud, I want to thank you for your time, effort and advice through the course of my thesis. For the technical assistance, Dr. Bill Cook and Jorge Sayat, Thank you. My amazing friends, Anshdha Rathore, Maharukh Jamil, Nahid Khalifa, Stephanie Verbeeck, Ashray Thrilok, Avishek Paul, Bassel Baydoun, Faraz Qamar, Keshav Mathur, Muhammad Imran Khan (Bhai), Musanna Shaikh, Vijaya Aditya Pawan Kumar Gutta and Waleed Usman, you all have etched your names deep into my heart for being there for me. You guys make me feel at home!

I would also like to thank Hydro-Québec, RTE France, NSERC and INNOVEE, the sponsors for their contribution towards the success of this study.

Contents

List of Tables

List of Illustrations

List of Abbreviations & Symbols

ACSR: Aluminium Core Steel Reinforced

ADINA: Automatic Dynamic Incremental Non-linear Analysis (commercial software)

ASCE: American Society of Civil Engineers

[C]: Damping Matrix

CEATI: The Centre for Energy Advancement through Technological Innovation

CIGRÉ: Conseil International des Grands Réseaux Électriques

E.H.V.: Extra – High- Voltage (Lines)

HQ: Hydro-Québec

H.V.: High Voltage (lines)

IEC: International Electrotechnical Commission

[K] : the total system stiffness matrix

[M]: the total system lumped mass matrix

OHL: Overhead Lines

RSL: Residual Static Load

TLC: Tower Load Controller

α: Rayleigh Damping Co-efficient

β: Rayleigh Damping Co-efficient

ζ : Critical Damping ratio

ω: Circular natural frequency in rad/sec

1. Introduction

Overhead power lines are among the most vital components of electric transmission infrastructure in the world. With the advent of electricity generation and transmission, the subsequent improvements in technology of the last century have made it economically viable to supply electric power to the remotest locations in any country. The power lines initiate the process of economic development of any region. As such, overhead lines must stand the test of time while being exposed to various climatic loads and weather conditions, as well as accidental loads. Figure 1-1 shows one of the failed lattice supports during the South Australian Blackout of 2016 which was a statewide power outage suffered due to a once-in-50-year event that saw winds upto 260kmph in two tornadoes. It is clearly seen that the cause of failure was foundation pull-out.

Figure 1-1: Transverse cascades during the South Australian Blackout of 2016. (Photo: The Australian issue: 12th October, 2016)

Transmission structures are designed to withstand loads subjected due to weather conditions, accidents, construction and maintenance. The design equations that deal with weather-induced

loads include the reliability-based load factors calculated for return periods of 50, 100, 200 and 400 years. (ASCE) American Society of Civil Engineers (1991). The transmission line infrastructure consists of a vast network of continuous lines and supports making them prone to domino type failures, which are termed as cascades. The question then remains as to which component failures are liable to trigger cascades. Longitudinal cascades are well known to be the result of conductor ruptures (fast cascades) or slower, quasi-static failures of successive towers whose capacity is insufficient to resist the imposed unbalanced environmental loads. CIGRÉ Brochure 515 (2012)

Figure 1-2*:* Transverse cascade on the 400 kV D/C Rubí-Vandellós-Pierola line in Spain during a 2008 a High Intensity Wind (HIW) storm (Photo: J. Santana López).

This study has been conducted to ratify if the transverse failure of a flexible tubular steel support could trigger a cascade. For this, the transmission line system which includes the support, lines

and insulators are modelled by means of finite elements most suitable to depict their behavior. Non-linear dynamic analysis is conducted to calculate the response of the system to the imposed transverse failure of a single support. Simulations are conducted by applying a rotation at specific nodes at a given support cross-section to initiate the transverse fall of the trigger/sacrificed support. Depending on the prescribed speed of the support falling movement, static or dynamic effects will be induced in the conductor system and transferred to adjacent supports. The failure propagation through the system has to be understood especially if the dynamic impact can be limited to reduce the likelihood of a cascade.

Transverse failures experienced in practice have mainly been caused due to extreme wind events (See Figure 1-2). The likelihood of transverse failures due to structural deficiencies, construction-related activities or man-induced causes like sabotage, vandalism or theft remains low and adequate maintenance and surveillance can reduce such occurrences. Other triggering high intensity wind events like tornadoes, downbursts and extra-tropical cyclones remain uncontrolled and appear to have been more frequent in recent years, or at least have caused more line failures.

It is understood that a transverse support failure will subject the adjacent supports to increased unbalanced forces. If these forces are large enough, the adjacent supports will collapse and the failure may progress until a stronger structure is reached. Thus, it is useful to derive appropriate tower design load combinations to ensure the resilience of supports to such failures. The main goal of this research thus, is to understand how a flexible support transverse failure propagates through a system and analyze the consequences to put forth mitigation measures.

The thesis will first present the main findings from the available research reported in the open literature about various line cascades in chapter 2, Literature Review. A comprehensive summary of the studies which have dealt with the mathematical modelling of overhead line systems, moving forth to understanding the effect of conductor ruptures is put together. The studies conducted pertaining to the effect of icing of cables and practical experiments on full-scale models of lines are also described. This chapter briefly documents only the research studies most relevant to the objective of the thesis.

Chapter 3 provides an overview of the problem of line cascades: definitions, most probable causes followed by mitigation practices. This chapter also summarizes the procedures adopted towards anti-cascade design in the American and Canadian Standard Codes.

Chapter 4 details the modelling assumptions for the study. It describes the finite element modelling procedure adopted, using the commercial software package ADINA. (ADINA 2012) The modelling assumptions include the justification for the element used based on the expected response, the sensitivity analysis conducted to ensure the correct mesh size and the mathematical methods used for the analysis.

Chapter 5 presents the free vibration analysis performed to calculate the Rayleigh Damping parameters. The free vibration analysis also provides the information on which the dynamic analysis results will be interpreted.

Chapter 6 presents the preliminary simulations conducted. The difference in longitudinal and transverse failures are simplified through idealized conditions. Some numerical modelling alternatives are discussed in relation to defining the appropriate material model for the supports.

Chapter 7 presents the simulations conducted and interprets the results. The proportion of unbalanced forces in terms of the RTS of the cables is provided for every case. The tension in the cables and axial forces in the insulator strings are tabulated. Additionally, results of simulations done on a modified support (with rigid cross-arms) are also summarized, and the failures leading to a conductor rupture are highlighted. The main observations and limitations of the study are summarized at the end of the chapter.

Chapter 8 presents the main conclusions of the study and suggests future research in this field.

2. Literature Review

The last decades have seen unprecedented progress in research pertaining to the effects of extreme loading scenarios associated with environmental conditions and failure of components on high voltage overhead transmission lines. The research activities completed during this time span were aimed at primarily understanding the modes of failure leading to longitudinal cascades and then developing computational models with capabilities to simulate the transient response of lines subjected to conductor failures and progressive collapses.

In the early 1900's, as line cascades started to occur in new overhead lines, researchers were drawn to the question of the capacity of an overhead line support to withstand longitudinal overloading. Mathematical models were developed to calculate the effect of failure of a component on the tensions in the ground wire and the phases. Lummis and Fiss (1969) presented their research on the effects of conductor imbalance on flexible transmission supports wherein the increment in tension in the conductors due to rupture was calculated based on the displacement of the support combined with the swing angle of the insulator. This was a relatively new concept at the time, as prior research considered the supports rigid. The effect of support flexibility in reducing the dynamic forces due to phase breakage were provided through a series of graphs. The idea of using tubular sections due to their inherent flexibility was propounded as a mitigation measure against domino type failure.

Lindsey (1978) put forth a mathematical model that calculated the longitudinal strength of transmission line system. The static response of overhead lines to events of rupture, imbalance due to ice and wind loading, was calculated by using a relaxation technique to maintain the static equilibrium of an overall non-linear system. See Figure 2-1. This formulation depended on maintaining the static equilibrium of the system through a redistribution of forces depending upon the stiffness of the components. Besides, the events were simulated using equivalent concentrated loads applied at the nodes in the model. An important new aspect of this research was consideration of an elastic-plastic moment rotation for the foundation of the supports. The

mathematical formulation was then used to analyze various full scale experimental results to prove its applicability.

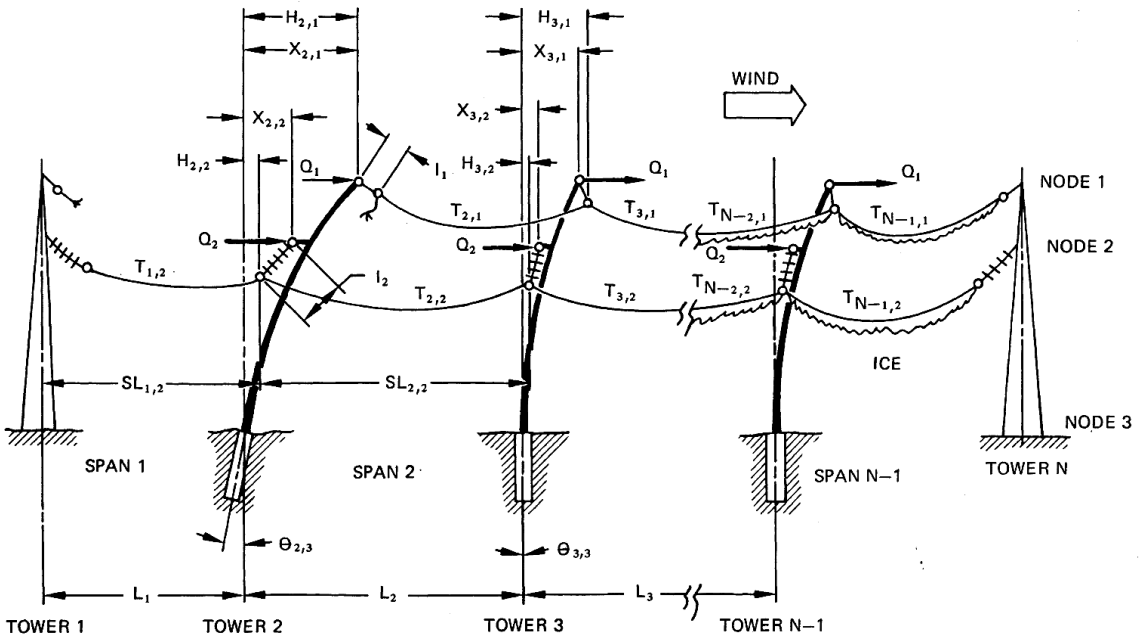

Figure 2-1 : Line profile with simultaneous wind, unbalanced ice and broken ground wire. (Lindsey 1978)

Peyrot, Kluge et al. (1980) conducted full scale tests on a decommissioned line to quantify the longitudinal imbalances associated with conductor rupture and insulator failure. They carried out tests on an 8-span configuration of latticed supports and, capitalizing on available techniques of instrumentation, were able to capture the transient dynamic effect of conductor rupture on the adjacent supports. They provided a method to calculate the maximum impact load based on the principle of energy conservation. The effects of length of the insulator, flexibility of the support, span length, and initial tension were considered on the impact factor and the residual loads on the supports.

(Mozer, Wood et al. 1981) through a research initiative funded by the American Electric Power Research Institute, prescribed a systematic approach to estimate the static and dynamic loads and the elastic response of the structure due to broken wire or ice-shedding. The project involved

conducting over 130 tests on a 1/30 scaled model of a *hypothetical 345kV line of 3 spans. See Figure 2-2.*

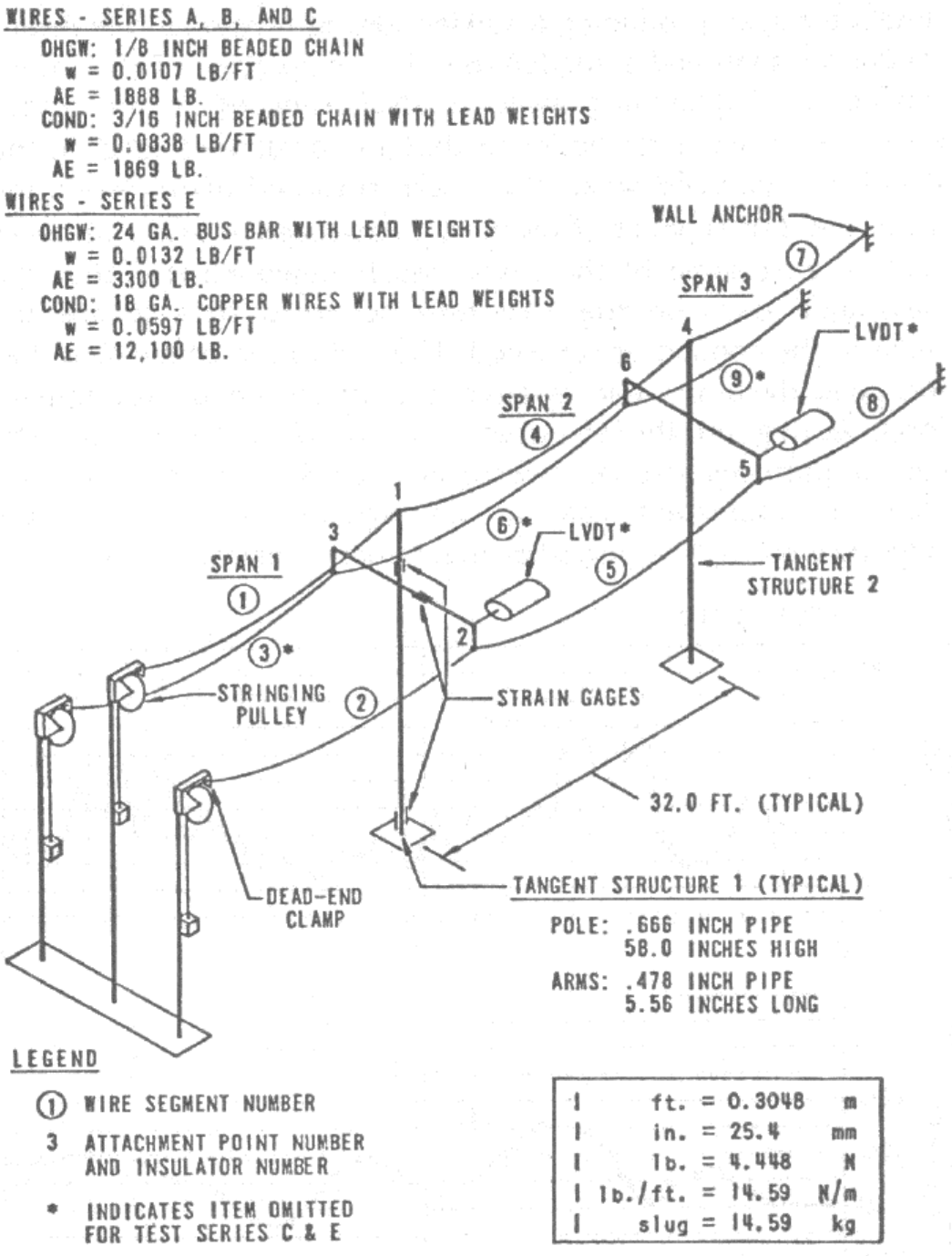

Figure 2-2: Schematic diagram of the test setup. (Mozer, Wood et al. 1981)

The majority of the results from test series E included 52 tests of broken conductors, 3 of broken shield wires and 1 was simulating sudden ice shedding. The parameters varied included stiffness, mass, conductor tension, shield wire tension, length of insulator, shield wire link and conductor type. The procedure involved comparing the initial and final conductor tensions measured during the experiment with those obtained from the static analysis of the same using a software BROD-I developed as a part of the EPRI Project. Besides, the natural period and damping of the model structures were measured by "plucking" them. The analysis was limited to elastic response.

(Richardson 1987) tested scaled models of transmission pole structures. His main objective was to examine the longitudinal dynamic loading on flexible transmission structures. He put forth a procedure to calculate the stiffness of a tubular support utilizing the information of tests carried out by the manufacturers provided during the bidding process. Besides, conducting more tests he included the additional stiffness provided by other components such as the pole shaft torsion due to forces at the upper end, pole arm support of upper conductor, lower phases and the underbuilt circuit. He constructed a 1/50 scaled model of an existing transmission line section on the roof of a building at the Massachusetts Institute of Technology, and he then ran a series of seven tests, involving broken conductor, ruptured shield wire, failed insulator, ice unload of a conductor followed by the same for a shield wire, and galloping conductor followed by the same for a shield wire. The results of these experiments were later compared with an actual line for broken wire under bare conditions, and they were found in close agreement. Besides the validation of the scaled model, the conclusions drawn regarding the resilience of flexible supports to dynamic loading was formidable. Another notable conclusion was that stiffer structures were subjected to twice the dynamic loading due to galloping compared to flexible supports.

The improvement of computational capabilities in the late 1980s coupled with the generation of sophisticated nonlinear finite element analysis commercial software fueled the idea of numerically modelling broken conductor problems as close to reality as possible. McClure and Tinawi (1987) conducted non-linear dynamic analysis of a 3-span model and validated the results against those obtained from the Mozer's experiments. The models studied evolved from those assuming completely rigid supports to more flexible ones, from only conductors to those including the ground wires to model the experiments performed. Succeeding this, various

research studies were carried out with the objective of numerically modelling the behavior of the various components of a transmission line system under component failure.

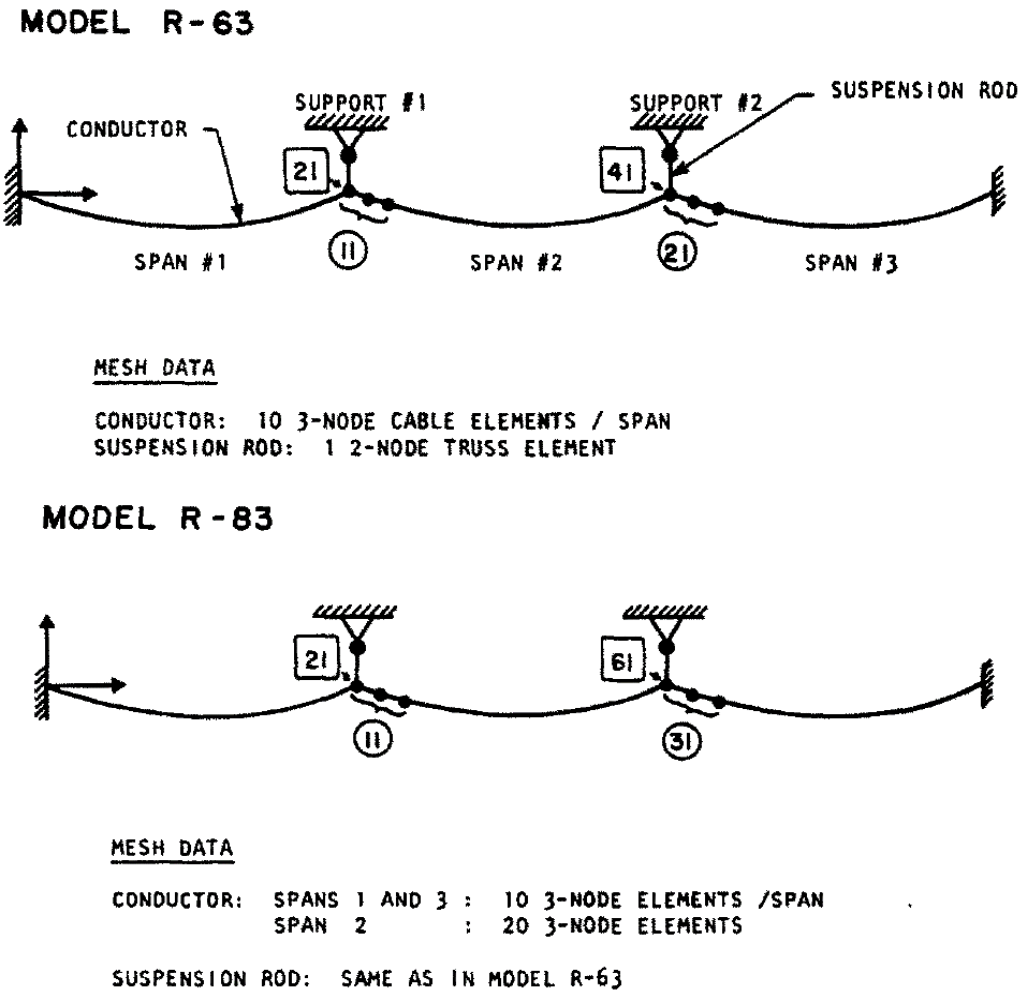

Figure 2-3*:* Simplified models for rigid supports. (McClure and Tinawi 1987)

Gupta, Wipf et al. (1994) carried out an investigation of the probable causes of a long cascade of 69 H-frame steel pole structures during an ice storm in Central Iowa on 7th March, 1990. The research involved non-linear dynamic analysis of a line section including the three supports which were speculated to have initiated the cascade based on field observations (see Figures 2-4 and 2-5). The fact that the post-disaster records of the observations were very well detailed, helped researchers to narrow down to such a zone. The finite element software ETADS was used for conducting the analysis on a model that included the material and geometric non-linearities in the system. The failure criteria were based on the rated tensile strength for the insulators,

conductors and shield wires. Whereas for the supports, material yielding combined with buckling of the main pole structures were considered. Static ice loads, dynamic broken insulators and conductor galloping loads were combined into several load cases. The loads were analyzed individually to ascertain their proportion needed to instigate a cascade i.e., loss of a tension bearing element in the conductor system. Besides, the resultant forces due to combination of loads were checked against the available failure data of certain components to decide on the cause most likely. It was concluded that dynamic effects of galloping coupled with radial ice of xx mm (1.5 in) caused the failure of an insulator that may have then triggered the cascade.

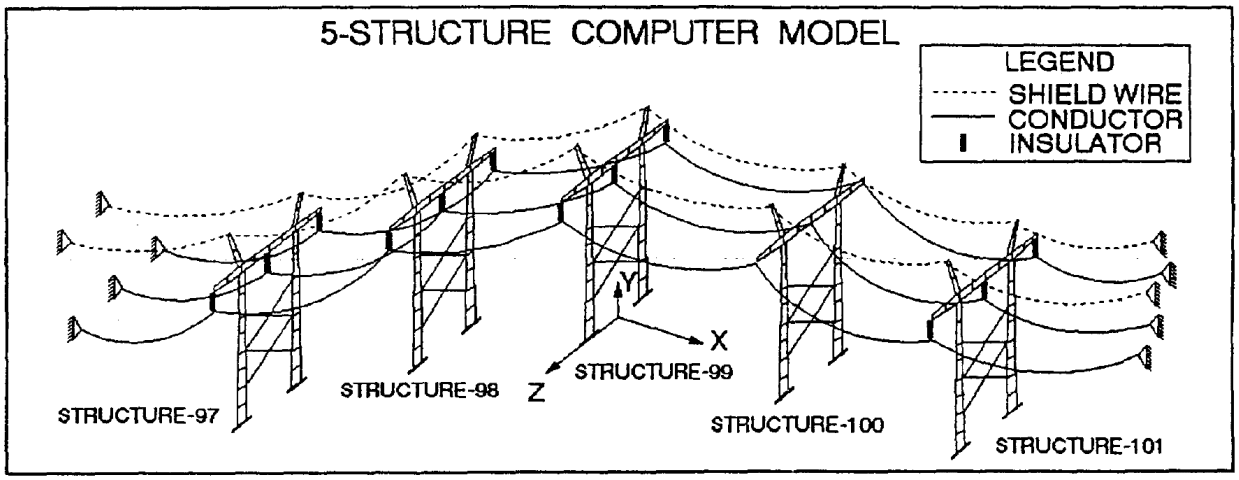

Figure 2-4: Three dimensional finite element computer model used for ETADS analysis. Gupta, Wipf et al. (1994)

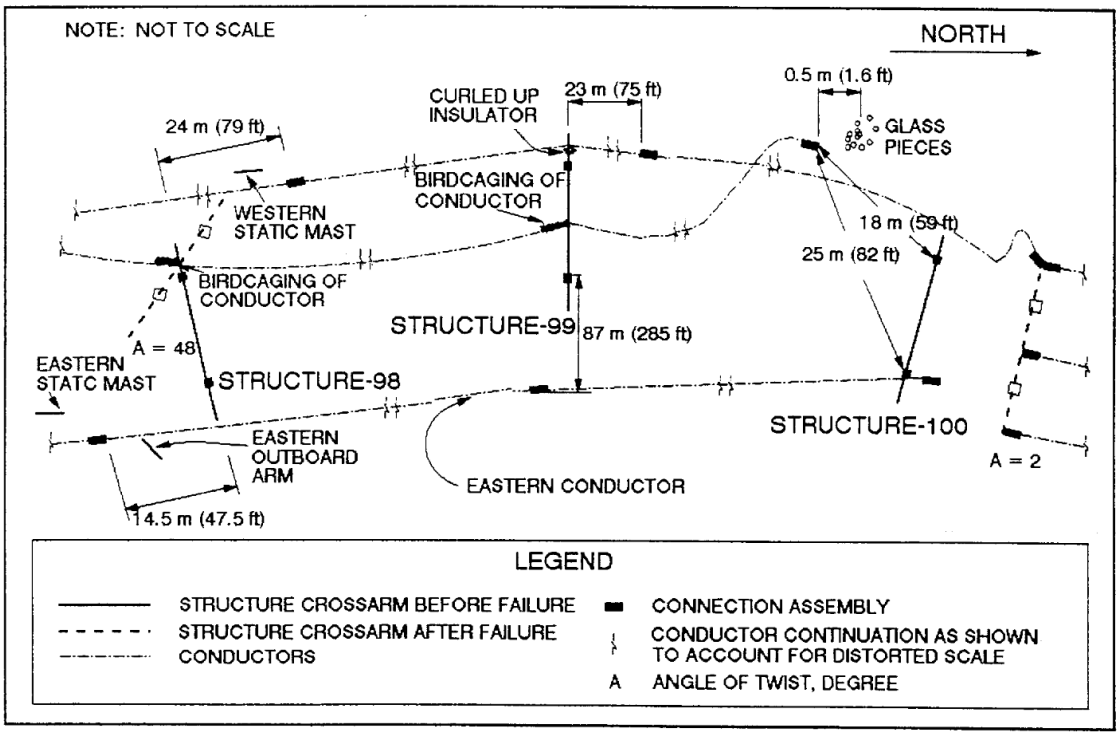

Figure 2-5: Plan view of area near Structure-98, 99 and 100 after transmission line failure. (Gupta, Wipf et al. 1994)

Lapointe (2003) suggested a rational approach to model the dynamic response of overhead lines due to sudden conductor rupture. The case study that was modelled in details was based on the failed latticed supports due to conductor breakage on account of ice. The simplified numerical model put forth assumed all the tower elements to be linear elastic truss elements except certain primary members which were assigned Hermitian beam elements. The model included internal damping of the system especially for the lines. Meshing considerations were studied to ensure that the model could capture the effects of the shock load. The finite element model was used to analyze the failure of supports due to rupture in two conductor spans due to icing. This model can be considered amongst the first few simplified models put forth on which one could study the effects of various conditions of exceptional or accidental loads on a system.

Alan Bowe Peabody (2004) in his PhD thesis put forth the idea of using supplemental springs and mechanical dampers to absorb the unbalanced longitudinal forces subjected on supports which

may propagate into a cascade. He invented the “Post Spring-Damper System” and “Rotating cross-arm Spring Damper system” to reduce the shock loads associated with conductor ruptures.

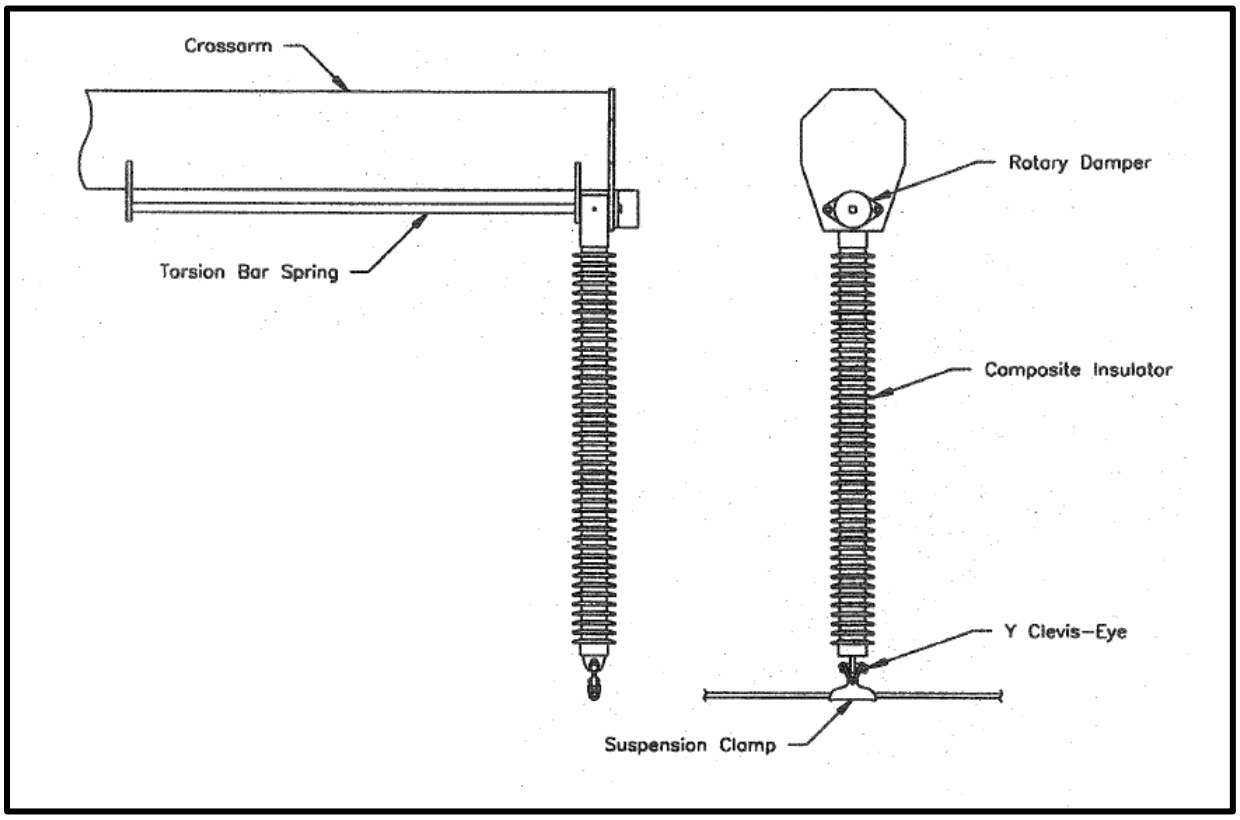

Figure 2-5: Post Spring-Damper System. Alan Bowe Peabody (2004)

The central idea of these inventions was to absorb the energy liberated into the system due to shocks by adding a mechanism within the support and line connection. In case of the Post Spring-Damper system, the rotary damper along with the torsional spring served the purpose. Whereas with the Rotating cross-arm Spring-Damper, the cross-arm was connected to the tower with a vertical axle. A torsional spring and damper are attached in between. Dynamic finite element analysis was conducted to test the suitability of the supplemental damping devices. The effectiveness of the system in case of iced cables was also checked.

Kalman, Farzaneh et al. (2007) proposed a numerical model using non-linear finite element analysis to quantify the dynamic effects of shock load induced ice shedding on a single span overhead line section. An important aspect of this study was the attempt to model ice as finite element compared to the previous studies, wherein a force equivalent to that of ice shedding

was applied on the lines to calculate the effects. Iso-beam and pipe-beam elements were compared for their efficiency in modelling the behavior of ice. The ice-shedding scenario was reproduced by using the plastic bilinear material model which supports the “Death upon rupture” option, which eliminates an element whose rupture criterion is satisfied at any integration point. The effectiveness of this approach was tested against the results of Roshan Fekr and McClure (1998) work on sudden ice shedding. A shock point load applied at 3m from the cable extremity caused failure of the ice elements under bending stresses due to its high deformation speed. Analysis were conducting by altering the parameters such as span length, initial tension and the pulse-load characteristics (12 ice-shedding scenarios). This research was amongst the first to model the rupture of ice deposits on the transmission lines.

Mirshafiei (2010) proceeded ahead with Lapointe’s and Kalman’s work by including accurate numerical modelling simulation of ice shedding due to initial shock loads or uncontrolled transient overloads due to cable rupture. This study tried to quantify the effects of ice dropping from the lines by accurately modelling the conditions of ice rupture prior to its shedding. The failure criterion for cylindrical glaze ice deposits based on maximum plastic strain was validated against the results of the reduced scale experiments performed by T. Ka´lma´n (February 2007). This was followed by applying the same on a single span to confirm the optimum mesh size to model ice deposits at real scale. Lapointe’s 3-dimensional model was then revised with these inputs and analysis was conducted emphasizing on a case of checking the effects of conductor rupture adjacent. The results indicated that ice shedding induced by cable rupture tends to attenuate the dynamic response of the system.

Siddam (May, 2014) further analyzed the effects of conductor rupture on adjacent supports and possibility of cascades. Unlike the previous studies wherein the supports were modelled as rigid initially slowly moving on to flexible, this study involved defining the supports as linear elastic truss elements moving to moment-curvature beam elements with inelastic properties and finally including the effects of Tower Load controlling devices on the dynamic response of the system. This study was successful in comparing the parametric results obtained from the various assumptions and stressed on the importance of considering the characteristic properties of the supports to reach the most realistic response. The final model included 31 tower structures

(Guyed V Steel Latticed Tower) of a single-circuit HV line section. See Figure 2-6. The consideration of moment-curvature beam elements in the tower model showed that if the middle span of the model was ruptured under bare conditions, two towers on either side of the failed conductor collapsed under the loads. Inclusion of 25 mm (1 inch) radial ice on the conductors propelled the failure to eight towers on either side of the failed span. The propagation of the cascade reduced including the Tower Load Controller (TLC's) in case of the iced condition wherein three adjacent supports instead of eight on either side of the ruptured span failed.

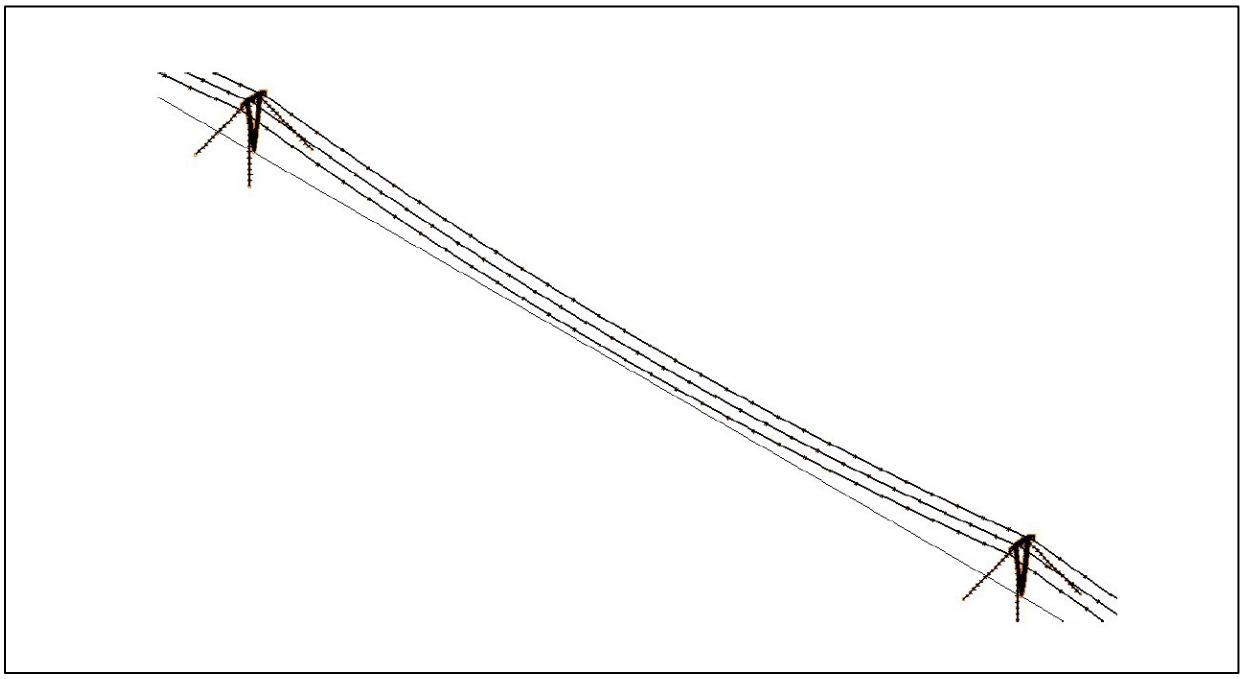

Figure 2-6: Section of the Finite Element Model of the Transmission Line Model. Siddam (May, 2014)

Alminhana, Mason et al. (2018) analyzed the response of an overhead line system to the failure of a latticed transmission tower developing in-house code for time-domain analysis using the central difference method. For accuracy at predicting the non-linear behavior of the angle sections of the tower, a special beam-column element was derived and utilized for the main members of the support. The formulation of the element allowed for detection of buckling and plastic hinge formation. The models were validated against available tests results conducted by Albermani (2009) and Peyrot, Kluge et al. (1980). The results obtained from the analysis were in concurrence with the available test results. This study is amongst the most recent ones that have

included intricate details especially in context of the non-linear response of lattice supports made of steel angle sections. Plastic hinging in the sections is controlled by means of a simplified approach to the principle of yield surface which was put forth by Al-Bermani and Kitipornchai (1990). The recent study conducted by Alminhana et al. can be regarded as the closest to the actual conditions.

Limited studies have been done concerning the dynamic response of lines on tubular supports. Most of the studies conducted were based on quantifying the effect of conductor rupture under various climatic conditions and achieving model validation by comparison with experimental results. The central idea of this case study is to evaluate the succession of events during the course of a tower failure, identify the dominant parameters governing the response and eventually suggesting further work and possible mitigating measures or design load cases.

3. Overhead Line Cascades – An Overview

The definition of a line cascade in IEC 60826 (2003) is: "… uncontrolled progression of failure (cascades) which might otherwise extend well beyond the failed section, whatever the extent of the initial failure."

The definition clearly indicates the uncontrolled nature of the failure, which is also commonly termed as a domino effect. As a line design objective, it is desirable to inhibit the progression of the initial failure at a section or span outside of this area (failure containment). How can it be done? The answer lies in understanding the response of a system to unbalanced loads. Generally, most overhead line cascades have been caused by extreme climatic conditions primarily involving wind and ice. Besides climatic conditions, another cause for line failures is termed as accidental loads, due to localized failures within a tower, vandalism, explosions, bushfires, etc. Through probabilistic models combined with available climatic data, one can approximate the probability of occurrence of the extreme loads due to natural phenomena and their values. The next step is termed as What-If analysis wherein the calculated extreme loads can be applied to a numerical model depicting the current design of the utility system.

The literature review in the previous chapter indicates how various studies have been done with the general aim to understand what happens when specific conditions cause unbalanced loading in the system. Until now, the majority of the studies aimed at analyzing the causes of longitudinal cascades because they are commonly observed than transverse cascades in cold climates. However, in regions exposed to tornadoes and high intensity wind storms CIGRÉ (Brochure 485) (2012) (such as localized downbursts) short transverse cascades, triggered by the transverse failures of a support have been observed.

The main aim of this chapter is to understand the causes of cascades and establish the necessity of studying them in detail to mitigate them. Causes of cascades can be classified as those due to failure of a single component and those which are due to multiple failures. An example of the latter is the dynamic failure of multiple of support insulator strings. On the other hand, a line

cascade caused by a localized conductor breakage is an example of a cascade due to failure of a single component.

As per the definition quoted above, for a cascade to occur, the zone of failure generally exceeds the region of the main triggering event.

3.1 Mechanisms of Cascades

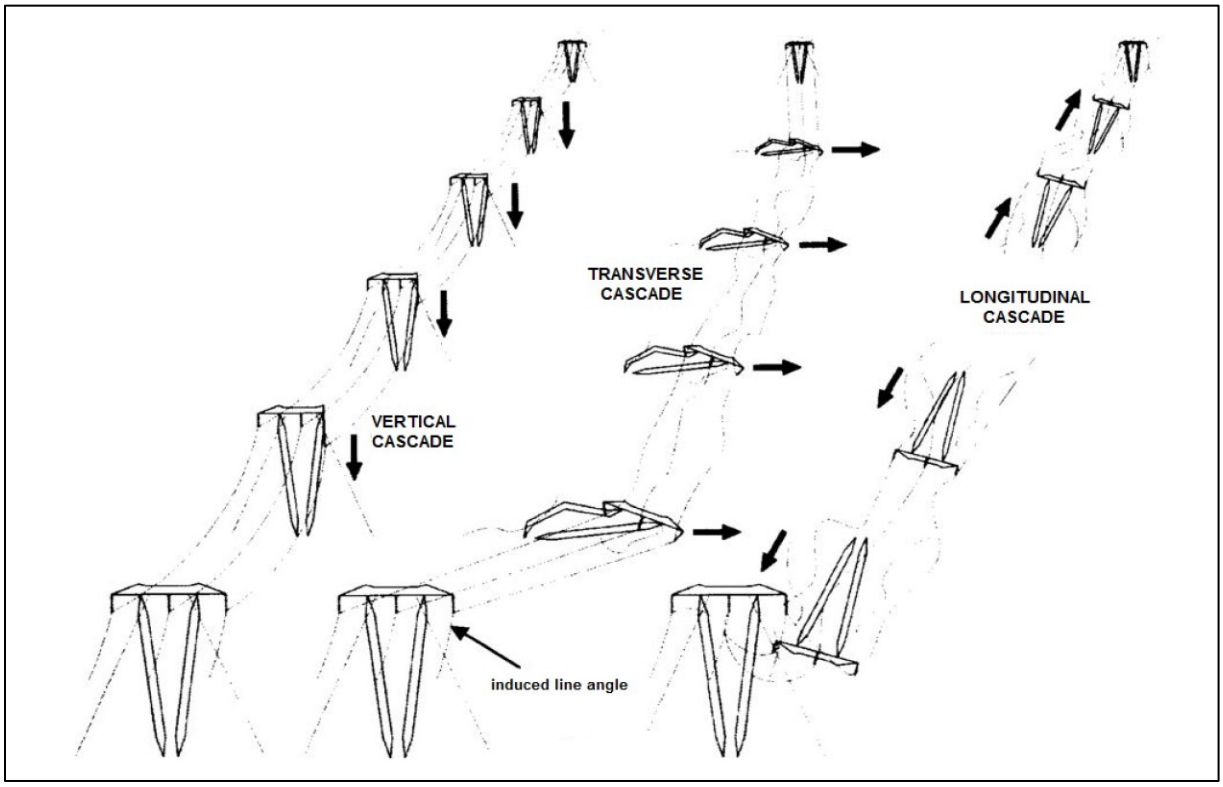

Figure 3-1: Transmission tower cascades mechanisms. Tucker (2007)

Cascades in transmission lines can be classified on the basis of their direction of propagation into three types: vertical, longitudinal and transverse. See Figure 3-1. A vertical cascade is triggered by loss of a component within the phase support assembly viz. cross arm, insulator etc. The dynamic effects following the component failure cause overloading of adjacent supports and cause multiple failures which are finally seen in the form of phases dropped to the ground.

Longitudinal cascades are the most common type seen to have caused huge economic losses to utilities, and occuring mostly in areas of cold climates. They are caused by the failure of a component within the system that maintains the tension in the lines. The potential energy of the

spans liberated due to the loss of tension is capable enough to overload the adjacent supports causing multiple failures due to longitudinal unbalanced loads. These failures propagate very fast such that the dynamic problem is compounded with a wave propagation problem. These failures continue until when the dynamic effects are attenuated to an extent that can be withstood by the intact supports and spans. Figure 3-2 shows a failed latticed tower during the 1998 ice storm in Québec.

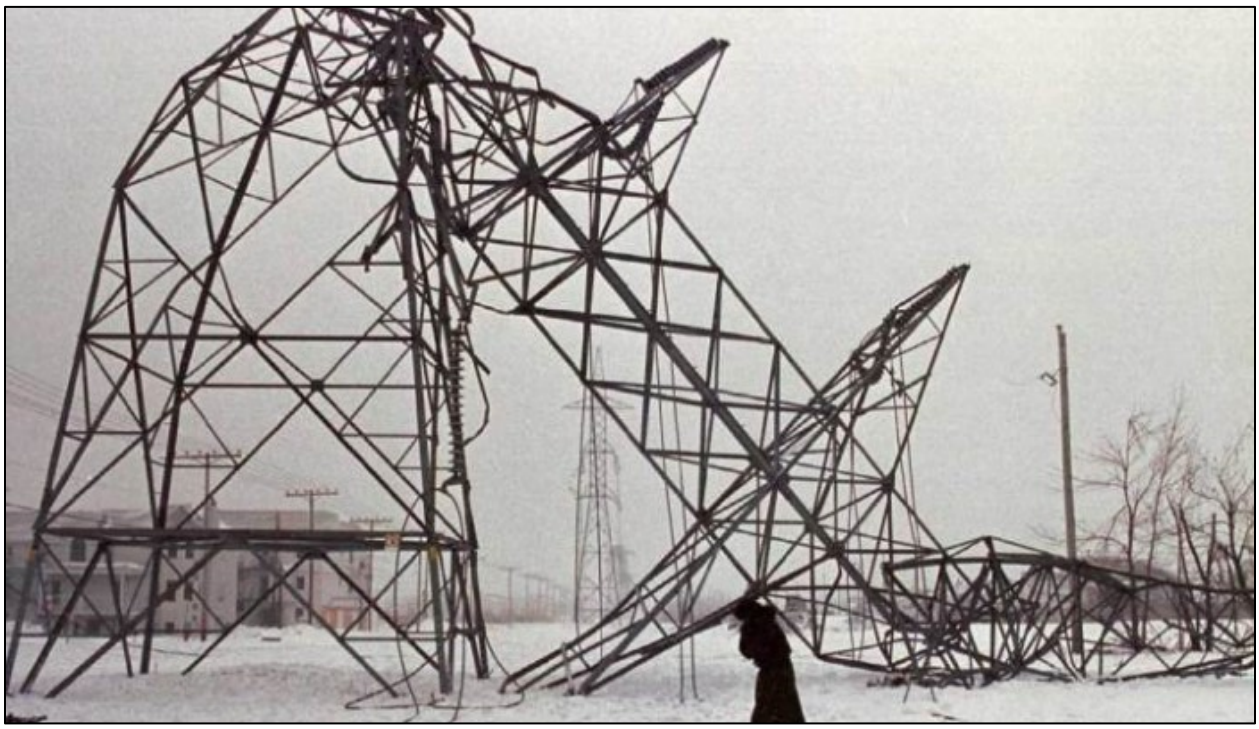

Figure 3-2: Longitudinal transmission towers cascade in Québec, January 1998, Photo by Robert Galbraith/CP PHOTO

Transverse cascades, as their name suggests, result in the failure of multiple supports in a direction perpendicular to the axis of the lines. These are generally believed to be caused due to extreme wind events (see Figure 3-3). The transverse failure of a support increases the effective length of the span propelling the rise in tension due to unavailability of slack until localized failures within the failing tower release the lines of these forces. The sequence of events in the failing tower completely depends on the allowable stresses of the components and the mode of failure. It is to be emphasized here that for a failing support, its own connections may be the weakest link when compared with the lines and insulators. The longitudinal and transverse load

imbalances created affect the entire system. However, the dynamic effects of support failures are less when compared against the longitudinal cascades and are thus termed as slow cascades. What needs to be understood through this numerical study is the quantum of dynamic effects the failure of a support has on its adjacent support and attached spans.

Figure 3-3: Transverse transmission towers cascade in by twin tornadoes near Melrose in South Australia, September 2016, Photo by ABC News: Tom Fedorowytsch

3.2 OHL cascading failures reported through the years:

Reports detailing devastations caused by extreme weather events are often heard and read in mainstream media, except that they do not detail the damage to overhead line systems. Generally, utility services (especially in private organizations) prefer to retain information pertaining to the detailed losses sufferred during such events. This makes it even more difficult for researchers to compile and study comprehensive information about the storms and associated types of cascades and their extent. Specialized groups such as Conseil International des Grands Réseaux Électriques (CIGRÉ) and The Centre for Energy Advancement through Technological Innovation (CEATI) provide for a protected forum for data sharing through their reports from time to time.

Table 3-1: Major Transmission line accidents from 1981-1996. (CIGRÉ 1996)

Cause of Failure	H.V. Lines (Voltage ≤ 240kV)		E.H.V. Lines (Voltage > 240kV)	
	No. of Events	No. of Tower failures	No. of Events	No. of Tower failures
Wind	94	606	45	240
Ice	28	205	9	469
Wind + Ice	65	122	16	24
Broken Conductor / Shield Wire	4	16		
Hardware Failure	4	4	6	6
Vandalism	1	1	3	4
Impact of Vehicles / Tractors	3	3	2	2
Soil Sliding Overflow	8	17	2	5
Others	8	8	1	1
Total	215	982	84	749

CIGRÉ in 1996 conducted a survey of countriesto establish the compliance of the prevalent codes of design for the OHL systems against the recommendations of IEC 826. A part of the survey involved collection of data pertaining to cascades due to extreme weather events. Table 3-1 had been compiled by listing the various storms worldwide spanning 15 years (1981-1996) with data collected from 42 electric utilities across the globe.

As indicated in the table, 299 events lead to the failure of 1731 supports for the period. 86% (257 out of 299) of the total failures in H.V and E.H.V lines have been attributed to either wind or ice or a combination of both, accounting for 96% (1666 out of 1731) of the total support failures. This indicates that extreme weather conditions whose occurrence can be predicted need to be accounted for in design to mitigate cascades. On the other hand, accidental events account for about 13% of failure events, leading to only 4% of the support failures.

Storms are clearly a major indirect cause of transmission line cascades as they create overloading of line components. Concentrating on the effects of wind storms (most likely to cause transverse cascades) the area affected due to high winds typically increases with the intensity of the storm (except for localized tornadoes and downbursts). A hurricane storm is classified into 5 categories (See Table 3-2) depending on the wind speed under the Saffir Simpson Scale. Taylor (2012). A category 1 storm includes a wind speed ranging between 119-153 kmph can cause failures within the utilities. A category 5 storm with wind speeds exceeding 252kmph can destroy the entire power grid network which has been seen in the Introductory note about the South Australian Blackout of 2016. The occurences of such storms has been rising in the past few years due to climate change.

The National Hurrican Centre (US) located at the Florida International University provides information according to the two zones of the Atlantic and Eastern Pacific. The Atlantic basin includes the Atlantic Ocean, Caribbean Sea, and Gulf of Mexico. The Eastern Pacific basin extends to 140°W. See Figure 3-4. The graphs provide the cumulative number of events per year depending on the time period of the year during which the storm season persists in the zone. It is seen from the graphs that at least 11 named systems occurred by the end of December in the Atlantic basin, 6 of which would be hurricanes and 2 amongst those would be Category 3 or greater, which roughly implies wind speeds ranging between 178-208 km/h.

Table 3-2: Saffir-Simpson Scale

Category Storm	Sustained Wind Speeds
1	119-153 kmph
2	154-177 kmph
3 (major)	178-208 kmph
4 (major)	209-251 kmph
5 (major)	252 kmph or higher

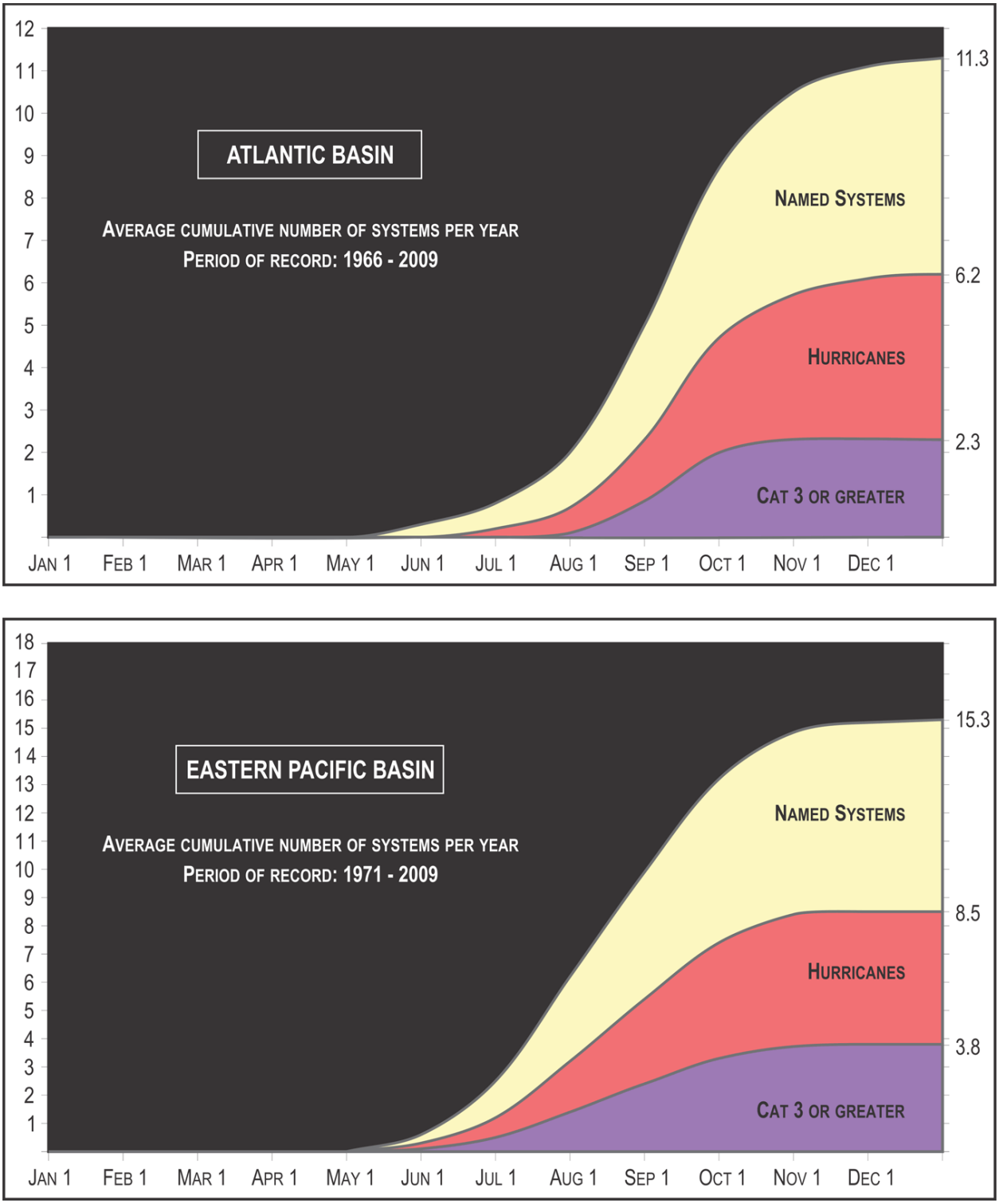

Figure 3-4*:* Statistical prediction of storms by National Hurricane Centre website.

In the year 2017 alone, The Atlantic basin experienced 18 storms, 10 amongst which were hurricanes , 2 of each categories. The United States had been ravaged by Harvey, a Category 4 storm with wind speed exceeding 200 km/h causing losses of about 75 billion USD. Hurricane Irma left a trail of devastation along its path from the Northeastern Carribean Islands, Dominican Republic, Cuba and Florida. The economic losses due to the hurricane systems in the Atlantic basin alone this year amount to 370 million USD.

3.3 Design for mitigation of Cascades

Designing towers that can withstand such high intensity wind events is impractical for economical reasons in large grids. Mitigation requires thorogh reliability analysis with careful consideration of the hazard levels, the grid configuration to assess redundancy of transmission routes, the vulnerability of strategic lines, etc. One of the structural mitigation alternatives is limiting the zone of failure combined with improving the emergency response delays, and developing rapid construction protocols. CIGRÉ Brochure 515 (2012)

Although the design procedures for the OHL systems have improved through the past decades, practical implementation of effective mitigation of cascades is still a concern. Transmission line engineers today are dealing with structures designed under different design principles, and structures designed prior to implementation of longitudinal loading criteria to avert cascades may be at a high risk of cascading failure.

The design procedure of OHL systems is based on the well-accepted reliability approach wherein weather induced loads are given a probability of occurrence based on climate data of the region and design load combinations are determined for tower design based on the limit state design approach. Most utilities also include load combinations that account for accidental loads (mainly represented by the effects of component failure) in the static regime. Depending on the nature of accidental loads, some impact factors may be applied to the static loads considered. These accidental loads are dealt separately by special load combinations applied longitudinally, transversely and vertically.

An important aspect of anti-cascade design of towers is utilizing the post-elastic response of the supports to sustain the unbalanced loads and their transient effects. Various degrees of

sophistication can be achieved in post-elastic analysis of towers, and most commercial nonlinear finite element analysis platforms offer adequate modeling capabilities, provider that their users have a good understanding of the theoretical model assumptions and limitations. The challenge in modelling complex nonlinear systems is to maintain realistic assumptions to achieve reasonable accuracy while trying to minimize computational loads. This was the motivation for a development of a special post-elastic beam element for tower analysis by Lee and McClure (2007). A 2-node L shaped beam element was formulated and tower analysis was validated with previous physical test results. Besides using the nonlinear beam formulation, the analysis of the tested structures included accurate representation of the various connections within the latticed supports, appropriately assumed as pinned or rigid by applying the necessary kinematic constraints. The numerical model also included the eccentricities for members connected at one leg. Despite its excellent performance in predicting tower failure modes in the post-elastic regime, the model was not put to use by the project sponsor.

Amongst the non-structural means of containment of cascades are the installation of control sliding clamps and load-limiting cross-arms. The governing principle of the sliding clamp is localized dissipation of energy to counterbalance the excess longitudinal loading by allowing controlled sliding of the conductor in the clamp, which provides extra slack in the conductor system and reduces shock loads. Load-limiting cross-arms involve installation of pivoting cross-arms with shear pins on poles; the cross-arms behave as structural fuses under shock loads by breaking in a controlled manner and protecting the rest of the support from overloading. Another effective design strategy developed and implemented by Bonneville Power Administration (in the Pacific North West of the United States) involves distributing the total load imbalance effects amongst a group of few supports designed with increasing longitudinal capacities (low, medium and high levels) and relying on the reduction in longitudinal imbalance at each support from the failing tower.

3.3.1 Standards for Anti-Cascade tower design

3.3.1.1 IEC 60826

IEC 60826 Standard provides for controlling of cascades by dividing the design procedure into fulfilling the requirements of reliability, security and safety. In terms of reliability, levels have

been defined with respect to the return periods of the design loads. In case of security, parameters have been defined to prevent the uncontrolled propagation of failures once they are triggered. These loads are applied longitudinally and for torsion also. Safety requirements pertain to prevention of injury considering the construction and maintenance loads. These loads are not accounted for while calculating climatic effects, but are dealt by applying overload factors to ensure reliability. For instance, construction loads during erection at a support are calculated by applying twice the static loads at sagging conditions to it. A major characteristic of the IEC is the complete designing of a structure based on probabilistic concept of reliability and deterministic concept of security.

While designing, the entire system is divided into sub systems such as the lines, supports foundations and insulators whose strengths are coordinated in a manner to account for, as also reduce the effects of the failure of a system on the efficiency of the whole. The whole concept of strength coordination is resting on the assumption that suspension supports will collapse in a relatively slow manner (dynamic effects are reduced) while the integrity of the conductor system is maintained, which means the sudden shock load created by a conductor rupture is absorbed by the system when it propagates in the line section. The main problem with this approach is that when conductor failures occur under ice and wind loads, the individual line supports are unable to resist the load imbalances created as the shock propagates in the section (until it reaches a stop).

Table 3.3 lists the limit states of strength defined for line components which are damage limit state for serviceability and failure limit state for security.

Table 3-3: Limit states of strength for line components according to IEC 60826.

Condition	Loads	Strength Limit State
Reliability	climatic, ice, wind + ice, with a return period T	Damage limit
Security	failure limit (torsional and longitudinal)	Failure limit
Safety	construction and maintenance loads	Damage limit

The damage limit for the lines are the lowest of: Vibration limit or infringement of critical clearances defined by appropriate regulations or 75% of the characteristic strength or rated tensile strength of the phase, while the failure limit is the ultimate tensile strength.

As explained earlier, security related loads to controlling the propagation of cascades put forth certain minimum requirements as below:

1. A broken phase load equivalent to the Residual Static load calculated for bare conductors at average room temperature is applied at any one phase.
2. An unbalanced longitudinal load is also prescribed in cold climates (see Figure 3-5), which is equivalent to simulating the static effects of an ice load equal to weight of the conductor span applied on one side of the tower., and bare cables on the other side.

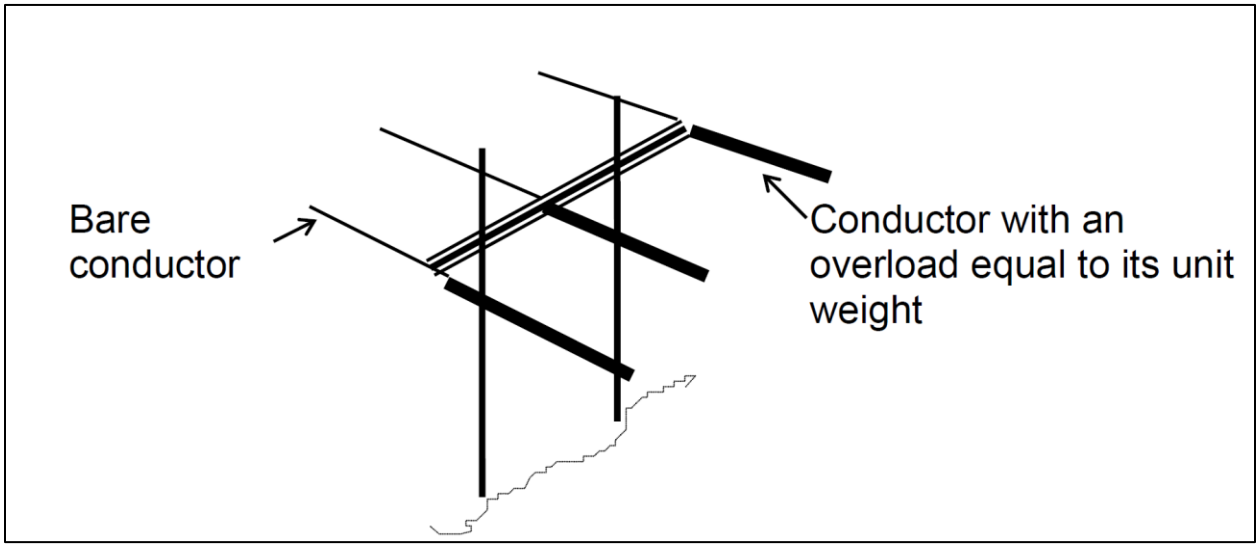

Figure 3-5: Example of longitudinal loads for cascade mitigation design. CIGRÉ Brochure 515 (2012)

For more important lines needing higher levels of security due to terrain or other reasons, additional measures are applied to meet the requirements, as listed in Table 3.4.

Table 3-4: Additional security measures listed in Table 9 under Clause 6.6.3.3 of IEC 60826 (2003).

Description of additional security measures	Comments
Increase the RSL by a factor of 1.5 at any one point. This requirement will increase the probability of a suspension tower to resist the dynamic load due to a broken conductor.	Lines where higher security is justified. But this strategy has been proved to be ineffective as the shock load propagates to the adjacent support faster than the energy dissipation in the tower.
Increase the number of RSL torsion/flexural load points to either two phases or two ground wires.	This option may apply to double or multi-circuit lines
Calculate the RSL for climatic conditions involving higher than everyday loads such as wind or ice loads corresponding to a 3-year return period	Advisable for angle structures or lines subjected to severe icing conditions
Insertion of anti-cascading towers (anchor towers) at intervals, typically every tenth tower. These towers shall be designed for all broken conductors subjected to limit ice and/or wind loads	To be considered for important lines in icing areas

3.3.1.2 ASCE Manual 74

The ASCE Manual 74 is widely practiced in various other countries besides the United States. It is quite similar to the IEC 60826 with respect to the design philosophy. It lists down three methods to contain cascades.

Method 1: Design all structures for a static residual longitudinal load.

Method 2: Installation of failure containment structures at specified intervals

Method 3: Installation of load release mechanisms.

Method 1 promotes the design of all structures for RSL applied longitudinally obtained by using reduction factors. The load obtained is an approximation of the final residual static tension in the lines after dynamic effects have subsided. These factors are a function of span-t- sag ratios and span-to-insulator length ratios. The ASCE prescribes that calculation of loads on intact spans should correspond to the climatic event assumed to cause failure, which covers in principle the

whole range of climatic conditions (heavy ice and wind in cold climate, high wind in warmer regions, or both).

Besides the static load reduction factors, the ASCE Manual includes methods to calculate dynamic impact load factors as a function of the span-to-sag, span-to-insulator ratios, and support stiffness. These methods have been developed through research completed by EPRI in the late 1980s. This approach guarantees a realistic approximation of the loads as it accounts for most of its governing parameters.

Method 2 of the ASCE is based on the principle of limiting the length of cascades through containment structures utilized mostly for existing lines with limited longitudinal strength. This option is cost-effective when compared against strengthening of each support. The failure containment structures such as stop structures, anchor structures, anti-cascading structures are constructed at regular intervals along the line. The manual doesn't specify any strict interval distance but suggests intervals shorter than ten miles or 16 km as a reference. The utility services can devise the interval distance depending on the design loading of the containment structure, importance of the line and other factors. The containment structures have to have the capacity to stop the failure shock.

Method 3 involves installation of load release mechanisms which allow for localized controlled energy dissipation to absorb the dynamic effects of longitudinal imbalances. Slip type or release type suspension clamps can be used.

This chapter summarizes the mechanism of cascades as also classifies it through the direction of propagation. The most plausible causes of cascades are listed and their reoccurrence specifically in the recent years has been documented. As designers bearing the responsibility of sustainable yet economically viable infrastructure, it is a necessity for us to understand the intricacies of the propagation of structural or mechanical failures in transmission lines to provide effective cascade mitigation solutions.

4. Modelling Considerations

The supports in the transmission line systems in use today can be classified broadly into tubular or latticed steel towers (guyed or self-supported) and wooden pole frames. There are multiple different configurations, as the geometry of the tower depends on the line voltage capacity and associated electrical conductor clearances to ground and to the supports.

In this study, to calculate the load imbalance due to transverse failure of a support, we have selected a case study of a tubular double-circuit tower because of its relatively simple geometry and anticipated simplicity in modeling. This type of support had not yet been investigated in the context of line failures and the study provided an opportunity to better understand the effects of their relatively higher flexibility when compared to lattice towers. Hydro-Québec employs tubular steel supports for voltage capacities ranging between 110kV to 315kV. The tower modelled in this study pertains to a suspension support for a capacity of 230kV.

4.1 Modelling of the Tubular Support

The particular tubular tower selected for the study supports spans ranging between 200 m to 400 m. The line design parameters and structural drawings were provided by Hydro-Québec. The elevation view of the tower is shown in figure 4-1.

The tower pole has a tapered geometry, and its actual dimensions are represented by 19 tapered pipe sections with thickness varying from 6 mm in the apex zone to 18 mm at the base, as indicated in table 4-1 by Hydro-Québec. The pipe-beam cross-section options available in the ADINA library of finite elements allows only for a uniform prismatic pipe. To account for the tapering cross-sections, the stem of the tower was divided into 31 cross-sectional groups depending on their outer diameters and thickness (about 1.7 m length each). Cross-arms are also tapered: the longer cross-arm was adequately represented by 9 segments whereas the shorter cross-arms were divided into 6. The tower finite elements are defined as 2 node pipe-shaped Hermitian beam elements with 6 degrees of freedom per node (the usual 3 orthogonal translations and 3 rotations at each node) (ADINA 2012)

The pipe-beam element is formulated with the Bernoulli-Euler Beam theory corrected for shear deformations. The element stiffness matrix is based on the Newton Cotes Method with the integration order of 5 along the longitudinal axis, 3 in the radial direction (through the thickness) and 8 (along the middle line of the circular cross-section). The location of integration points is illustrated in Figure 4-2. The label points at which the results are calculated consist of 3 digits in the following order, the first digit is along the longitudinal (1-5), 2nd digit is for the points along thickness (1-3) and the last is the points along the middle line of the circular cross-section (1-8). Thus for 1 element it calculates a total of 120 results (ADINA 2012). The large number of integration points is necessary to capture the inelastic effects that may develop in the tower. This approach is numerically very taxing as all supports have been modelled in such detail even if they are not going to sustain inelastic effects in the simulation.

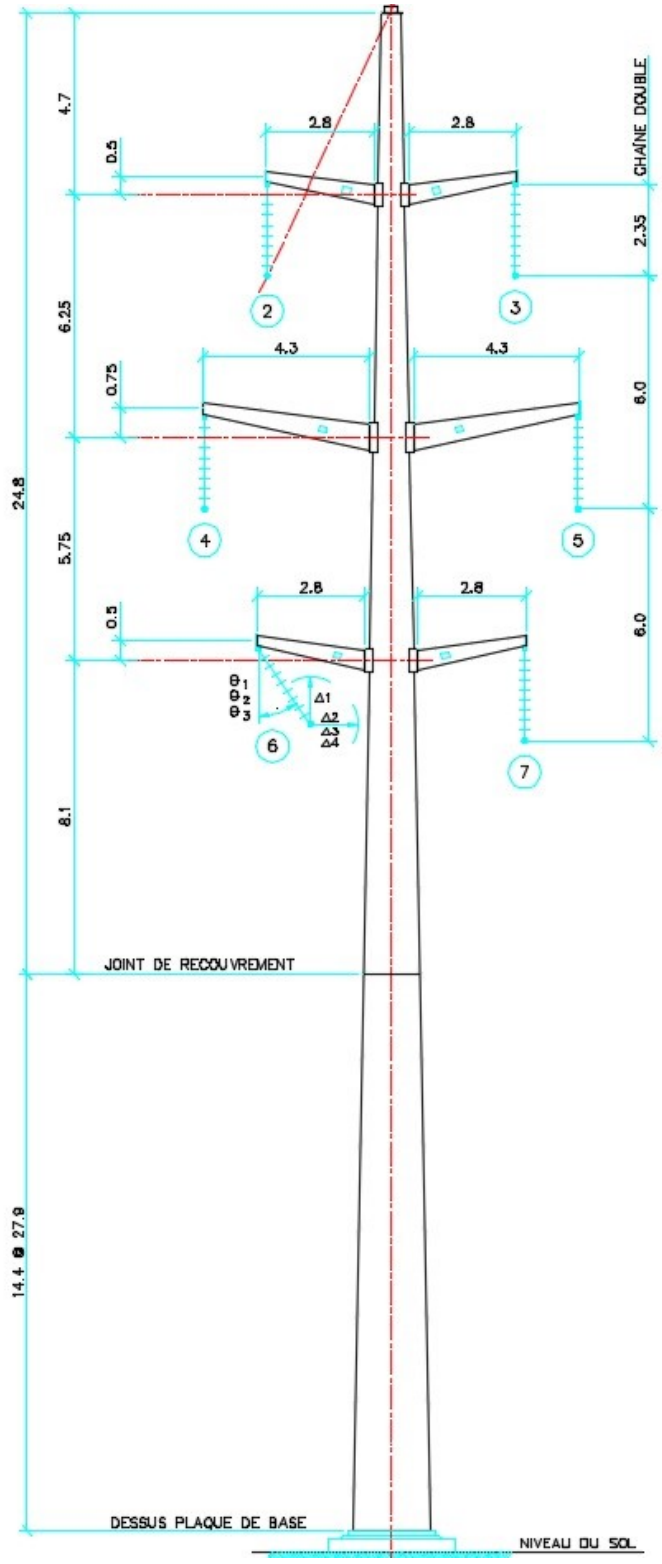

Figure 4-1 Elevation View of the Tubular Support (Source Hydro-Québec)

Table 4-1: Geometry of cross-sections of the Tubular support provided by Hydro-Québec

Beam Section Number	Height (mm)	Outer Diameter (mm)	Thickness (mm)
1	4700	500 636	6
2	3125	640 730	8
3	3125	734 824	10
4	2875	828 911	12
5	2875	915 998	14
6	3300	1002 1098	16
7	4800	1101 1240	18
8	4800	1240 1343	18
9	4800	1343 1481	18
10	4800	1481 1620	18
11	1500	1620 1663	18
12	1500	1663 1707	18
13	1500	1707 1750	18
14	1500	1750 1793	18
15	1500	1793 1837	18
16	1500	1837 1880	18

17	1500	1880 1923	18
18	1500	1923 1967	18
19	1500	1967 2010	18

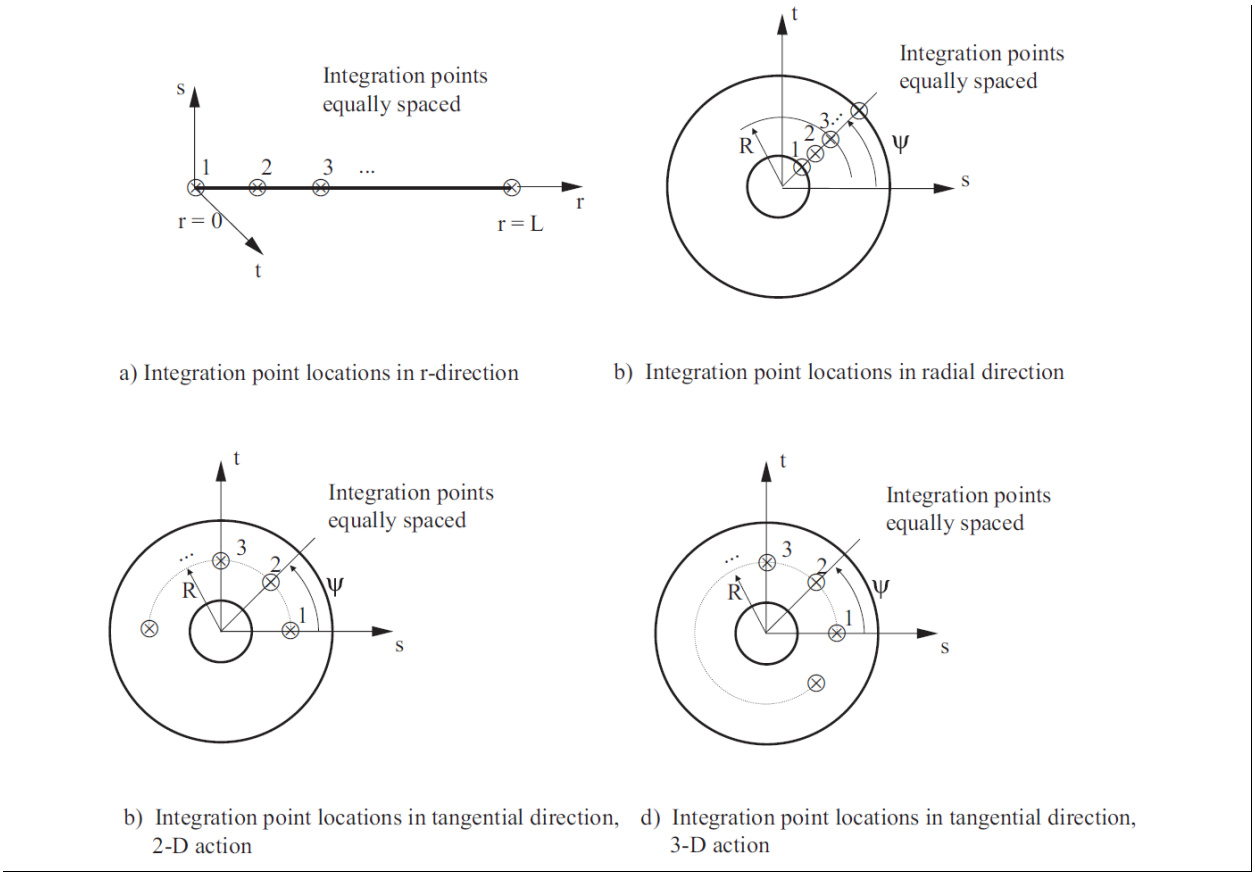

a) Integration point locations in r-direction

b) Integration point locations in radial direction

b) Integration point locations in tangential direction, 2-D action

d) Integration point locations in tangential direction, 3-D action

Figure 4-2: Integration point locations in elasto-plastic beam analysis, pipe section. (ADINA 2012)

For determining the length of the beam elements most effective in approximating the behavior of the tubular structure, a sensitivity analysis of lengths varying between 1m and 0.1m was done when calculating the natural frequencies of the tower stem (tubular pole) using the proposed meshes and a more refined model using thin shell finite elements. The shell model consisted of 9-node shell elements (quadrilateral shaped elements with 4 on the top and bottom faces and 1 mid-surface node). The meshing in ADINA is a 2-step procedure. In the first, mesh density is

assigned to the entire model wherein each line in the model is divided into parts depending on the length. This was kept as 0.1m. The next step is the actual generation of the mesh wherein the software creates elements by joining the previously divided edges. Effectively a minimum edge length of 10cm was used to create the shell elements. The conclusion of the sensitivity analysis was that in the stem, an element length of 0.1 m was sufficient.

Figure 4-3 shows the fundamental mode shape of the pole stem using the detailed shell model (on the left) and the beam model on the right using element lengths of 0.1 m. Table 4.2 lists the lowest natural frequencies obtained from the two models. Overall, it is seen that the pipe-beam model is effective in estimating the natural frequency response of the support as the different between the two models is of the order of 1% or less for the lowest three modes. Note also that the pipe-ovalizing effects are neglected in the analysis to simplify the calculations.

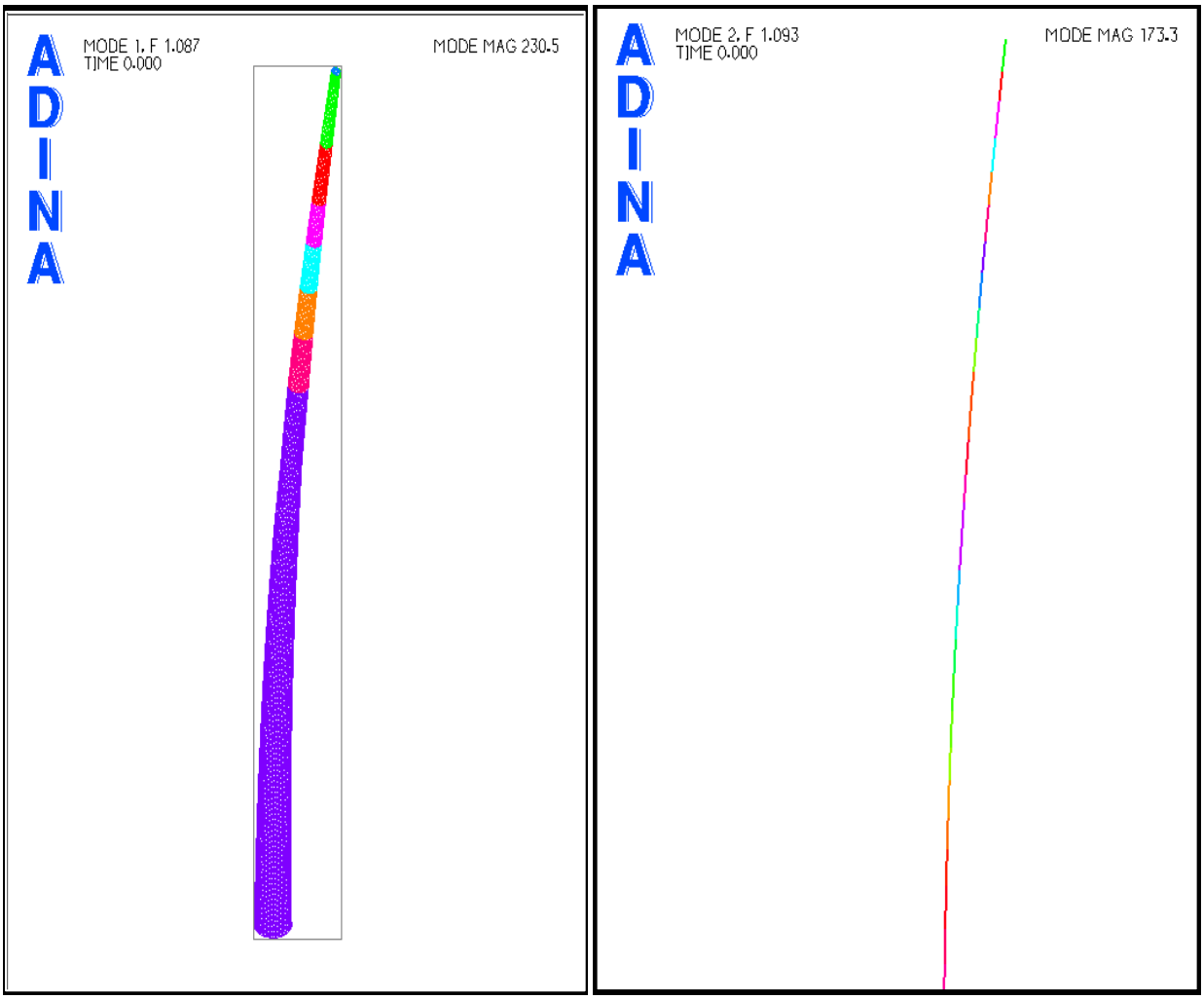

Figure 4-3: Comparison of Shell and Beam elements fundamental mode and frequency.

Table 4-2: Comparison of tower stem natural frequencies using two models

Shell Model	Beam Model	Ratio (Beam:Shell)
1.087Hz	1.093Hz	1.005
3.762Hz	3.738Hz	.994
8.136Hz	8.041Hz	.988
14.54Hz	14.66Hz	1.01
17.49Hz (pipe mode)	23.21Hz	1.32

The material model assigned to the tower pipe-beam elements is a trilinear curve yielding at 345 MPa and allowing for an ultimate stress of 450 MPa. The Young's Modulus is 200 GPa and the strain hardening modulus is 50 GPa. See Figure 4-4.

An important assumption used in the model concerns the failure criterion of the pipe-beam elements modelling the supports. Two options were considered along the course of this project:

1) Perfectly elastic behavior of the support until reaching the ground (in preliminary runs)
2) Elasto-plastic behavior of the support followed by the death of an element when reaching a maximum deformation criterion.
3) Elasto-plastic behavior of the support with no ultimate failure criterion when comparing a shell model and a pipe-beam model of the mast only.

The first option was ruled out during preliminary analyses because it yielded unrealistic forces at adjacent supports as it created excessive cable tensions first in the ground wires and then in the conductors. In the second option, which was retained for the complete line section simulations with prescribed support rotations at various mast elevations, the elasto-plastic behavior of the supports is included and the pipe-beam elements of all towers are provided a material model that allows for post-rupture analysis. It is termed as Plastic-Cyclic material model in ADINA. It implies that on reaching its maximum plastification at any integration point, the complete pipe-beam element is considered dead for the succeeding analysis, automatically removing its contribution to the stiffness matrix of the system. In this study, since a support will fail, the elements of all towers have been provided a material model that allows for post-rupture analysis. It is termed as Plastic-Cyclic material model in ADINA. It implies that on reaching its maximum plastification at an integration point, an element shall be considered dead for the succeeding analysis, automatically removing its contribution to the stiffness matrix of the system.

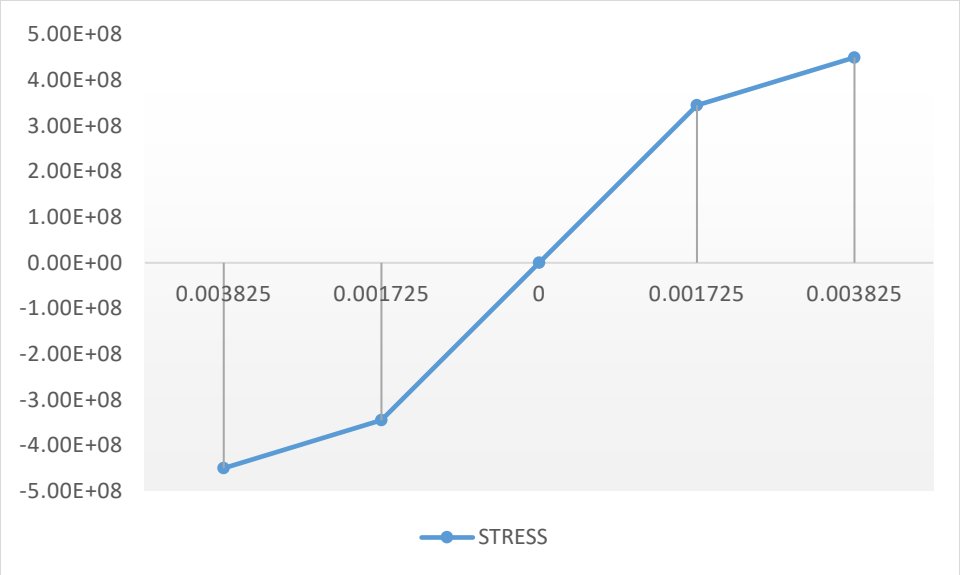

Figure 4-4: Material curve for the tower steel.

In the third option, tested only on a mast section, the model accounted for the elasto-plastic behavior of the thin-walled structure when reaching structural failure without specific death-upon-rupture. Although this is rather straightforward with a shell element formulation, it proved difficult to duplicate the actual behavior of a pipe cross-sectional element using the pipe-beam formulation. Two simplified models of the pole alone using pipe-beam elements and shell elements were analyzed and compared to further study the possible effect of the pole failure criterion assumptions. This analysis aided the understanding of the working of the Death upon rupture of the pipe-beam element and its suitability and inherent limitations to study the section failures in the sacrificed support. ADINA doesn't allow to model the pipe-beam element selected without death upon rupture if non-linearity has to be included in the material model, thus it is either elastic or plastic cyclic. In this case, only the model with shell elements can be modelled as infinitely elastic or bilinear without a rupture criterion.

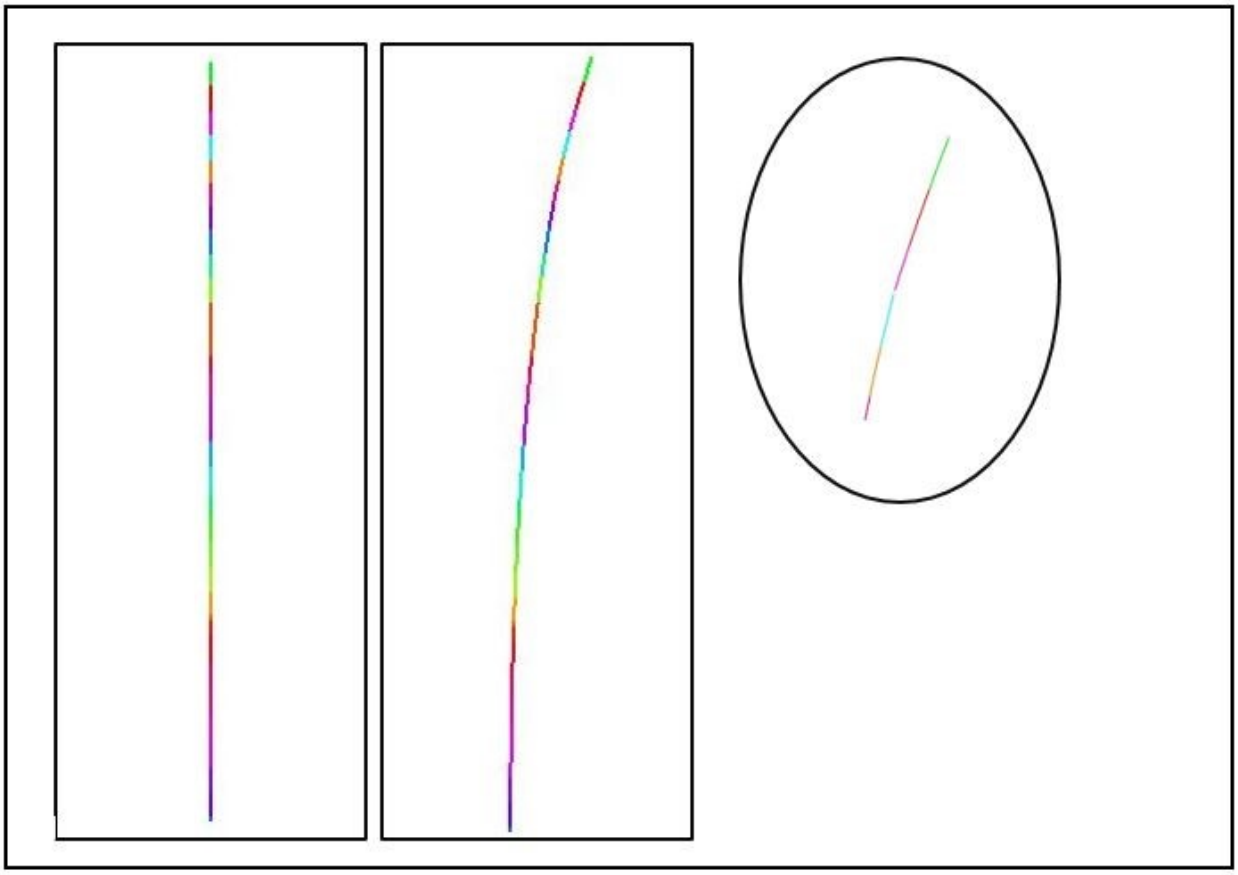

Figure 4-5: Deflected Shape of the beam model

First, Figure 4-5 depicts the stages of deflection within the tubular mast made of pipe beam elements when a monotonically increasing load at the rate of 50kN/sec is applied on it transversely. This analysis runs showing the failure of an element when the force reaches a value of 180.25kN. At this point, the element about 5m below the apex node is removed from the support as its integration points breach the failure criterion that allows a plastic straining in compression of 10%.

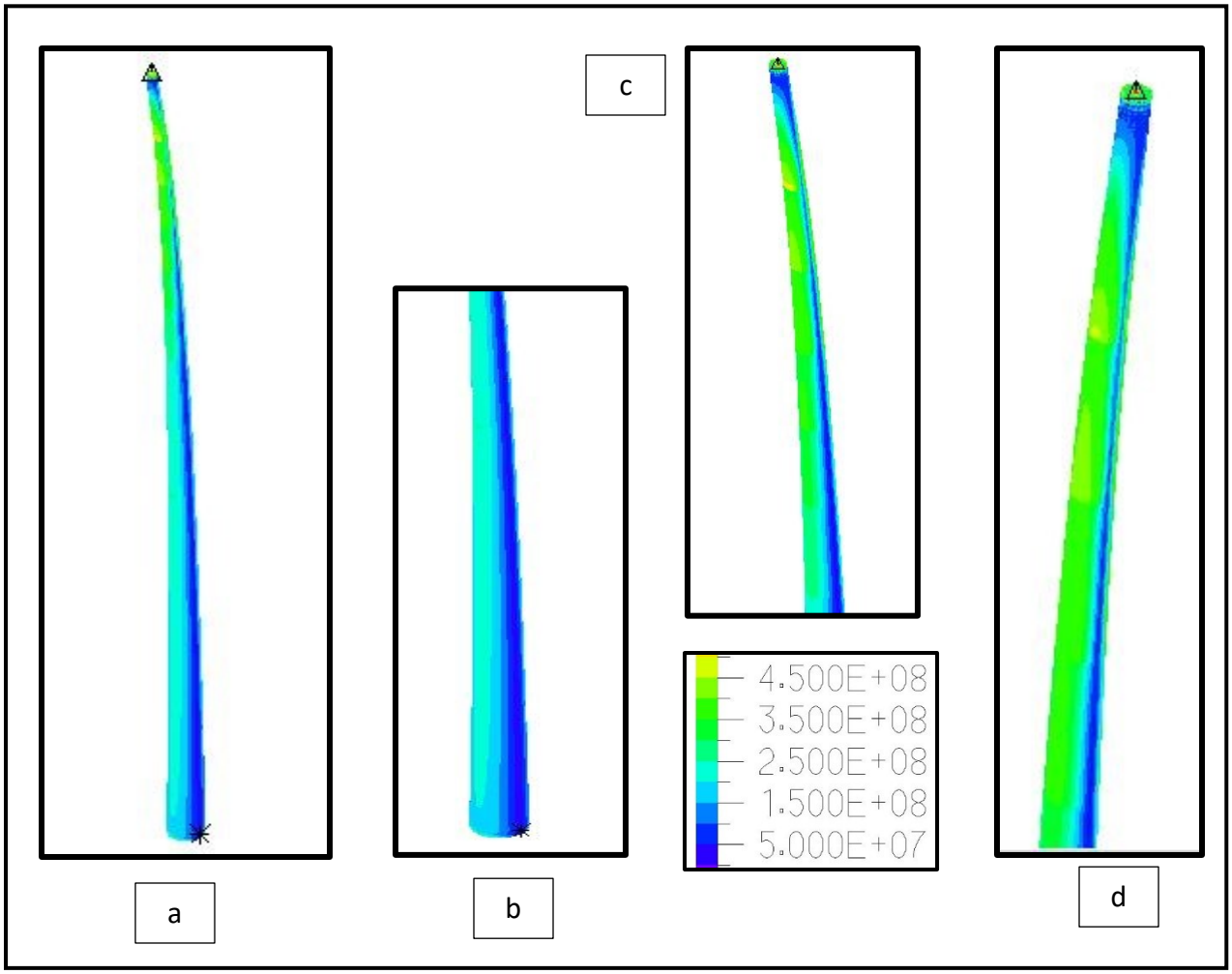

Figure 4-6: Deflected shape of the shell model.

Second, Figure 4-6 depicts the final stage of deflection of the shell model when a major portion of the apex undergoing compression has plastified. The figure 'a' denotes the stresses in various regions within the support which are depicted by the bands which follow the legend as shown in the figure. The figure 'b' denotes the region undergoing compression in the base of the support. As is evident through the legend, the maximum stress within this region is about 200 MPa. The figure 'c' denotes the stresses in the apex region which is maximum affected due to the applied transverse force undergoing a compression at its ultimate strength of 450 MPa. The next important section of the support is depicted in figure 'd'. It is the region in the apex which is undergoing tension due to the applied force. This region shows a maximum stress around 350 MPa thus it has yielded.

The force at which the shell model undergoes maximum plastification is 213.18 kN. The beam model thus under-estimates the strength of the section to an extent. Also, another important aspect of the beam formulation, is that it eliminates an element having an integration point reaching the failure criterion although the entire cross-section has not plastified to that extent. Once the element is eliminated from the stiffness matrix, it will lead to release of strain energy in the system causing some amount of excitation besides, it will also influence the trajectory of downward motion of the support. This analysis implies that, in case of a transverse failure, the tubular section of the support will fail in compression but remain attached to the support, the associated movement of the failed region of this support will increase the span length, however it remains to be seen whether this leads to a partial cascade of supports.

4.2 Modelling of the Insulators

The insulators used by Hydro Québec are manufactured by Sediver of the type N21/171 conforming to CS11A Sediver (2015). They are toughened glass ball and socket type insulators with a maximum load capacity of 222 kN. Figure 4-4 shows their typical arrangement.

The insulators are linked together like a rigid chain, to model the movement of the same, they are defined as steel rods using 2-node truss elements having 3 degrees of freedom (translations) at each node. This measure ensures that the behaviour of the insulator swinging about a pivot is approximated satisfactorily. The length of the insulator is 2.355 m and it is assigned an elastic steel (tension only) material model with a modulus of Elasticity of 200 GPa not allowing any compression in the string to account for its real chain-like behavior. The insulator rod is considered having a diameter of 83 mm (critical cross-sectional area).

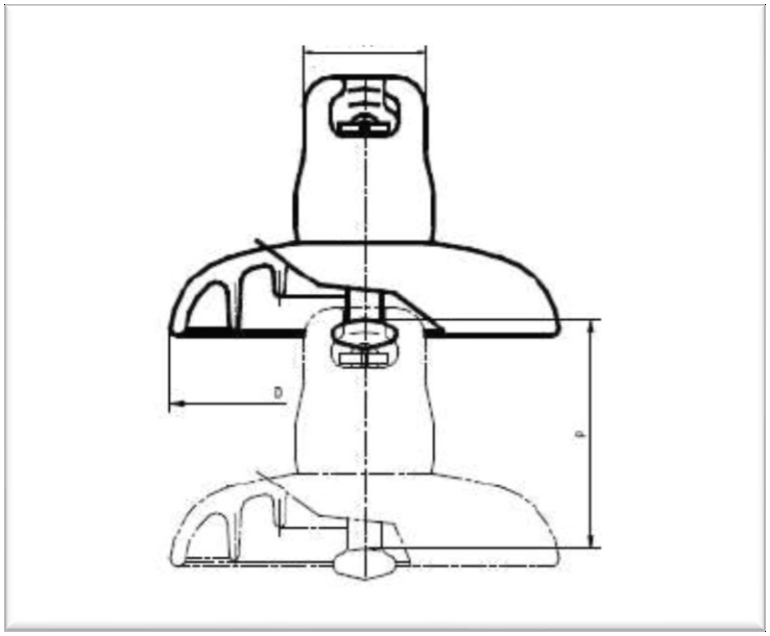

Figure 4-7: Insulator Ball and socket arrangement

4.3 Modelling of the overhead conductors

The steel overhead ground wire CDG16D is modelled in this study. The ACSR (Aluminium Conductor Steel Reinforced) trade name BER-A4 was modelled as the conductor. The cable properties are listed below (See Tables 4-3 & 4-4), as provided by Hydro-Québec.

Table 4-3: Overhead lines Conductor Characteristics

Conductor Characteristic	Value
Type	BER-A4
Area of Aluminum	60.60 mm^2
Area of Steel	686.50 mm^2
Total Cross-sectional Area	747.10 mm^2
Weight/length	23.21 N/m
Rated Tensile Strength	238.285 kN
Young's modulus	66489 MPa

Table 4-4: Overhead lines Ground Wire Characteristics

Ground Wire Characteristic	Value
Type of Conductor	CDG 16D
Area of Steel	153.84 mm^2
Weight/length	11.89 N/m
Rated Tensile Strength	209.904 kN
Young's modulus	172400 MPa

The geometry of the cables strung between two supports was calculated using the elastic catenary equation. Thus the sag calculated depends upon the span length, initial horizontal tension, the weight of the lines and their axial rigidity. The initial pre-tensioning of the lines depends on the span length. Tables 4-5 & 4-6 provided by Hydro Québec list the initial pre-tensioning and the associated maximum sag at the mid span.

The ground wire and conductors are modelled as linear elastic 2-node truss elements with tension only properties with a boundary condition of maximum allowable stress corresponding to their RTS. The span is divided into elements having a length of 10 m. The ground wire and conductors are specified an initial strain that corresponds to the initial axial pretension corresponding to bare line conditions, i.e., no wind or ice. The effect of meshing for overhead lines had been studied in detail by Lapointe (2003) wherein 30 elements for a 300m span were found efficient when compared with 80 elements for the same span. The following tables summarize the sag and tension values for various span lengths.

Table 4-5: Sag-Tension for BER-A4 conductor at 15°C (Initial conditions from HQ drawing No. 6474-60148-002-01)

Span (m)	Horizontal Tension (kN)	Sag (m)
200	22.85	5.08
250	23.55	7.71
300	24.03	10.89
350	24.36	14.62
400	24.54	18.97

Table 4-6: Sag-Tension for CDG 16D conductor at 0°C (Initial conditions from HQ drawing No. 6474-60148-001-01)

Span (m)	Horizontal Tension (kN)	Sag (m)
200	13.81	4.31
250	13.79	6.74
300	13.74	9.75
350	13.69	13.32
400	12.97	18.39

Does one expect an overhead line rupture due to the longitudinal imbalances caused by the transverse failure? This question cannot be answered at the onset, however, considering the available literature which has calculated the transient effects of conductor rupture, it was deemed convenient to not model the elements of the conductors for post-rupture analysis. To

reduce the computational requirements of a model demanding post rupture analysis for the supports and span, the axial forces in the conductors shall be monitored and checked for scenarios of rupture. The same assumption holds good for the insulators too.

4.4 Structural Damping

The governing equations of motion to be solved in dynamic analysis of any system in still air conditions depend on physical parameters such as mass (inertia), stiffness and internal damping. In this study, the effects of a transverse failure of a support on the adjacent spans and towers are being modeled while neglecting any possible aerodynamic effects due to wind – still air conditions are used. It would be highly conservative to not include the internal damping characteristics of the system in estimating the transient dynamic effects of such a failure.

The initial runs do not include any damping, however, it has been defined for the later runs as small amounts of structural damping contribute to filter out spurious high frequency components of the finite element model response due to discretization. Rayleigh damping was used, with the Rayleigh damping coefficients defined as in Equation 5.1 to provide a linear combination of effects due to mass and stiffness. The Rayleigh damping matrix is given by-

$$[C] = \alpha[M] + \beta[K] \quad \text{Equation 5.1}$$

Where,

α and β are the Rayleigh damping coefficients

[M] is the total system mass matrix here it is lumped

[K] is the initial total system stiffness matrix (corresponding to zero initial displacements).

The critical damping ratio ζ_i for mode '*i*' is given with respect to the Rayleigh damping co-efficients as-

$$\zeta_i = \frac{\alpha}{2\omega_i} + \frac{\beta\omega_i}{2} \quad \text{Equation 5.2}$$

In this study, the damping matrix is used under an implicit time integration scheme. The Rayleigh Damping matrix is diagonal and is set to update at every time step wherein the mass matrix changes in order to account for the loss of ruptured elements.

The Rayleigh damping coefficients were calculated using equation 5.2. Damping is taken as 1% for the tower and the conductors. The values of the Rayleigh coefficients are calculated using the frequencies of the three element groups obtained through the free vibration analysis. Using the consecutive frequencies about the same axis, the values for the mass and stiffness coefficients are calculated and input into the model. The values for alpha and beta for both the shield wire and the conductors are 0.010 and 0.030 respectively.

4.5 Modelling the effects of the transverse failure of a support

The main objective of the study is to calculate the unbalanced forces generated due to the transverse failure of a support. To understand the speed of progression of these loads, a six-span model is generated, where the end points of the end spans are assumed perfectly fixed. Figure 4-5 illustrates the model as displayed in the ADINA user interface: X is the transverse axis, Y is longitudinal and Z is vertical. The finite element model prepared includes all the properties listed and discussed in the preceding sections. The elements of the five suspension towers are defined into 46 different groups depending on their cross-sectional properties. Figure 4-8 depicts the complete model indicating the naming of the supports: TF for the failing support, T1 for the first support adjacent to TF and T2 follows after T1.

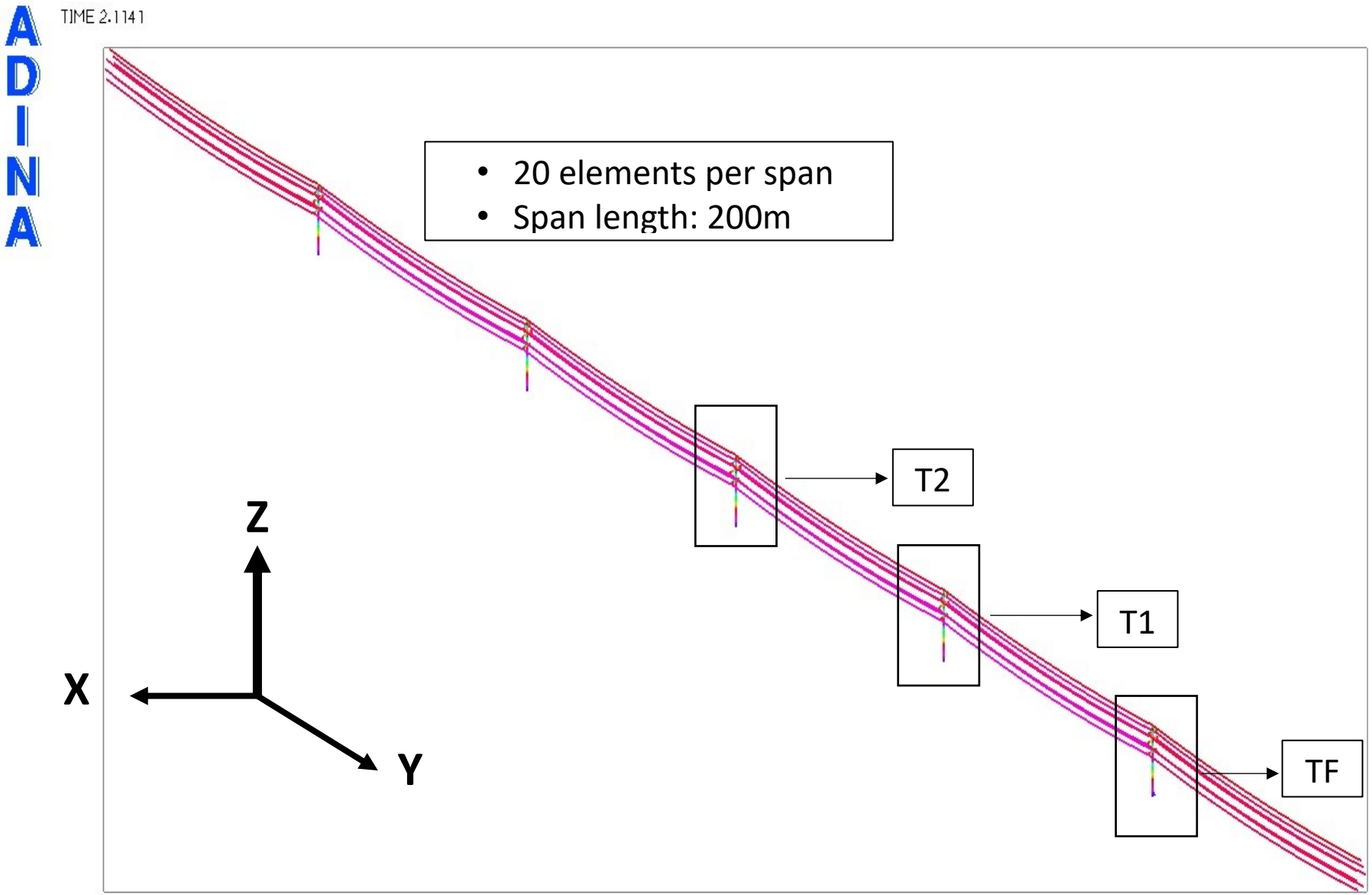

Figure 4-8: 6-span line section configuration

5. Free Vibration Analysis

The sudden failure of any element within a tower creates a shock wave which then propagates through the system. To comprehend the effects of such a failure, it is important to determine the range of the natural frequencies of vibration of the supports and the line conductors to explain the transient response calculated, keeping in mind, that the numerical simulation provides results with a considerable amount of high frequency noise that may require post-processing filtering.

5.1. Free vibration analysis of the tubular support

A modal (eigenvalue) analysis was carried out for the model of the support including the cross-arms without the insulators. The list of transverse and longitudinal frequencies obtained is given in Table 5-1. The support modes can be compared to that of a cantilever beam. However, in reality the tower is attached to the overhead ground wire on both sides of the apex, which provides a boundary condition that is flexible but not completely unrestrained in the longitudinal direction while being assumed free in the transverse direction. The combined effect of the conductors on the support is assessed next.

In the first instance, we shall compare the frequency modes of a cantilever support against those of a support fixed on both ends (base and apex). Next, the support attached to the ground wire on either ends shall be dealt with, such that a range of more realistic natural frequencies is defined for the longitudinal modes.

The frequency of the models discussed here are influenced by the support conditions as also the lumped masses representing the conductors and ground wires. A tower fixed at its base and free at the apex is obviously less stiff compared to the same tower with a fixed base and pinned apex.

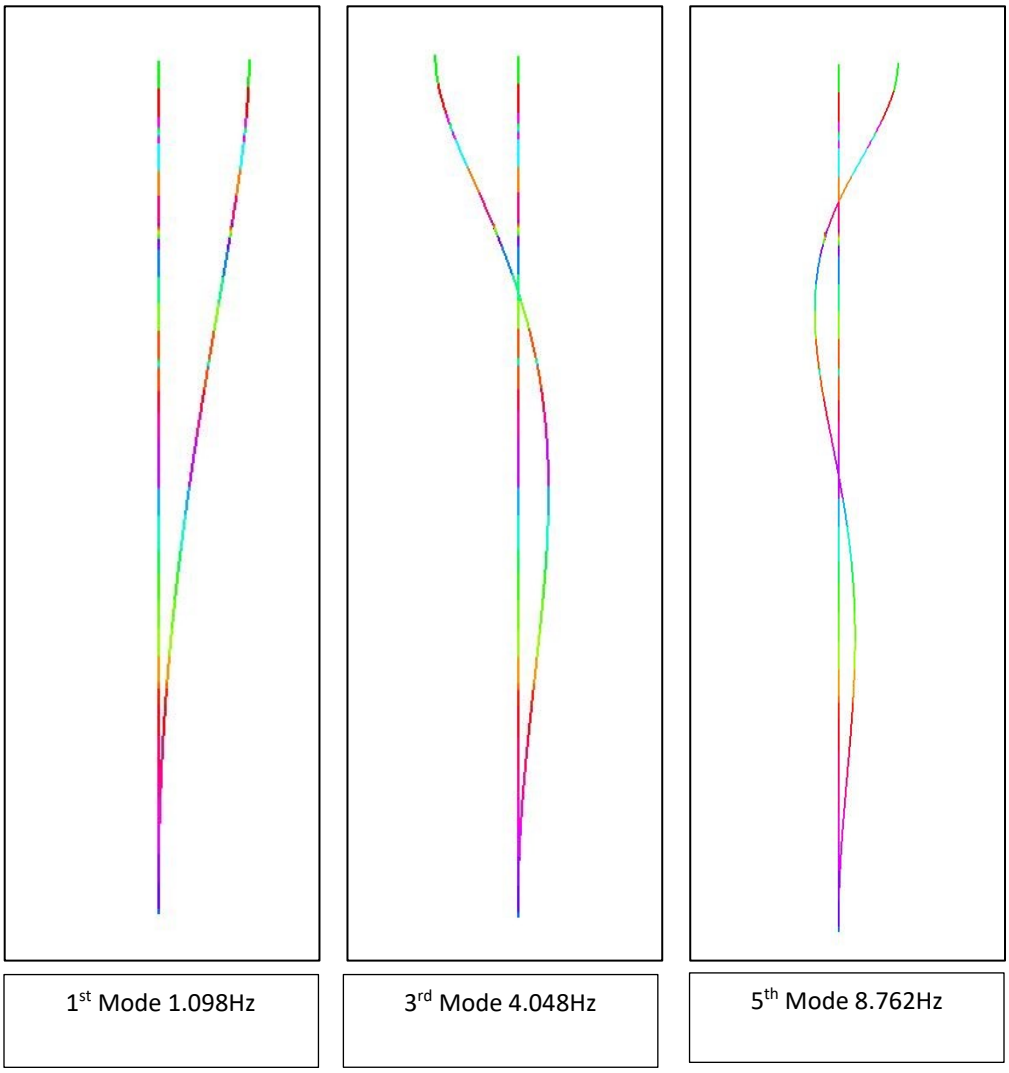

Figure 5-1: Lower frequency longitudinal modes of the tubular support with fixed base and free apex

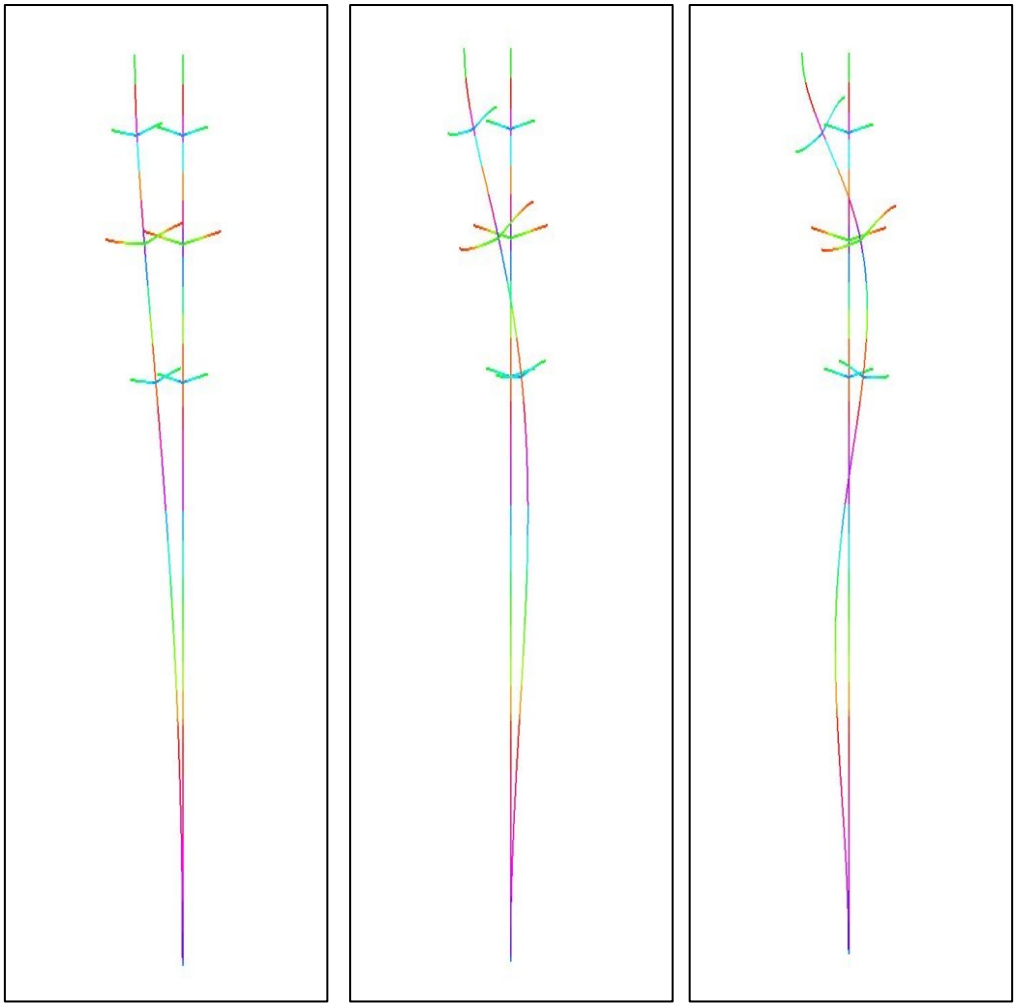

2nd Mode 1.114Hz	4th Mode 4.091Hz	6th Mode 8.772Hz

Figure 5-2: Lower frequency transverse modes of the tubular support with free apex and fixed base

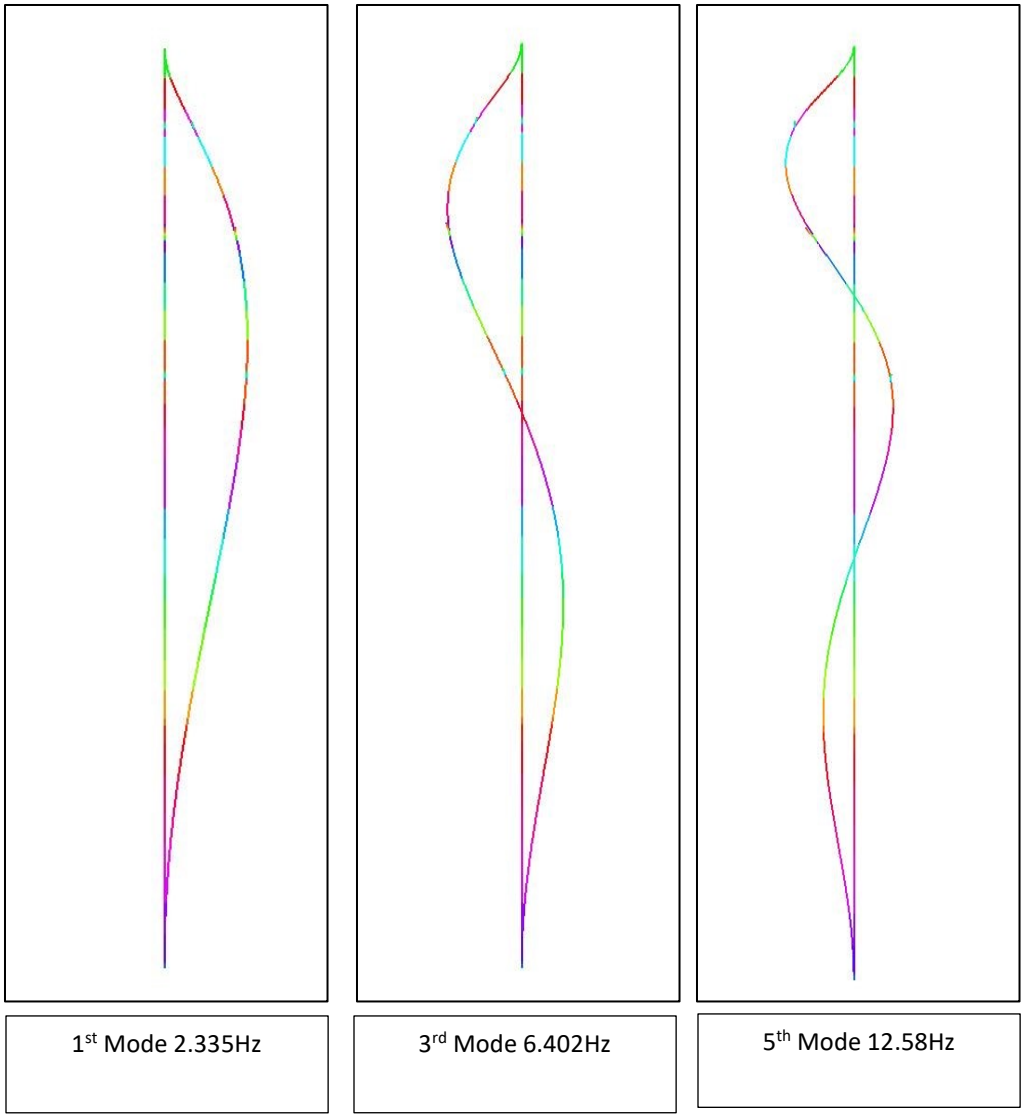

Figure 5-3: Lower frequency longitudinal modes of the tubular support with pinned apex and fixed base

Table 5-1: Comparison of the longitudinal modes for the two apex support conditions.

Comparison of the Modes		
	Cantilevered(Hz)	Pinned-Fixed (Hz)
1st	1.10	2.34
3rd	4.05	6.40
5th	8.76	12.6

5.2. Free vibration analysis of the tubular support attached to a shield wire

The above comparison between different apex support conditions outlines the effect of the stiffness on the calculated frequencies of the support for the longitudinal modes, assuming the apex of the support when attached to the ground wire can be simplified to behave like a pinned support in the longitudinal direction. However, the actual natural frequencies of the support will also depend on the mass and the stiffness attributed to the ground wire. A new model was created where the tower was attached to the ground wire span on each side, and the first longitudinal mode was observed at 1.30Hz. The first transverse mode was found at 1.12 Hz. These frequencies lie within the range determined in the previous section for the longitudinal modes and it is seen that the presence of the ground wire has practically no effect in the transverse direction. See Figure 5-4.

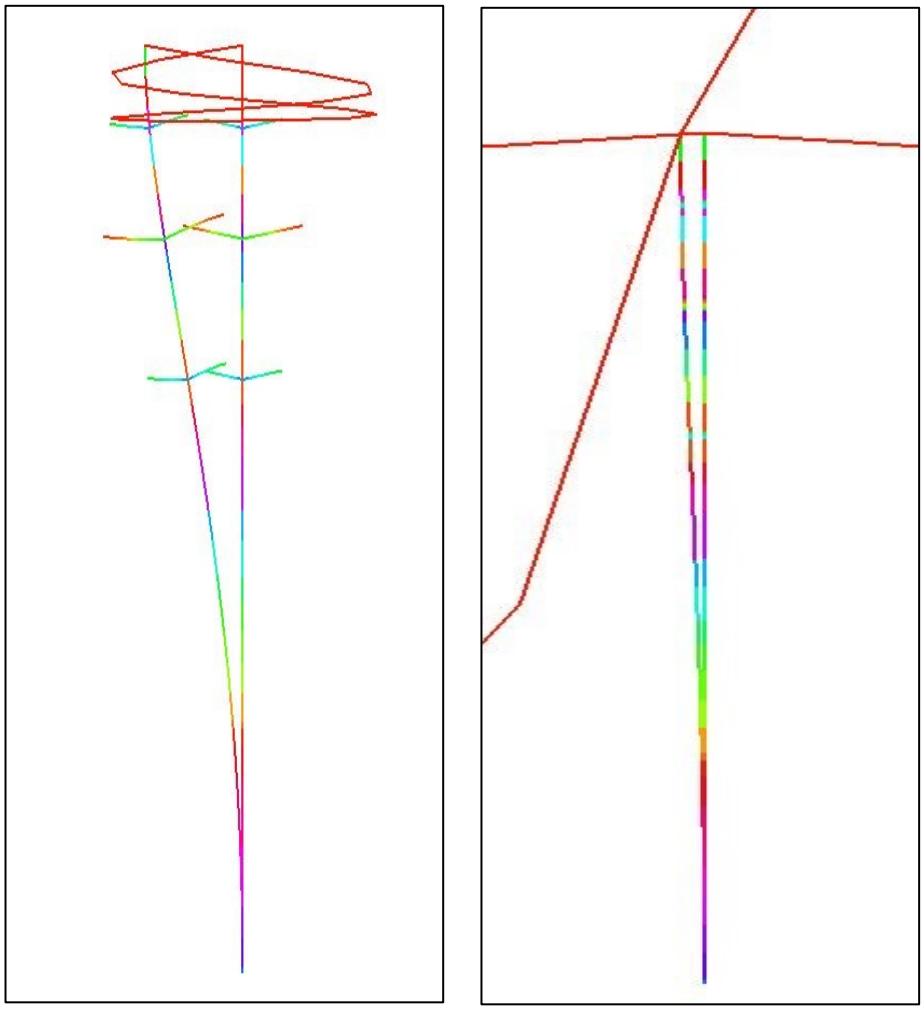

1st Transverse Mode at 1.12Hz	1st Longitudinal Mode at 1.30Hz

Figure 5-4: Fundamental modes of the tower attached to the shield wire.

The combined stiffness of the system with the addition of the components will reduce the natural frequencies if compared to the first 3 modes of vibration of the support alone. A frequency analysis of the complete line section (6 spans) was carried out including all the components and the lowest frequencies were found in the range of 0.03Hz to 0.25Hz. This information is important to interpret the results of the non-linear dynamic analysis of the failure. Numerical simulations tend to create high frequency disturbances while trying to account for the mechanical shock generated in the system due to failures. The real physical system will not vibrate at exceptionally high frequencies (above 50Hz) and it becomes important to identify the frequency range that is

physically significant to filter the spurious response using a low pass filter (discussed in Chapter 7 in detail)

6. Preliminary Simulations

This chapter charts the course of developments made through this study with respect to the modelling. The aim is to share the background of the research to facilitate fellow researchers to evaluate their paths for someone who decides to work on a similar objective. Preliminary runs had to be conducted to study the effect of selection of modelling options to reach approximation of the behavior of the numerical model.

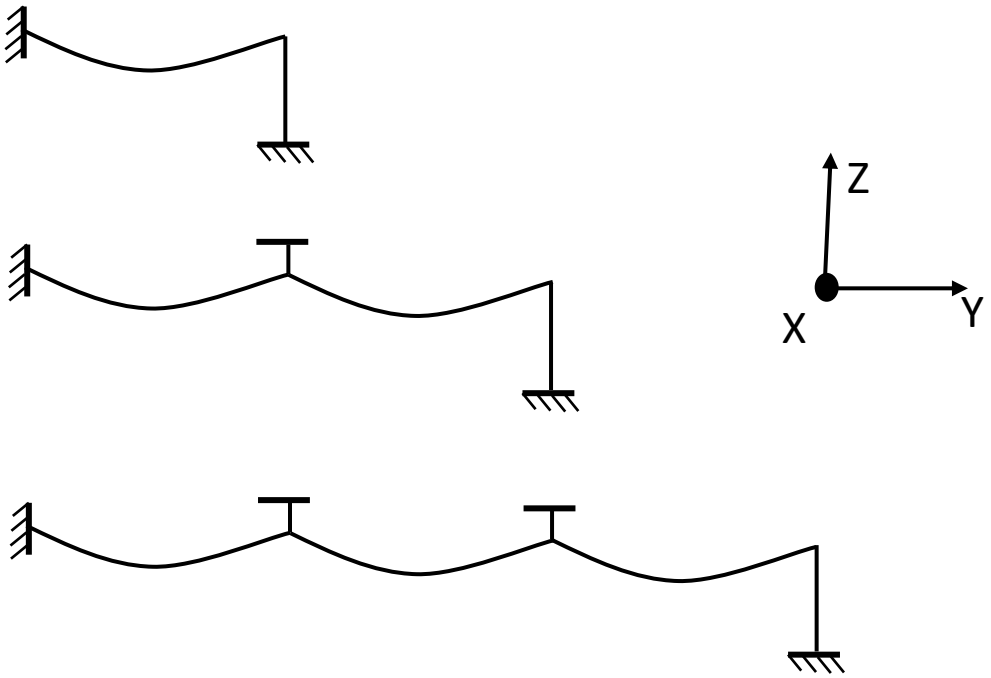

Figure 6-1: Illustration of the first models studied

Figure 6-1 illustrates the first set of runs conducted with the aim to quantify the difference between longitudinal and transverse failures. As the figure indicates, only one flexible tower was modelled using 2-node pipe elements (1m length each) with a hyper elastic material model. The tower was attached to one, two and 3 spans to understand the transmission of forces through the suspension strings, assuming the other supports were rigid. The right support was failed in 3 ways: applying a longitudinal displacement only, applying an angular displacement in the longitudinal plane, and applying an angular displacement in the transverse plane. These displacements were applied at the apex of the support.

Table 6-1: Comparison of longitudinal and transverse failures

Spans Configuration	Longitudinal Failure	Transverse Failure
1 span	Conductor rupture at displacement of 1.725m	Conductor rupture at displacement of 23.4m
2 span	Conductor rupture at displacement of 3.325m	Conductor rupture at displacement of 30.42m
3 span	Conductor rupture at displacement of 3.425m	Conductor rupture at displacement of 32m

Table 6-1 quantifies the difference in displacements needed between longitudinal and transverse failures to create a significant tension imbalance to cause a failure of the conductors. Other parameters such as insulator swing angles and also conductor tensions were monitored in these runs. These preliminary runs have helped understand the dominance of the available slack with additional spans on the overall response of a system to longitudinal and transverse displacements.

Moving on, the detail of the tower in the models was improved by then designing the complete support but the failing tower was modelled elastic so that it could be failed until it reached the ground by applying a controlled rotation at the base. A 6-span configuration was put together with a span length of 250m with the tower elements having a length of 1m. The runs were conducted by varying durations of the rotation application. The displacement applied was angular with a constant velocity. Duration of failure was checked between 3 s and 10 s.

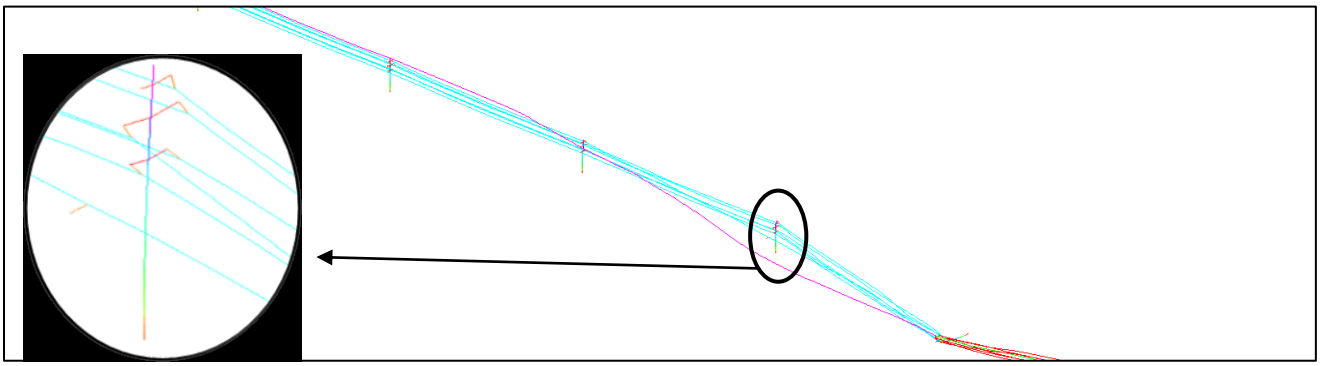

Figure 6-2: Failure of the support in 3 s

Figure 6-2 shows the final condition of the line section when the tower reaches the ground. The major outcome is the failure of the apex of two adjacent supports, while the ground wire is not ruptured (creation of super span). The figure above also indicates failure of the topmost cross-arm of the first adjacent support along the transverse direction, coupled with large swings of the insulators in the adjacent support. The increase in time duration of failure allowed for smooth absorption of imbalanced forces thus lowering the likelihood for a cascade. In this case, there were a few localized failures within the 1st adjacent support only.

Besides these, another mode of failure that was tried was applying a large distributed transverse load on all the phase conductors and ground wires only for the wind span around the support to be failed.

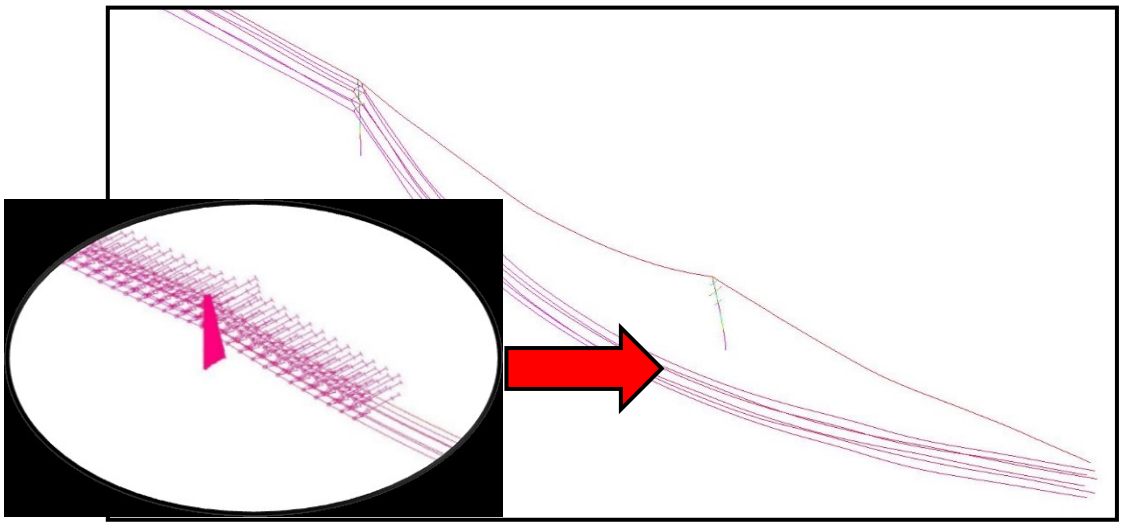

Figure 6-3: Failure of the tower under localized wind loads.

Figure 6-3 illustrates the simplified application of the transverse load wherein a uniformly distributed load (UDL) having an intensity of 10kN/m is applied on the support to be failed and also its associated wind span. This load is applied within a duration of 3 seconds. As is evident, the support sustains multiple failures at its cross-arms. But the first two adjacent supports suffer yielding at their apex only. These failures can be attributed to the applied transverse force much more than the transverse failure of a support.

Another important simulation to be discussed also assumes the failing support being elastic. However, this model was detailed as the meshing of the elements was limited to 0.1m for the tower. All the supports were considered elastic. The overhead conductors were not modelled for post-rupture analysis. A transverse rotation is applied at the junction of the bottom cross-arm in 0.5 seconds.

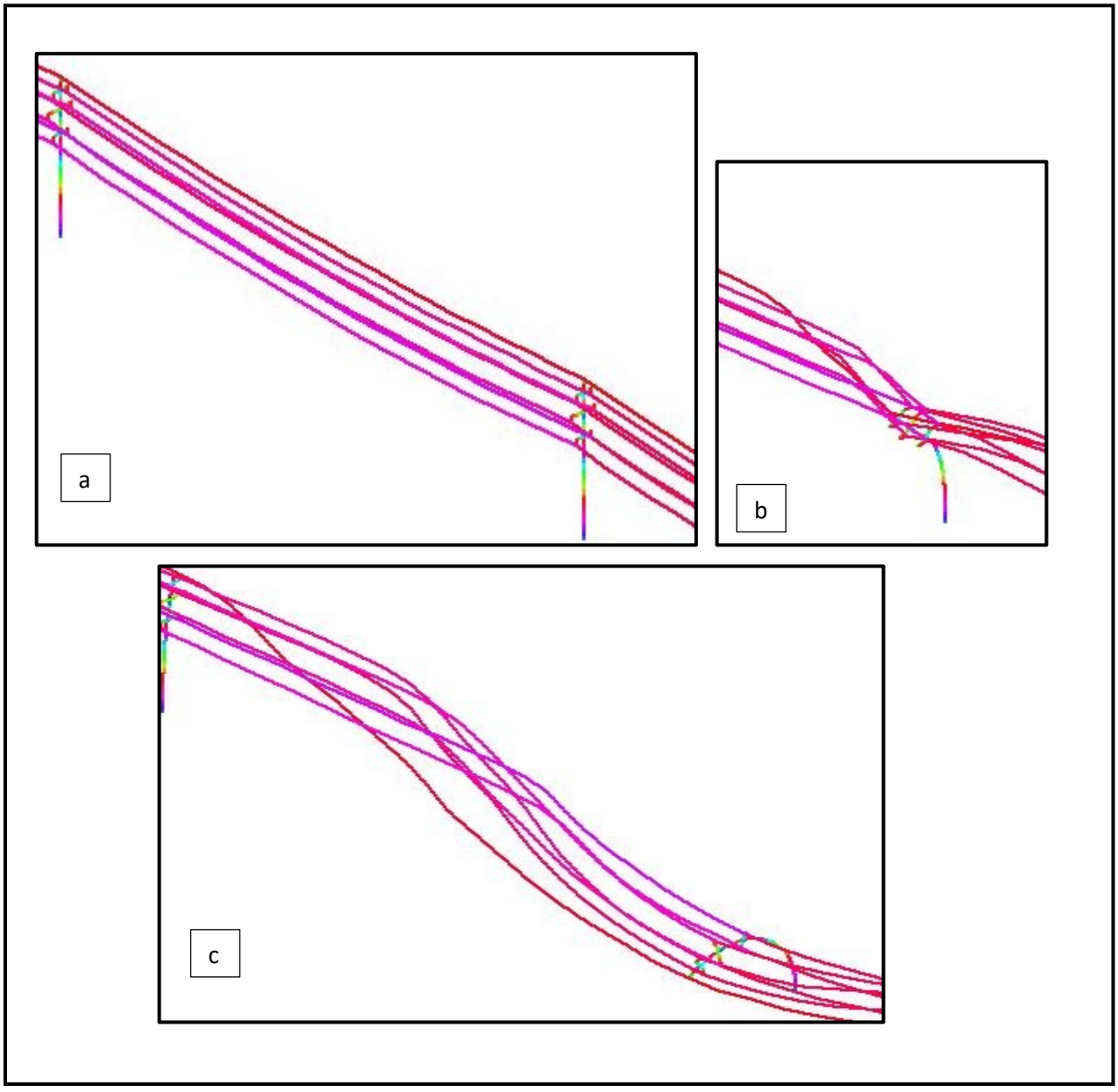

Figure 6-4: Rotation applied at the bottom cross-arm junction of an elastic tower

The figure 6-4 depicts the stages of displacement in the failing support under the influence of the applied rotation. The initial condition is depicted by stage ‘a’, an intermediate by stage ‘b’ and the final by stage ‘c’. The elastic material model allows for the tower to completely fall to the ground, this being the worst scenario would lead to large longitudinal imbalances in the line section. As expected, we do see that the overhead ground wire ruptures with the onset of the rotation at 2.30 seconds which is 0.3 seconds into the application of the rotational displacement. The rupture of a line will lead to dynamic excitations within the system and translate to a cascade. This simulation over-estimates the strength of the section as under normal conditions the support will suffer bending and axial stresses thus failing at certain sections. The tubular mast of the support will suffer compressive and tensile stresses along the periphery of the section leading to a collapse of the plastified region.

The above discussed simulations illustrate the effect of modelling assumptions on the analysis of the transverse failure. As the failing support is modelled as elastic, it accelerates the increase in effective span length, thus we see a cascade of apexes or rupture of cables depending upon the duration of failure. On the other hand, these failures lead to the creation of super spans which prevented the rupture of the cables. Another important conclusion can be the effect of time duration of failure, the slower the failure, the easier is the absorption of the longitudinal imbalance. The overall response was quasi-static but the same has to be validated in case of impulse loads causing failures. In view of these observations, it was considered essential to model the failing support to depict non-linear behavior. The time duration of failure was sort to be reduced to check for dynamic effects and model the shortest span supported by these supports as they are most prone to failures. Besides, the mode of failure to be adopted was a subject open for multiple opinions from the fellow researchers at Hydro Québec and Université de Sherbrooke. By including a realistic failing tower, it was understood that this tower would suffer several failures within itself while it is brought down to the ground. These failures would serve as temporary stop to the increasing effective length of the span although there would be dynamic excitation in the system. To check for the influence of the mode of failure on the response of the line, it was decided to apply rotational displacement at certain joints of the failing support.

7. Results

In this section we present the simulation plan and results to observe the effects of various transverse failures of the support on the adjacent spans and supports. The question which shall be addressed is “Can a transverse support failure lead to a cascade?” Transverse failures are generally attributed to high intensity wind events such as cyclones, tornadoes, downbursts and hurricanes. After the storm, inspection of the site will determine whether there was conductor or insulating string rupture or essentially collapse of the support while the conductor system remained intact or at least not severed. In this study we do not model the evolution of the damage in the failed support, but rather we postulate some failure modes with different parameters and we study their effects on the rest of the line components to determine whether a cascading failure will occur.

The different failure load scenarios that were successfully modelled and reported next are as follows:

- Localized tower failure in the apex region;

- Transverse failure at the mid cross-arm level;

- Transverse failure at the bottom cross-arm junction with the pole;

- Transverse failure at the base of the support;

The elements whose results are discussed next follow a naming pattern as described below in Figure 7-1. For the overhead conductors, tensile forces in the end span elements are reported. The first span is the one attached to the failing support followed by the rest. The failing tower (or sacrificed support) is referred to as TF, T1 its first adjacent support. The naming of the overhead conductors is uniform depending on their type and location: CS stands for Conducting spans and OGW for the Overhead Ground wire. Depending on the span it belongs to as also the direction of the X axis it lies on, the conducting spans for the 1st spans attached to the failing support are termed as follows.

- CS+XT1 for the end span element attached at the topmost cross-arm of the first support along +X direction
- CS-XT1 for the end span element attached at the topmost cross-arm of the first support along the -X direction.
- CS+XM1 for the end span element attached at the middle cross-arm of the first support along the +X direction.
- CS-XM1 for the end span element attached at the middle cross-arm of the first support along the -X direction.
- CS+XB1 for the end span element attached at the bottom cross-arm of the first support along the +X direction.
- CS-XB1 for the end span element attached at the bottom cross-arm of the first support along the -X direction.

For the 2nd span from the failing support, the naming convention shall remain the same eg., CS+XB2, CS-XB2 and so on.

The naming of the elements of the supports is depicted in Figure 7-2. It follows the same pattern as the conductors except that the Prefix for the cross-arms is CR

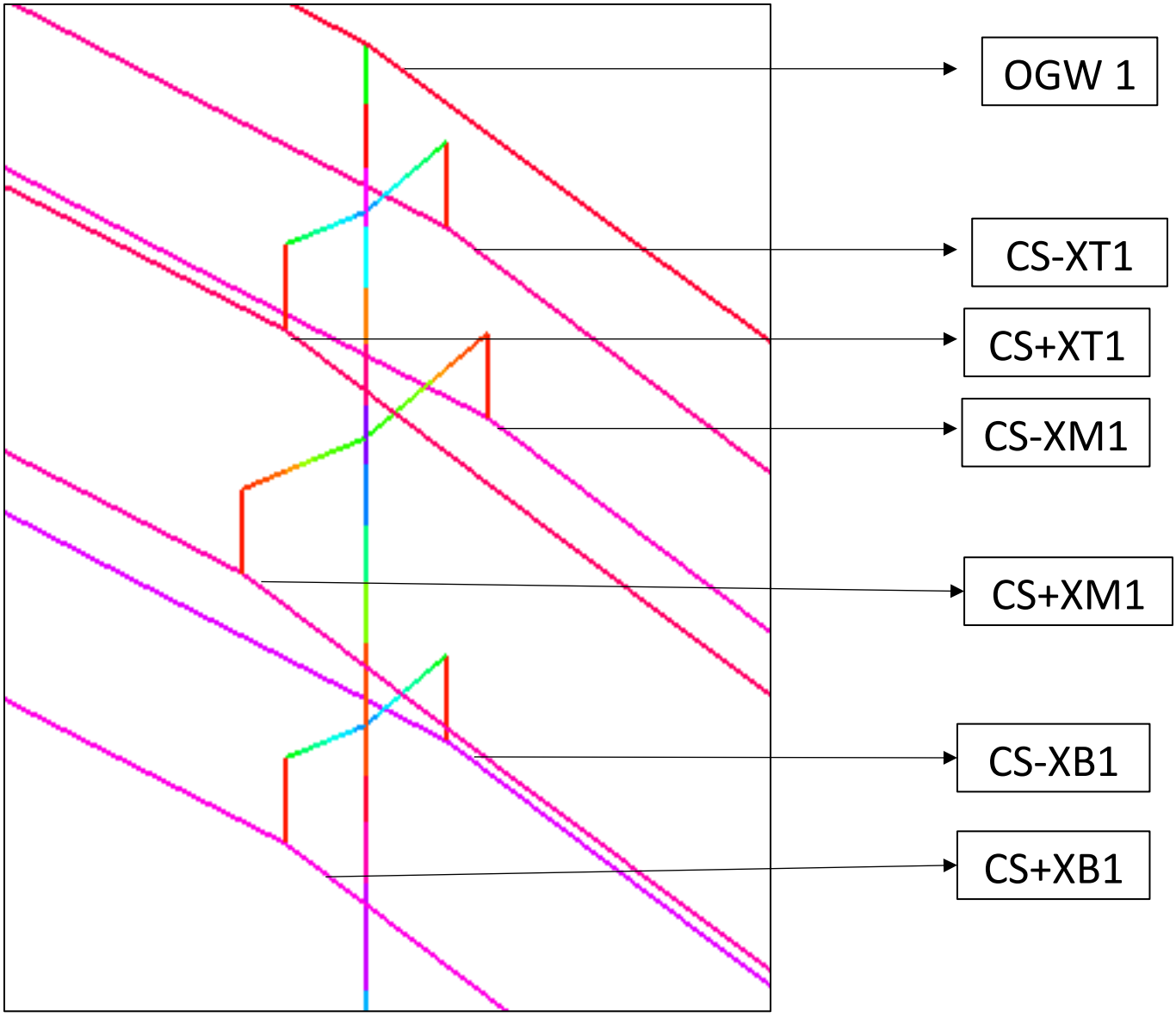

Figure 7-1*:* Naming of end span elements of Tower 1

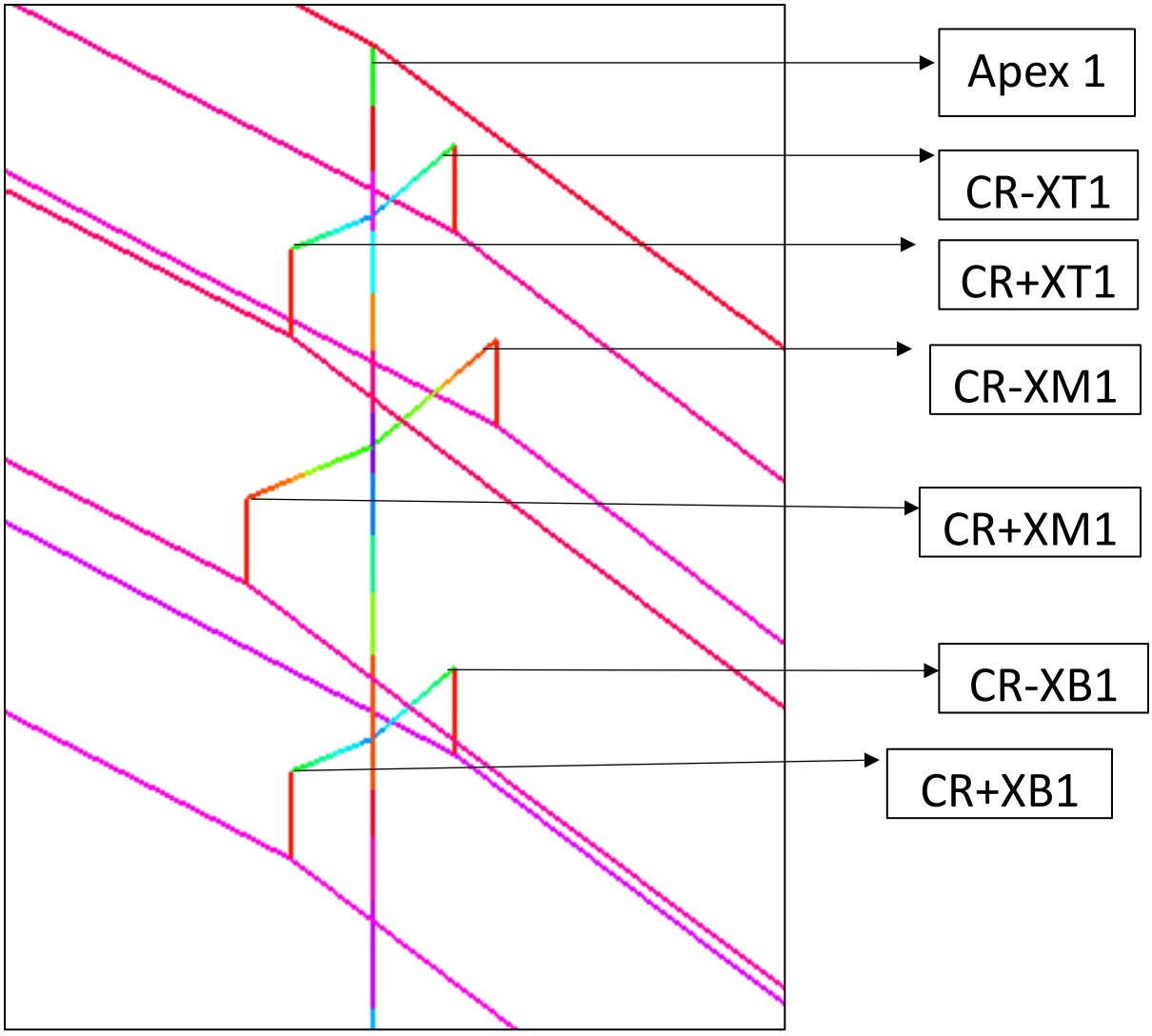

Figure 7-2: Naming of cross-arm elements of Tower 1

7.1 Simulations of transverse failure on actual support

7.1.1 Transverse failure of a support at its apex region

For this first localized damage scenario, the node connecting the top cross-arms to the tower is subjected to a prescribed rotational monotonic applied displacement within a time span 0.5 seconds, which is approximately half of the support's fundamental period.

The entire simulation is divided into two time zones depending on the analysis type and forces to be accounted for. From t = 0 to 2 s, a static analysis is conducted under self-weight of the model and initial tensions in the conductors to obtain a proper initial static equilibrium state for the system. The time step or the loading interval for this analysis is 0.1 s (20 increments in total)

to allow for convergence at the integration points of the beam elements. The failure simulation imposing the rotational displacement restarts at t = 2 s and the nonlinear dynamic analysis continues for 5 seconds post rotation application. The time step used is 0.0001s (or 0.1 ms) for the iterations.

Imposing this increasing rotational displacement at the joint connecting the topmost cross arms leads to failure within the apex zone of the tower as the bending stresses combined with the axial compression exceed the post-elastic capacity of the pole section. The rupture of the most solicited pole element is followed by the detachment and free fall of the severed section of the apex with the attached ground wire.

Tension waves are propagating in the conductors by the sudden onset of the transverse displacement and the support element failures. A Fourier transform analysis of the time histories of ground wire tension in the failure region provides an assessment of the spectrum of the tension waves generated. Examples are shown in Figure 7-3 for ground wire sections OGW 1 and OGW 2.

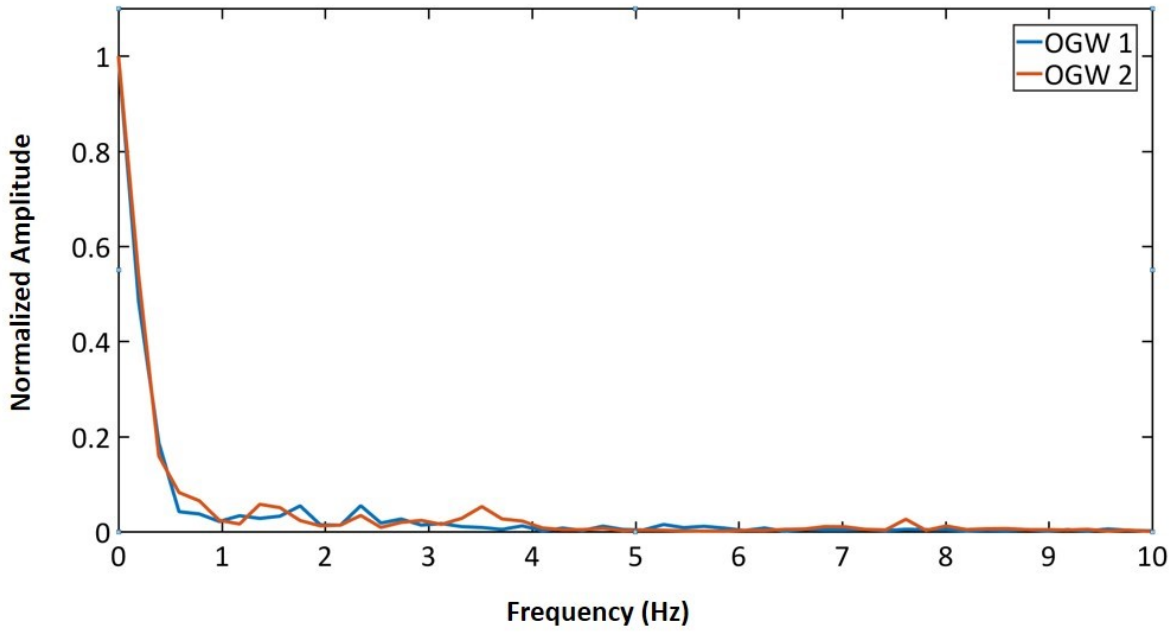

Figure 7-3: Fourier Frequency Analysis of the Tension Ground wire (Case1.1)

OGW 1 is attached to the first support directly adjacent to the failed tower while OGW 2 is attached to the 2nd tower peak. It is seen that the transverse failure simulated generates very low frequency waves, within the 0-5Hz band for OGW 1 and up to 8 Hz for OGW 2. Figure 7-3 shows the filtered time histories of the cable tensions during the failure for the two OGW positions monitored.

It is seen that the OGW tension increases with the onset of the failure and the peak values are obtained about 2 s after the imposed failure in the sacrificed support (See Figure 7-4). The peak tension obtained in the simulation is 86.8 kN at OGW 1 and drops to 41.9 kN in the successive span at position OGW 2. The corresponding longitudinal displacement of the tower apex at position OGW 1 is 80 cm and 30 cm at the next support (see Figure 7-5). The transverse displacements of the adjacent supports can be considered insignificant compared to their longitudinal counterparts.

The effect of the support failure is also seen in the time histories of the resulting cross arm loads induced by conductor tensions (see Figure 7-6) in the longitudinal (Y) direction.

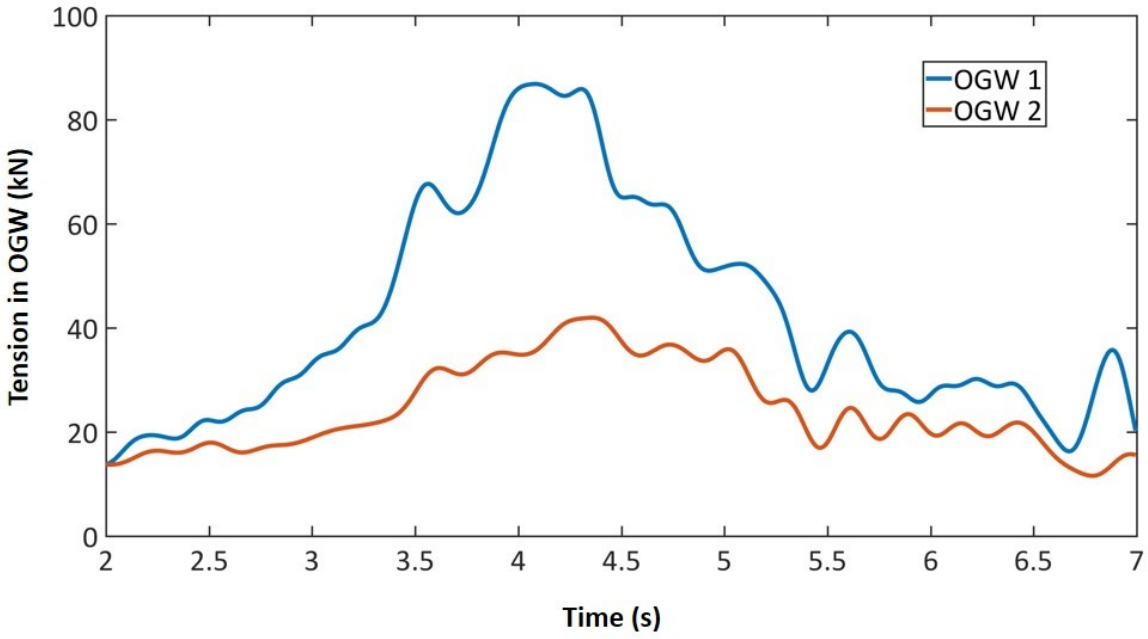

Figure 7-4: Ground wire tensions in end span elements of spans 1 and 2 (Case 1.1)

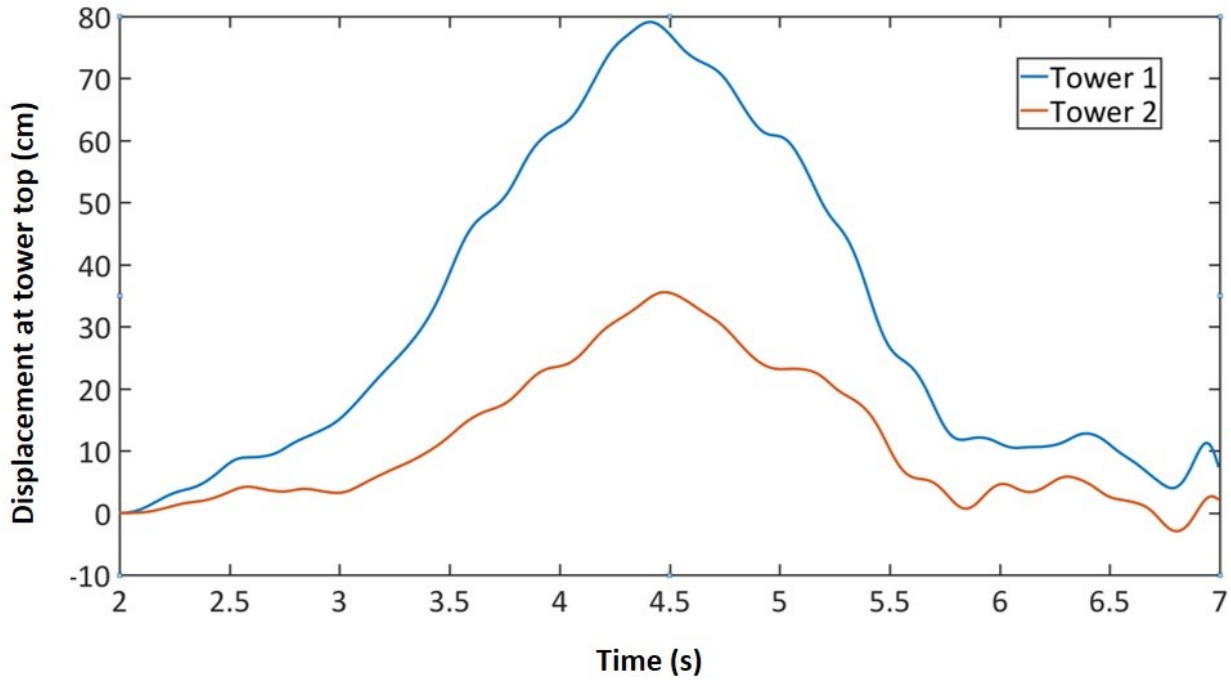

Figure 7-5: Longitudinal displacements of adjacent support apexes (Case 1.1)

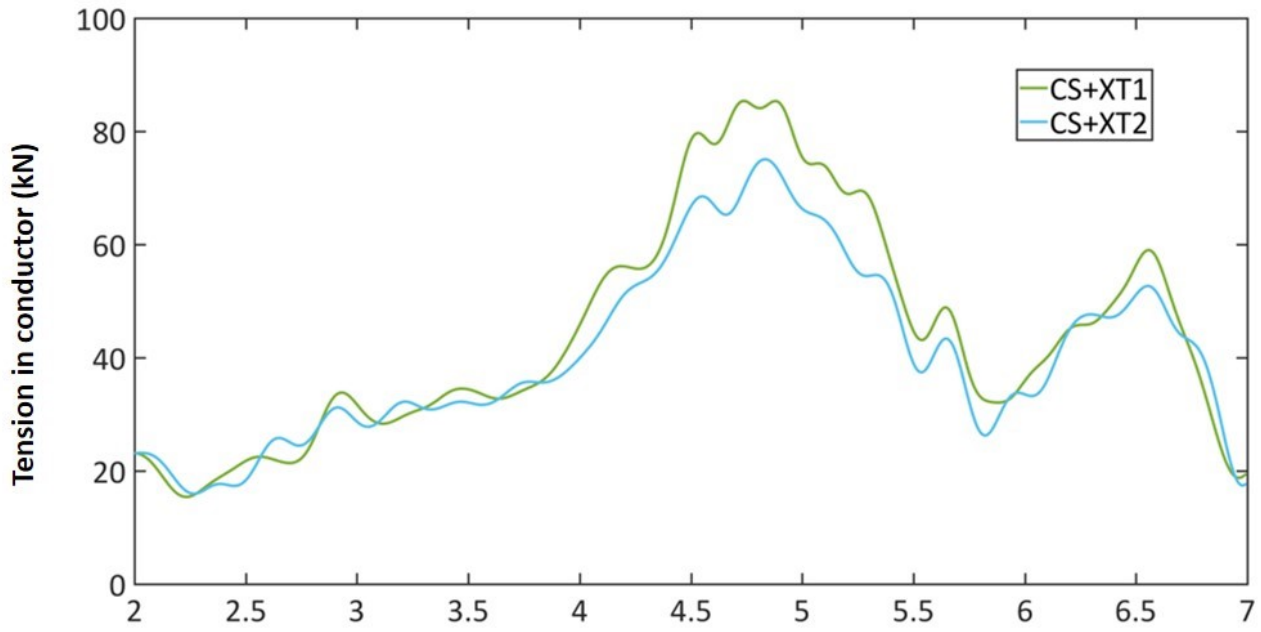

Figure 7-6: Conductor tensions at Tower 1 and 2 along +X direction (Case1.1)

CS +XT1 is the end span conductor element attached to Tower 1 directly adjacent to the failed support and CS+XT2 is the end span element of the next span. The peak axial tension in the first

span element is 85.3kN and it reduces to 75.0kN in the consecutive span. The swing of the insulator strings governs the loads that are transferred to the tower cross arms. In the initial phase of the failure, the insulator swings in the opposite direction of the failure trigger point thus creating a small relaxation in the tension. But as the failure progresses and the tower top and the cross arms fail, the insulator strings swing towards the failed support and the tension loads transferred to the consecutive supports increase. The peak forces occur when the insulator strings reach their maximum amplitude (and swing angle). Thereon, due to their inherent flexibility, the conductors, insulators and supports will continue to vibrate with lesser amplitude and reach a new equilibrium position corresponding to the super span of 400 m. Further analysis in time would show an attenuation of the tension in the lines as the vibrations will attenuate and the residual static steady-state would be reached. Such analysis was not done here as the main interest is the peak loads transferred to the adjacent supports. An important aspect to bear in mind is the pointed difference in the tensions observed in the spans on either sides of the failed support. As the failure is simulated along the positive X direction (previous results reported in +X), the conductor tension in the intact span on the opposite direction will be higher due to the pronounced displacement: in this case, the peak tension in CS-XT1 is 114.0 kN and that of the following span is 88.6 kN (See Figure 7-7).

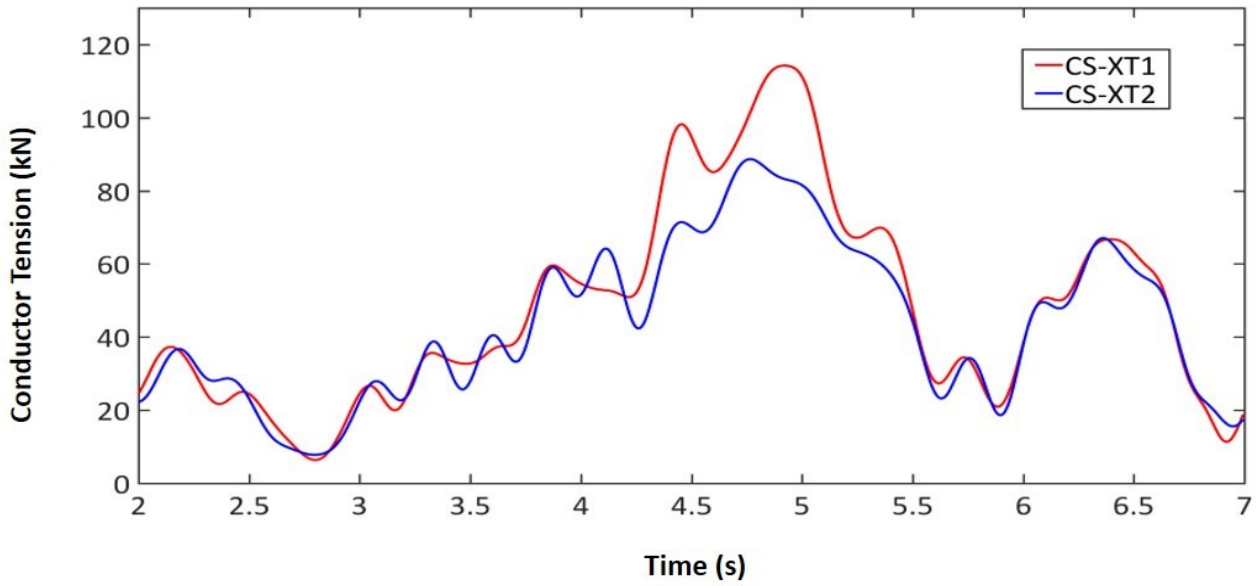

Figure 7-7: Conducting span tensions in end span elements along the –X axis of spans 1 and 2 (Case1.1)

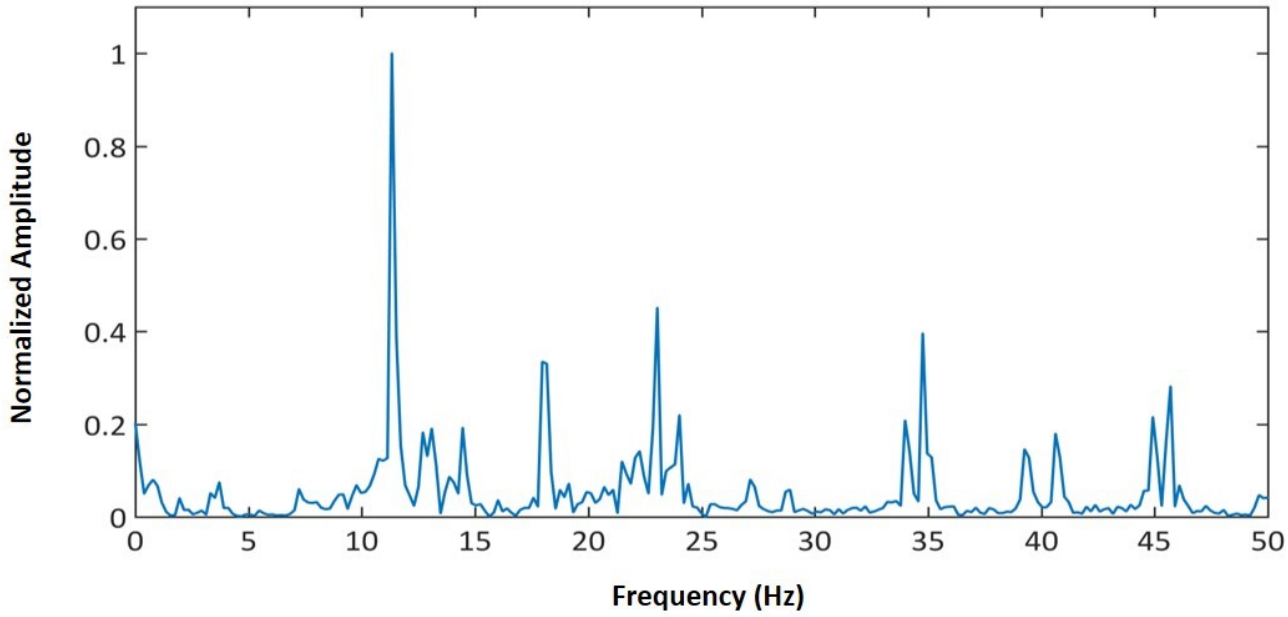

Figure 7-8: Fourier Frequency Analysis of the Tension in CS+XM1 (Case1.1)

The spans within the zone of failure ought to be affected whereas the remaining spans attached to the lower cross-arms show a marginal rise in tension from the initial 22.8 kN to a maximum value of 23.5 kN. An important aspect of the intact span response outside of the failure zone is

the high frequency vibrations calculated by the model. These are spurious high frequencies (especially in the zone exceeding 20Hz – see Figure 7-8) following the shock failure that excites all the discretized elements of the model, with no physical significance in the physical line section. These results are therefore filtered from the calculated results using a low pass filter of 0-10 Hz.

The effect of the localized failure on the adjacent supports can be quantified through the resultant forces (longitudinal & transverse) observed at all the connection points (tips of cross arms and ground wire peaks) of the support with the conductors. The peak values of these forces are listed in Table 7-1 and 7-2.

Table 7-1*:* Forces at the points of connections of Towers 1 & 2 (Case1.1)

Point of Connection	Longitudinal Forces	Use Factor	MF
Apex 1	50.7	0.24	3.7
Apex 2	21.6	0.10	1.6
CR +XT1	21.6	0.09	0.9
CR +XT2	13.3	0.06	0.6
CR +XM1	10.0	0.04	0.4
CR +XM2	8.7	0.04	0.4
CR +XB1	9.6	0.04	0.4
CR +XB2	10.0	0.04	0.4
CR -XT1	30.0	0.13	1.3
CR -XT2	17.6	0.07	0.8
CR -XM1	8.4	0.04	0.4
CR -XM2	8.0	0.03	0.4
CR -XB1	9.3	0.04	0.4
CR -XB2	8.7	0.04	0.38

The use factor represents the ratio of the maximum force to the rated tensile strength (RTS) of the attached cable. It is for instance, the RTS for the OGW is 209 kN and this value is used in the calculated ratio at the apex. The last column lists the ratio between the forces and initial

horizontal tension (13.8kN for OGW and 22.8kN for the conductors) of the lines. This is termed as MF or Multiplication Factor.

Table 7-2: Transverse forces at the points of connections of Tower 1 & 2. Case 1.1

Point of Connection	Transverse Forces	Use Factor	MF
Apex 1	9.3	0.04	0.7
Apex 2	3.3	0.02	0.2
CR +XT1	5.5	0.02	0.2
CR +XT2	5.4	0.02	0.2
CR +XM1	2.9	0.01	0.1
CR +XM2	2.7	0.01	0.1
CR +XB1	9.5	0.04	0.4
CR +XB2	6.8	0.03	0.3
CR -XT1	8.3	0.04	0.4
CR -XT2	6.8	0.03	0.3
CR -XM1	3.3	0.01	0.1
CR -XM2	3.3	0.01	0.1
CR -XB1	8.9	0.04	0.4
CR -XB2	5.8	0.03	0.3

The Table 7-2 lists the transverse forces along the various points of connection of the adjacent supports. It is seen that the transverse imbalance is less critical compared to the longitudinal. (See Figure 7-9) The forces on the adjacent supports are transmitted through the lines which have a predominantly longitudinal movement as the effective span length increases due to the localized failure.

The total tensile forces in the insulator strings of the adjacent supports are listed in Table 7-3. The maximum tensile strength of the insulator is 220 kN and this is the value used to calculate the use factor.

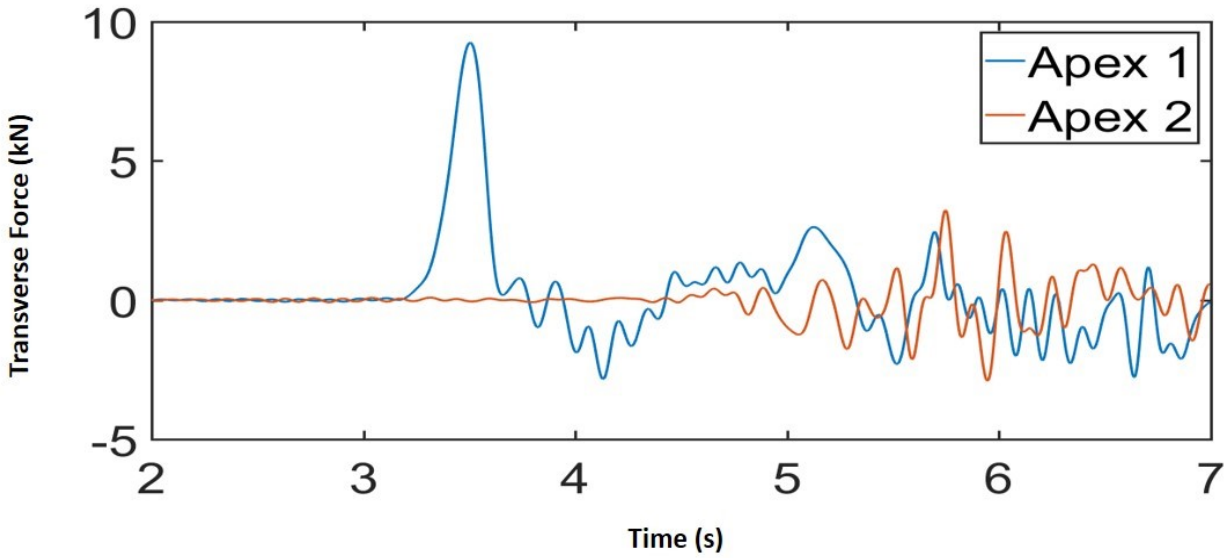

Figure 7-9: Transverse Forces at the Apex of Towers 1 & 2 against Time. (Case 1.1)

Table 7-3: Axial forces in the insulator strings at Towers 1 & 2. (Case 1.1)

Insulators	Forces (kN)	Use Factor	MF
INS +XT1	25.48	0.12	1.1
INS +XT2	12.13	0.06	0.5
INS +XM1	11.16	0.05	0.5
INS +XM2	8.66	0.04	0.4
INS +XB1	12.14	0.06	0.5
INS +XB2	9.96	0.05	0.4
INS -XT1	34.82	0.16	1.5
INS -XT2	19.06	0.09	0.8
INS -XM1	9.82	0.04	0.4
INS -XM2	8.31	0.04	0.4
INS -XB1	8.88	0.04	0.4
INS -XB2	7.96	0.04	0.4

7.1.2 Transverse failure at the mid cross arm level

In this failure scenario, the failure is assumed to occur in the steel pole at the level of the mid cross arms of 4.6 m length, and similar results as presented for the first scenario are presented for comparison and discussion here. In this run, the node joining the two middle cross-arms has been subjected to a rotational displacement within a time-span of 0.5 s. Firstly, the time histories of tension in the ground wire (Figure 7-10) and the longitudinal displacement of the tower apexes (Figure 7-11) are presented next.

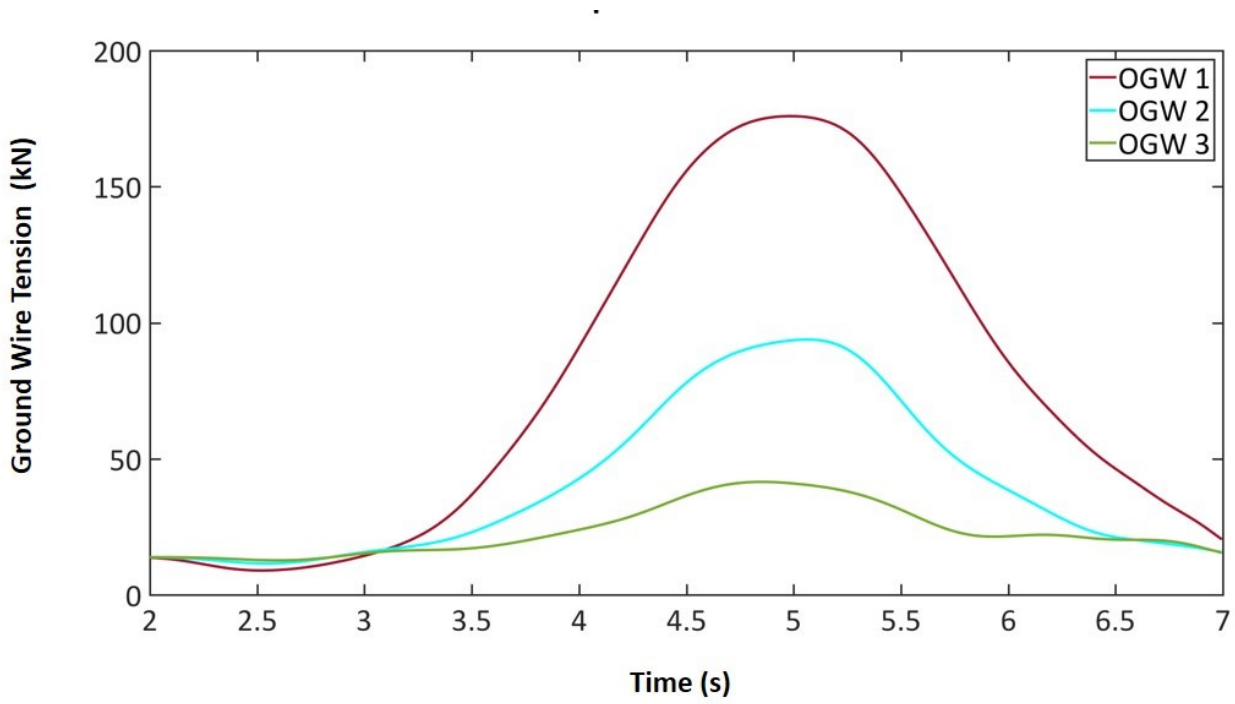

Figure 7-10: Ground wire tensions in end span elements of spans 1, 2 and 3. (Case 1.2)

Compared to the prior case study, the peak tension in this case is significantly higher for OGW1 at 175.9 kN which is 0.84 RTS. The succeeding span shows a peak tension of 93.8 kN, which corresponds to 0.45 RTS.

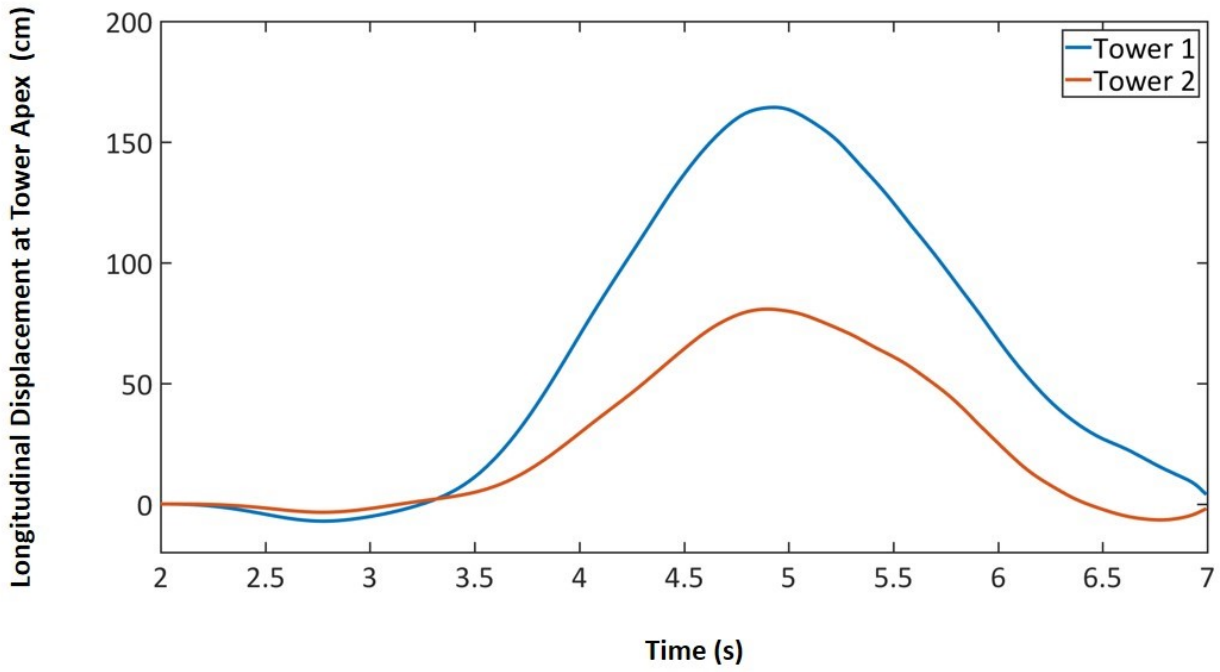

Figure 7-11: Longitudinal displacement of adjacent support apex 1 & 2 (Case 1.2)

The change in location of the failure within the support (lowering failure point from 4.7m below the apex to 11m from the apex) has almost doubled the effect on the parameters governing the tension in the shield wire. The maximum longitudinal displacement of the tower apex is quite significant at 164.3 cm. As the cross-sectional area of the support increases towards its base, it takes longer for the mast cross section to completely fail and larger displacements are imposed in the line section to accommodate the prescribed rotational motion. As a result of these larger displacements, the adjacent supports are affected to a larger extent than in the first failure location scenario.

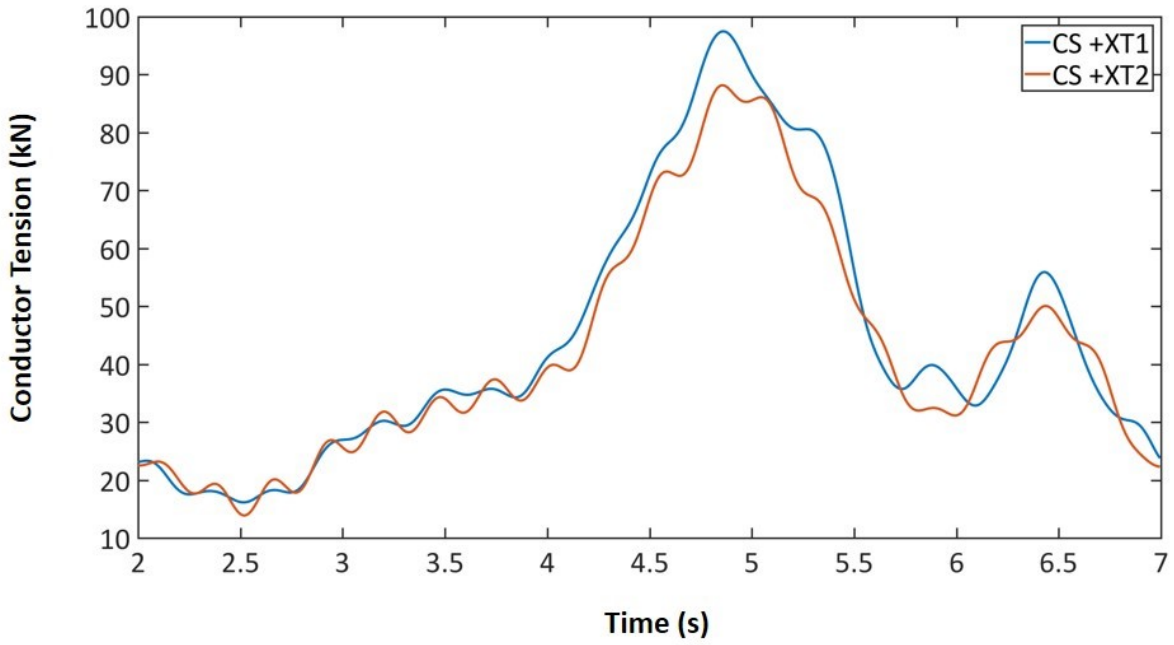

Figure 7-12: Conductor tensions in top end span elements of spans 1 and 2. (Case 1.2)

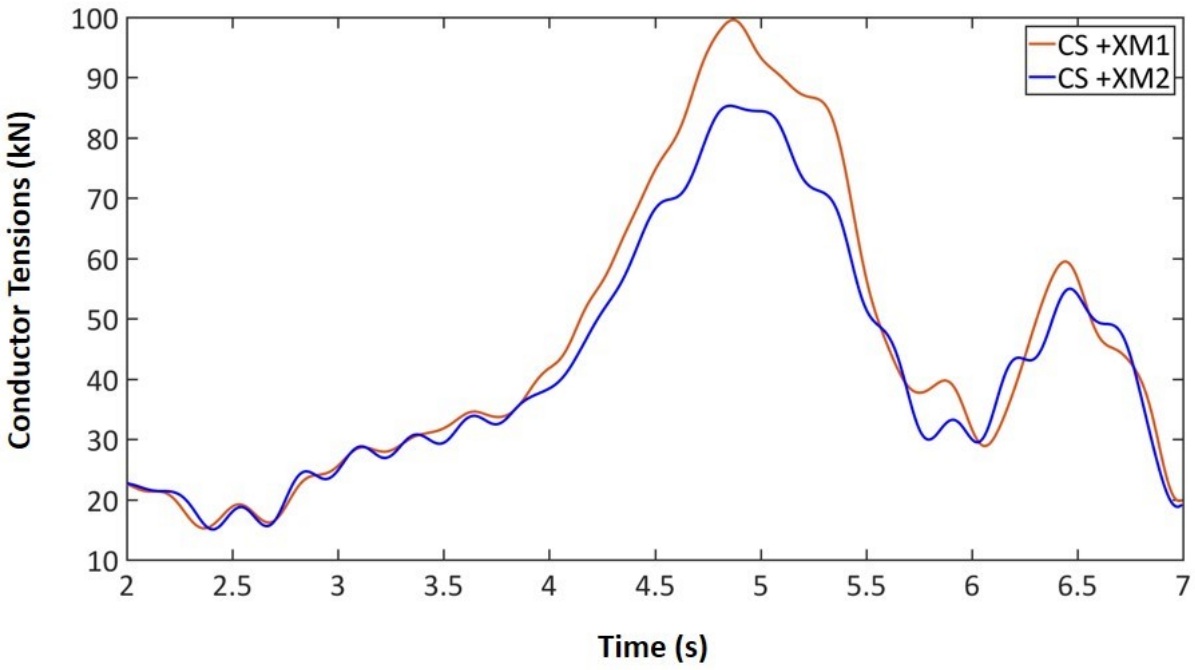

Figure 7-13: Conductor tensions in mid end span elements of spans 1 and 2. (Case 1.2)

It is seen that the time taken for the tension in the spans to reach its peak value is 2 s as the pole ultimate capacity is larger in the lower section (See Figures 7-12 & 7-13). Each pipe-beam element being defined by 2 nodes, when the element whose node connects the two longer cross-arms is rotated, it fails when any of its integration points reaches the rupture criterion. The portion of the support that lies between the ground wire and the junction of the middle cross-arms is severed from the support due to the pipe-beam element death. Post rupture, the top tower section detaches and falls under its weight (a limitation of the analysis discussed in detail in Chapters 4 & 8) while the super span created also continues its downward motion. The maximum tension in the previous graphs coincides with the maximum sag of the new span created. Following the similar convention established for previous scenarios, the peak response values are summarized in the following tables.

Table 7-4: Conductor tension in the spans adjacent to of Towers 1 & 2. (Case 1.2)

Conductor	Tension (kN)	Use factor	MF
CS +XT1	98.0	0.41	4.3
CS +XT2	88.2	0.37	3.9
CS +XM1	100.0	0.42	4.4
CS +XM2	85.3	0.36	3.7
CS +XB1	23.5	0.10	1.0
CS +XB2	24.1	0.10	1.1
CS -XT1	102.4	0.43	4.5
CS -XT2	93.0	0.39	4.1
CS -XM1	109.0	0.46	4.8
CS -XM2	94.0	0.39	4.1
CS -XB1	24.2	0.10	1.0
CS -XB2	25.7	0.11	1.1

Table 7-5: Axial forces in the insulators of Towers 1 & 2. (Case 1.2)

Insulator	Tension (kN)	Use factor	MF
INS +XT1	19.8	0.09	0.9
INS +XT2	10.2	0.05	0.5
INS +XM1	22.8	0.10	1.0
INS +XM2	14.4	0.07	0.6
INS +XB1	9.1	0.04	0.4
INS +XB2	9.3	0.04	0.4
INS -XT1	21.5	0.10	0.9
INS -XT2	16.1	0.07	0.7
INS -XM1	24.8	0.11	1.1
INS -XM2	19.3	0.09	0.8
INS -XB1	11.3	0.05	0.5
INS -XB2	11.9	0.05	0.5

With an increase in the transverse displacement of the failing support, the increase in tension in the conductors and the associated insulator swings will exert forces on the support cross arms which tend to be pulled downward. These forces also create additional moments on the pole segment of the support. At the adjacent support (tower 1), the central portion of the pole is subjected to large axial compressions while its apex sustains an axial compression of 25 kN.

Table 7-6: Longitudinal forces at all points of connection of Towers 1 & 2. (Case 1.2)

Point of Connection	Longitudinal force (kN)	Use factor	MF
Apex 1	84.1	0.40	6.1
Apex 2	54.6	0.26	4.0
CR +XT1	17.8	0.07	0.8
CR +XT2	11.0	0.05	0.5
CR +XM1	19.3	0.08	0.8
CR +XM2	12.5	0.05	0.5
CR +XB1	7.8	0.03	0.3
CR +XB2	7.7	0.03	0.3
CR -XT1	18.1	0.08	0.8
CR -XT2	12.6	0.05	0.5
CR -XM1	19.3	0.08	0.8
CR -XM2	12.4	0.05	0.5
CR -XB1	7.8	0.03	0.3
CR -XB2	7.8	0.03	0.3

Table 7-7: Transverse forces at all points of connection of Towers 1 & 2. (Case 1.2)

Point of Connection	Transverse Forces (kN)	Use factor	MF
Apex 1	2.9	0.01	0.2
Apex 2	2.6	0.01	0.2
CR +XT1	5	0.02	0.2
CR +XT2	5.7	0.02	0.2
CR +XM1	3.1	0.01	0.1
CR +XM2	2.86	0.01	0.1
CR +XB1	9.5	0.04	0.4
CR +XB2	8.85	0.04	0.4
CR -XT1	6.3	0.03	0.3
CR -XT2	6.5	0.03	0.3
CR -XM1	7.2	0.03	0.3
CR -XM2	5.8	0.02	0.3
CR -XB1	8.6	0.04	0.4
CR -XB2	8.1	0.03	0.4

7.1.3 Transverse failure at the bottom cross arm junction with the pole

It is expected that as the point of constrained displacement application moves away from the apex, the magnitude of unbalanced forces generated in the system increases. In the same manner as in the previous cases, the rotational displacement is applied at the lowest cross-arm junction with the mast. In this scenario, the section of the tower between the apex until the constrained node breaks into three parts due to excessive bending stresses and axial compression. Thus all six cross-arms along with the apex of the support are lost.

Similar to the previous results, the tension in the ground wire and the longitudinal displacement of the adjacent apexes are documented. (See Figures 7-14 & 7-15)

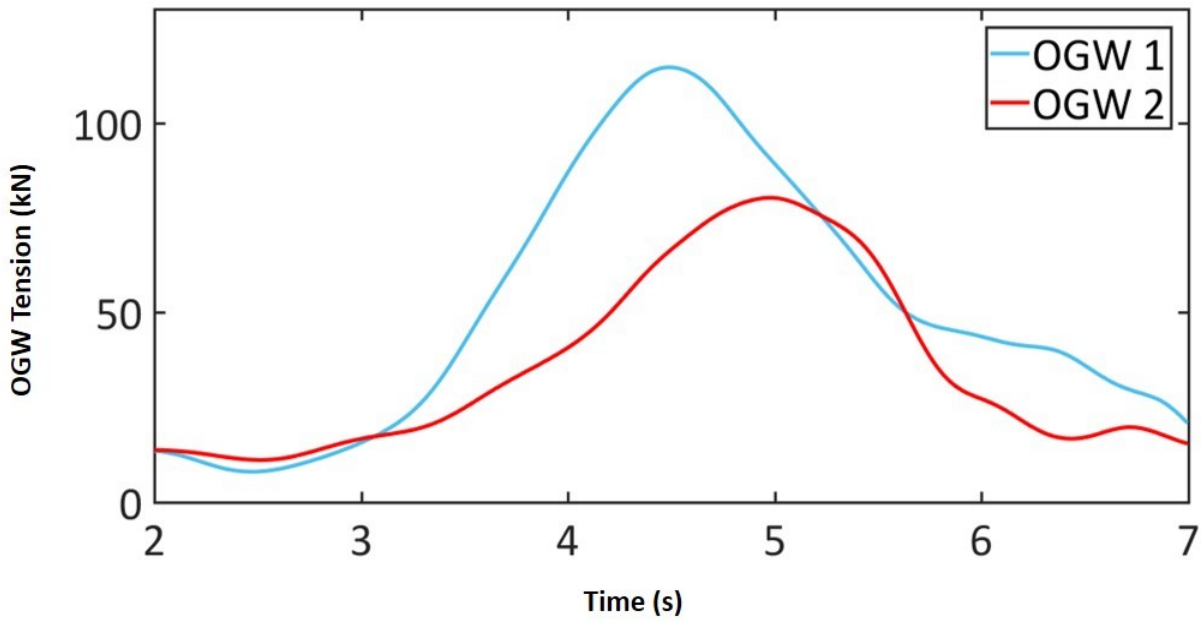

Figure 7-14: Ground wire tensions in end span elements of spans 1 and 2. (Case 1.3)

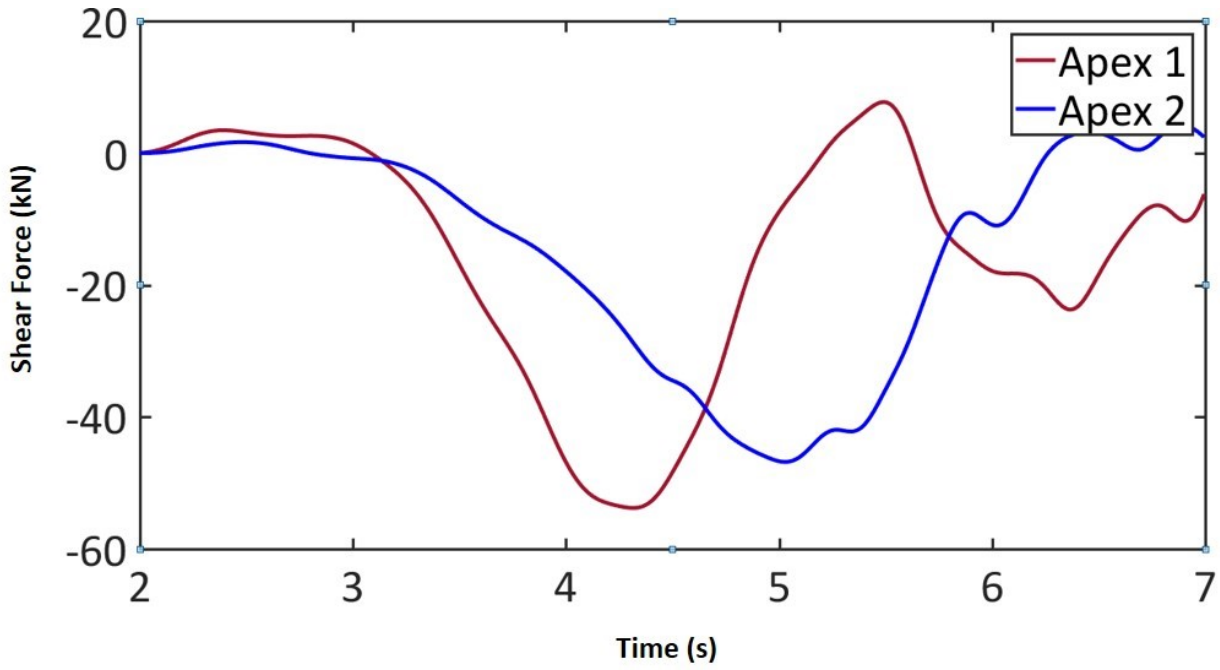

Figure 7-15: Longitudinal forces at the Apex of towers 1 and 2. (Case 1.3)

As explained for the previous failure scenario, the localized ruptures within the failing support are the most dominant factors in ensuing line response rather than the tension in the shield wires. This run is important when considering the conductor tensions in the spans attached to

the middle cross-arm. As indicated in Table 7-8, the conductor tension at position CS+XM1 reaches 93% of the RTS, which indicates a possible conductor rupture.

Table 7-8: Tension in the Conducting spans of Towers 1 & 2. (Case 1.3)

Conductors	Tension (kN)	Use Factor	MF
OGW 1	114.6	0.55	8.0
OGW 2	80.11	0.38	5.8
CS +XT1	75.85	0.32	3.3
CS +XT2	70.97	0.30	3.1
CS +XM1	221.31	0.93	9.7
CS +XM2	128.24	0.54	5.6
CS +XB1	90.73	0.38	3.9
CS +XB2	75.12	0.32	3.3
CS -XT1	64.20	0.27	2.8
CS -XT2	59.19	0.25	2.6
CS -XM1	197.24	0.83	8.7
CS -XM2	127.72	0.54	5.6
CS -XB1	102.15	0.43	4.5
CS -XB2	81.47	0.34	3.6

The larger conductor tensions also lead to more important vibrations for the successive supports. It can be observed that the transverse failure of the trigger support acts quasi-statically for the adjacent support but causes dynamic impulses of lesser magnitude in the successive supports (see for example Figure 7-16).

Table 7-9: Longitudinal forces at all connection points of connection of Towers 1 & 2. (Case 1.3)

Point of Connection	Longitudinal Force (kN)	Use Factor	MF
Apex 1	53.8	0.26	3.9
Apex 2	46.8	0.22	3.4
CR +XT1	16.7	0.07	0.7
CR +XT2	16.3	0.07	0.7
CR +XM1	46.6	0.20	2.0
CR +XM2	15.6	0.07	0.7
CR +XB1	20.2	0.09	0.9
CR +XB2	14.2	0.06	0.6
CR -XT1	14.4	0.06	0.6
CR -XT2	22.2	0.10	0.9
CR -XM1	37.2	0.16	1.6
CR -XM2	16.9	0.07	0.7
CR -XB1	23.3	0.10	1.0
CR -XB2	18.8	0.08	0.8

The peak transverse forces exerted at the connection points of the support are listed in Table 7-10.

Table 7-10: Transverse forces at the points of Connections for Towers 1 & 2. (Case 1.3)

Point of Connection	Transverse Force (kN)	Use Factor	MF
Apex 1	3.2	0.02	0.2
Apex 2	2.2	0.01	0.1
CR +XT1	14.8	0.04	0.6
CR +XT2	5.0	0.02	0.2
CR +XM1	9.0	0.04	0.4
CR +XM2	4.7	0.02	0.2
CR +XB1	23.2	0.10	1.0
CR +XB2	20.5	0.09	0.9
CR -XT1	14.3	0.06	0.6
CR -XT2	7.3	0.03	0.3
CR -XM1	16.2	0.07	0.7
CR -XM2	5.0	0.02	0.2
CR -XB1	23.9	0.10	1.1
CR -XB2	20.9	0.09	0.9

Table 7-11: Axial forces in the insulators of Towers 1 & 2. (Case 1.3)

Insulators	Axial Force (kN)	Use Factor	MF
INS +XT1	19.6	0.09	0.9
INS +XT2	17.7	0.08	0.7
INS +XM1	104.5	0.48	4.6
INS +XM2	27.6	0.13	1.2
INS +XB1	25.0	0.11	1.1
INS +XB2	23.1	0.11	1.0
INS -XT1	19.5	0.09	0.8
INS -XT2	14.6	0.07	0.6
INS -XM1	83.2	0.38	3.6
INS -XM2	15.7	0.07	0.7
INS -XB1	27.1	0.12	1.2
INS -XB2	20.6	0.09	0.9

The forces subjected at the various components have been determined. But the effect of these forces in terms of stresses at various points along the adjacent support more vulnerable to rupture need to be checked. Figure 7-16 illustrates the effective stress in the base of the support at the integration point with maximum stress. As is evident from the curve, the base of the adjacent support is within its elastic zone.

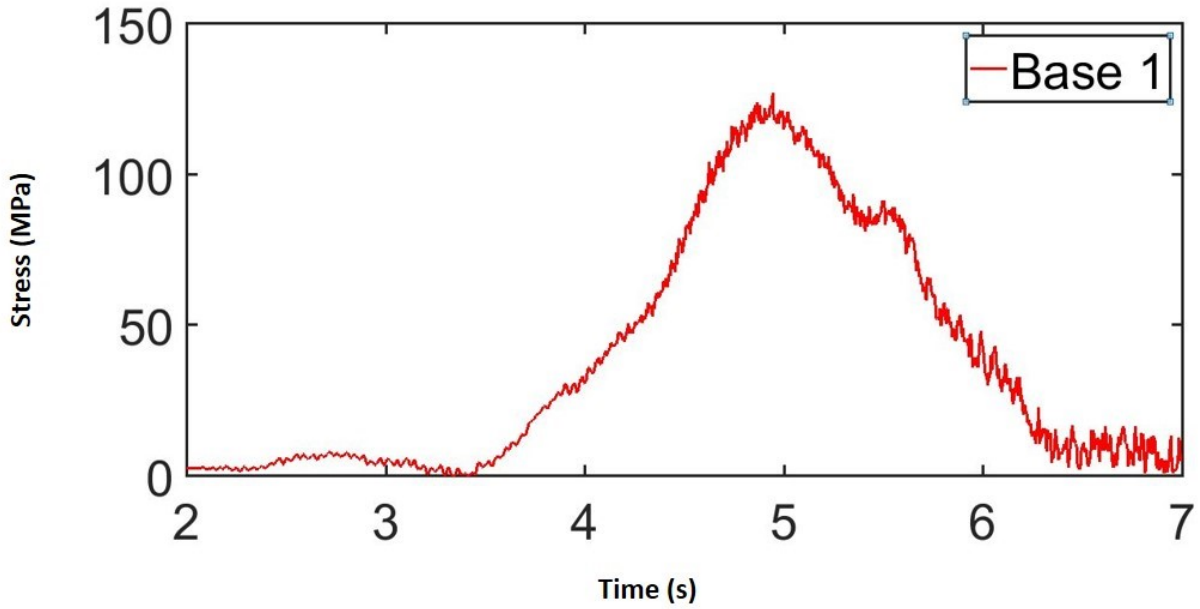

Figure 7-16: Time History for stress-strain in the base of Tower 1. (Case 1.3)

Next the stresses at the element within the apex zone of the support are examined for inelastic behavior. Prior to the same, the slight change in the naming convention has been made for stress results which have been denoted in Figure 7-17. The major change is the monitoring of the first element of the cross-arms that is connected to the mast of the support.

Figure 7-18 shows the stresses in the Apex region of the support. It reaches a maximum value of around 20MPa. The stresses in the elements of the cross-arms depicted in the figures 7-19 to 7-21 are within their allowable limits too. This confirms that the adjacent support is not overloaded.

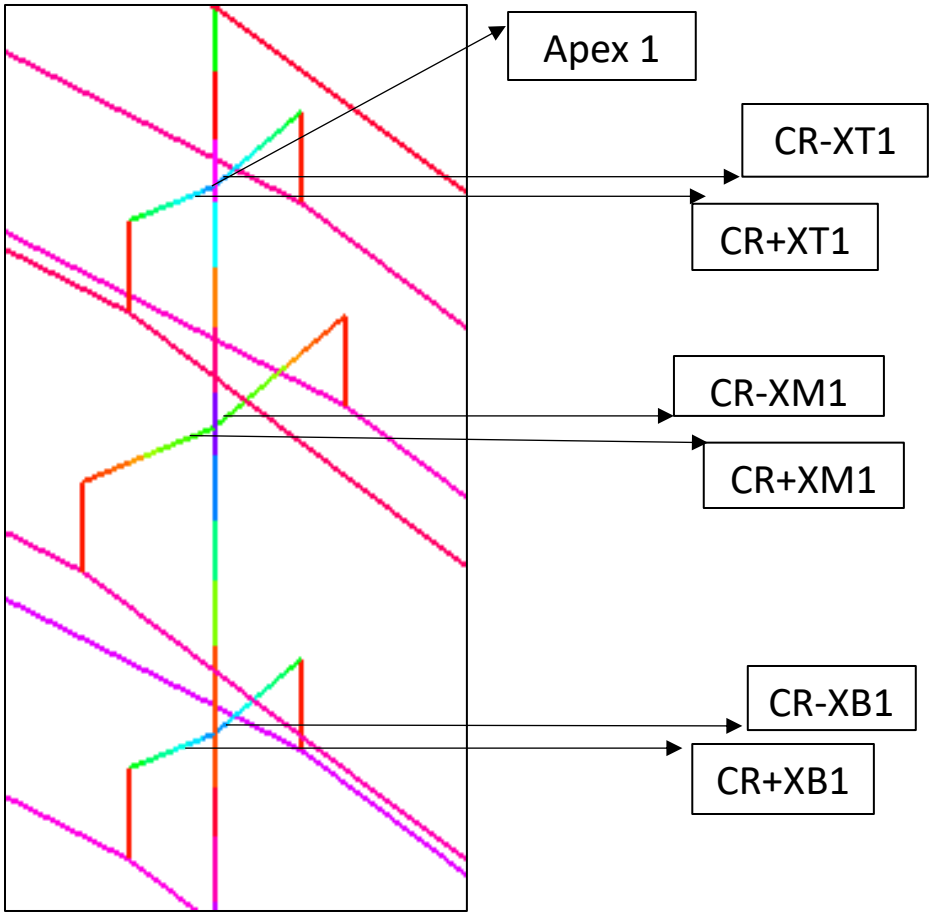

Figure 7-17: Naming of the elements being monitored for stresses.

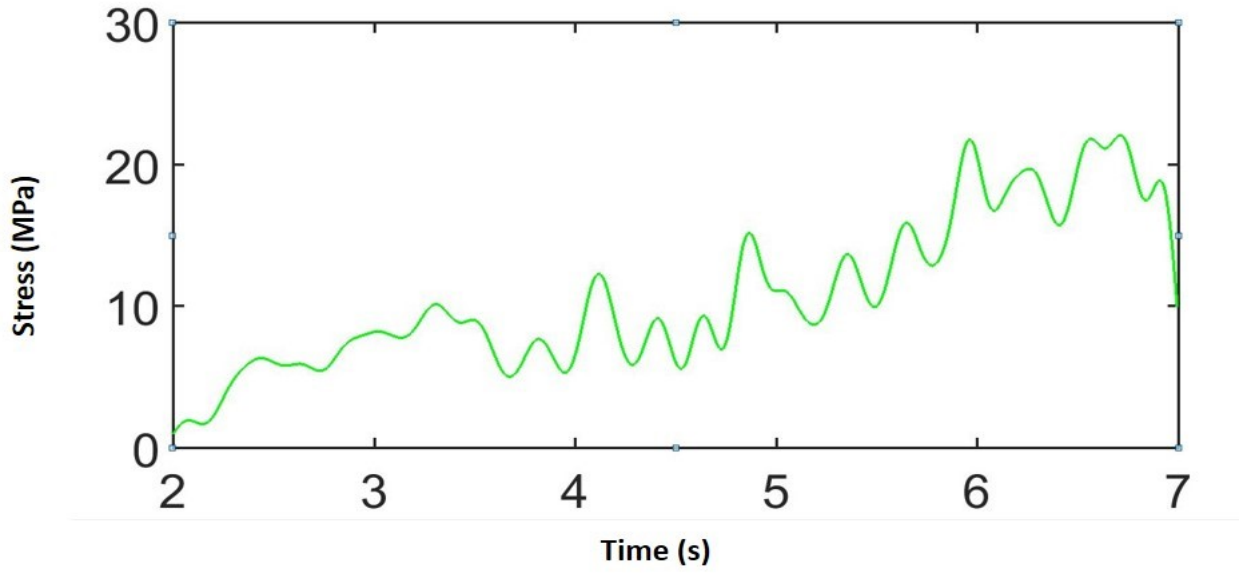

Figure 7-18: Stress-strain time history for the element in the Apex of T1. (Case 1.3)

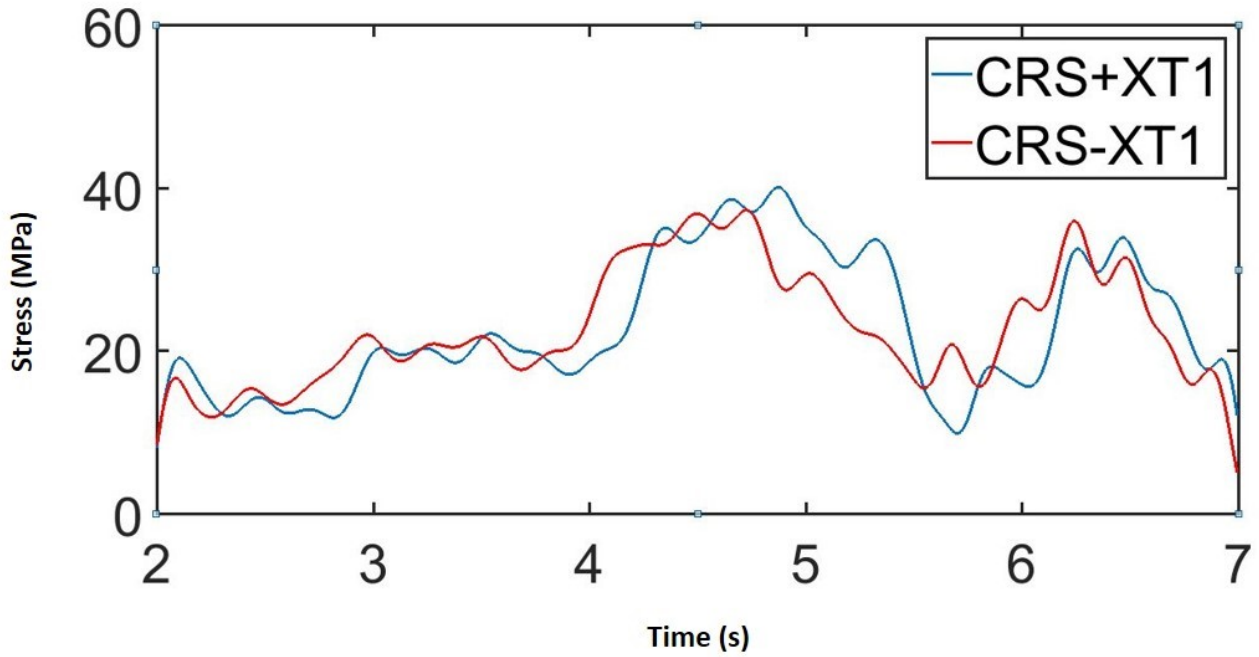

Figure 7-19: Stress-strain time history for the element in the topmost Cross-arms of T1. (Case 1.3)

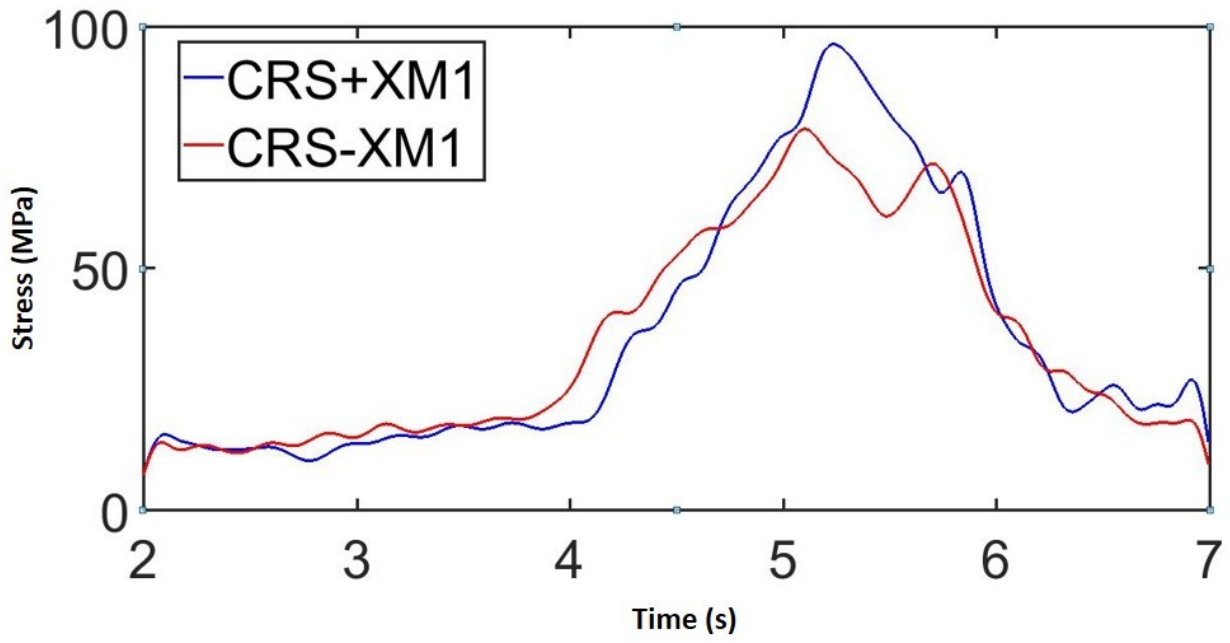

Figure 7-20: Stress-strain time history for the element in the middle Cross-arms of T1. (Case 1.3)

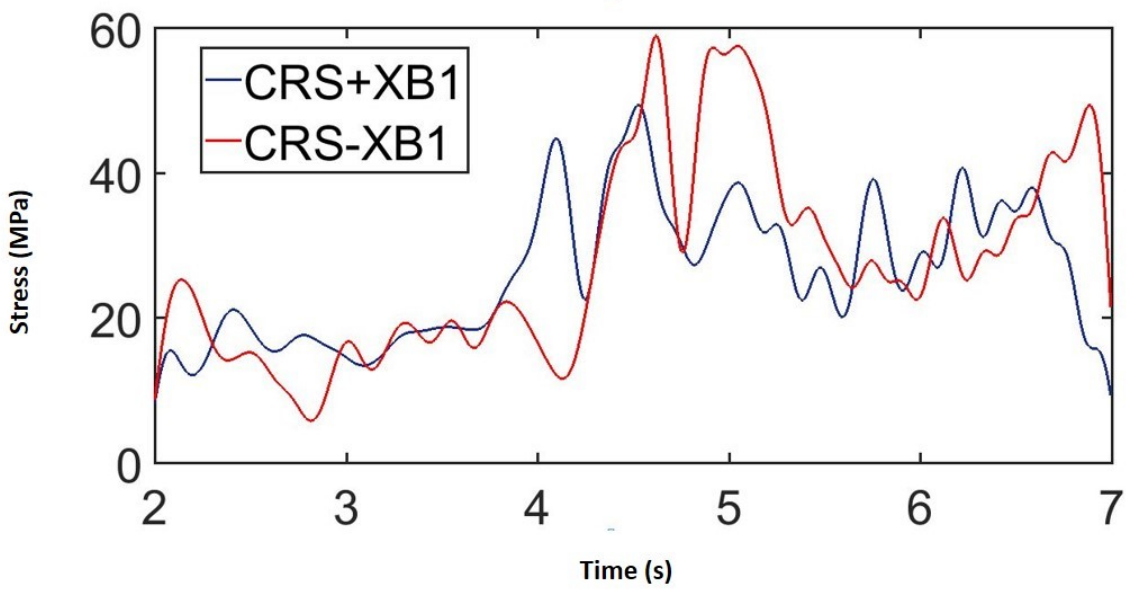

Figure 7-21: Stress-strain time history for the element in the bottom Cross-arms of T1. (Case 1.3)

7.1.4 Transverse failure at the base of a support

This is the last trigger failure scenario to be studied for the tubular support. In this case, a node located at 10 cm from the base is subjected to a controlled rotational displacement that will force the transverse motion of the whole support. This motion is further amplified by the self-weight of the support and attached conductors. The resulting forces will cause large bending stresses in the pole section in the zones connected to the cross-arms. Besides, the axial compression in the pole acts eccentrically and creates important secondary bending due to P-delta effects. These regions of the support will eventually fail and the whole support will fall to the ground.

The detailed sequence of failure of the trigger support is not the primary concern as the model is built to simulate the response of the rest of the line system after the initial failure. However, this response necessarily depends on the sequence of failures in the trigger failure support. This scenario appears to create mostly monotonic quasi static response in the initial stage as the adjacent support and attached spans sustain the bulk of the load imbalances. After the peak response is obtained, the inertial forces within the components then start dominating the latter part of the response which is seen in the vibrational response of these intact components to reach a new residual static steady state.

The response to the failure at the base of the support is not very different compared to the failure at the bottom cross-arm connection. The tower elements now fail earlier compared to the prior cases and the displacements and forces are comparable in trend but lower in amplitude. This is illustrated in Figures 7-22 & 7-23.

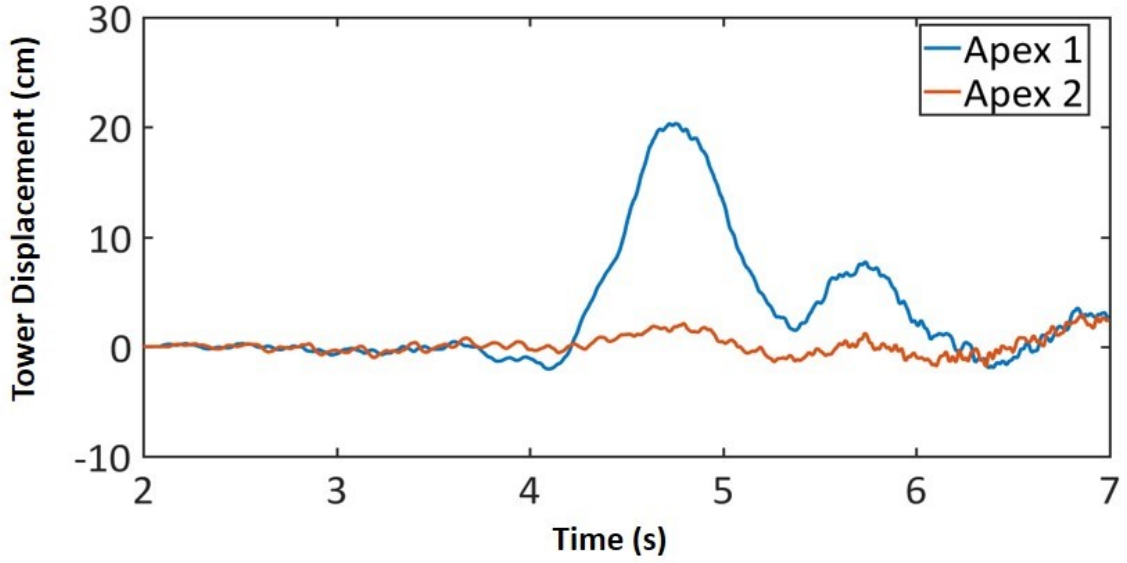

Figure 7-22: Transverse displacement at the apex of adjacent supports 1 & 2. (Case 1.4)

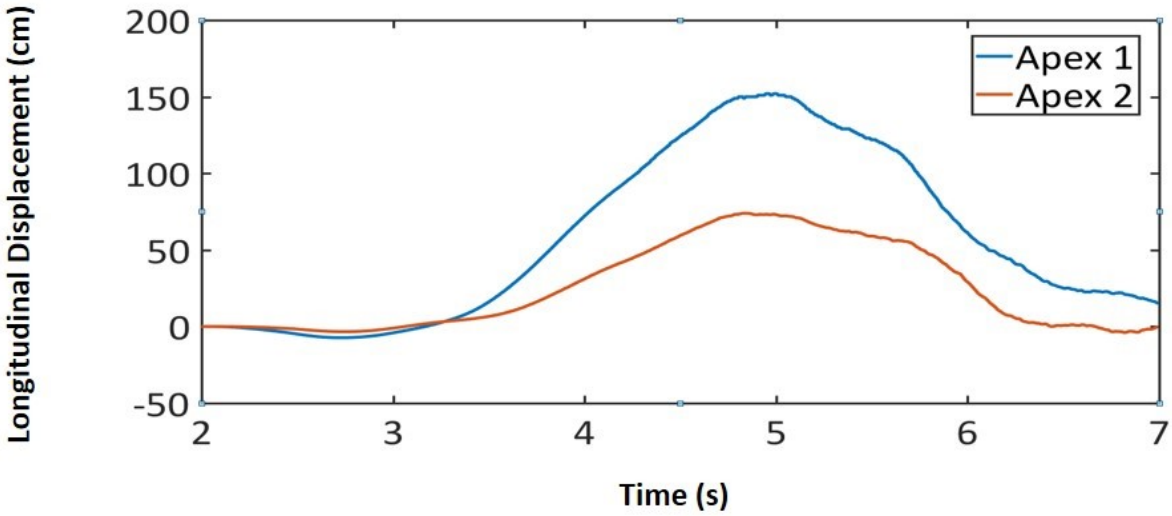

Figure 7-23: Longitudinal displacement at the apex of adjacent supports 1 & 2. (Case 1.4)

The movement of the tower apex is restrained by the stiffening effect of the ground wires. It is seen again that the transverse failure induces a dominantly longitudinal response.

Table 7-12: Conductor tension in the spans of Towers 1 & 2. (Case 1.4)

Conductors	Tension (kN)	Use Factor	MF
OGW 1	113.8	0.54	8.3
OGW 2	87.3	0.42	6.3
CS +XT1	74.8	0.31	3.3
CS +XT2	70.3	0.30	3.1
CS +XM1	219.5	0.92	9.6
CS +XM2	132.6	0.56	5.8
CS +XB1	167.6	0.70	7.4
CS +XB2	110.1	0.46	4.8
CS -XT1	63.3	0.27	2.7
CS -XT2	58.7	0.25	2.6
CS -XM1	194.5	0.82	8.5
CS -XM2	133.28	0.56	5.8
CS -XB1	171.36	0.72	7.5
CS -XB2	114.96	0.48	5.1

The tension in the conductors although quite high does not surpass their RTS. The cross-arm end of the adjacent support is subjected to a dominant downward force primarily due to the motion of the spans. This force creates bending stresses in the pole section of the support but the numerical simulation does not show any localized failures. The numerical results of the peak response indicators are listed next in Table 7-13

Table 7-13: Longitudinal forces at all connection points of connection of Towers 1 & 2. (Case 1.4)

Point of Connection	Longitudinal Force (kN)	Use Factor	MF
Apex 1	54.8	0.26	4.0
Apex 2	51.1	0.24	3.7
CR +XT1	16.4	0.07	0.7
CR +XT2	17.8	0.08	0.8
CR +XM1	45.8	0.20	2.0
CR +XM2	13.0	0.06	0.6
CR +XB1	31.3	0.14	1.4
CR +XB2	14.3	0.06	0.6
CR -XT1	14.4	0.06	0.6
CR -XT2	17	0.07	0.7
CR -XM1	36.9	0.16	1.6
CR -XM2	12.9	0.06	0.6
CR -XB1	33.6	0.15	1.5
CR -XB2	17.1	0.07	0.7

7.2 Simulations of transverse failure with a stiffer support assumption

The possibility of the tubular support transverse failure causing a cascade has been ruled out from the previous simulations owing to the trigger support flexibility for the transmission lines in the bare conditions. However, these conditions may change and so will the consequences. The tower modelled in the prior simulations (section 7.1) was designed with steel of a yield strength of 350 MPa. In the next series of simulations, the towers have been assigned an increased material yield strength of 450 MPa and the thickness of the sections has been increased to three times their original values to also create stiffer supports. The same failure scenarios as discussed in the beginning of Section 7 are repeated and the results are summarized in similar formats.

7.2.1. Transverse failure at the top cross-arm of a stiff support

The increment in the pole thickness combined with the stronger material property translates into larger displacements prior to localized failures within the support, leading to increased response in the other elements of the line adjacent to the failed support. (See Figure 7-24)

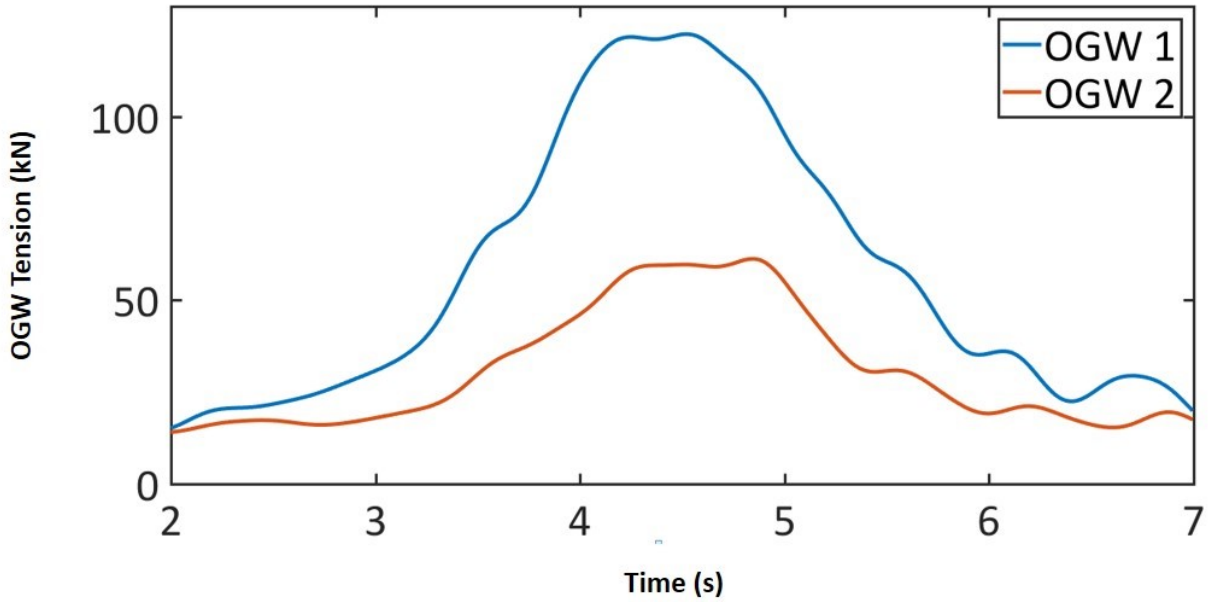

Figure 7-24: Ground wire tensions in end span elements of spans 1 and 2. (Case 2.1)

The same rotational displacement was imposed to the support as in the previous models and generated a maximum OGW tension of 122.4 kN (Table 7-14), compared to 86.8 kN in the previous case, an increase of 41%. Besides, the conducting spans attached to the cross-arm bear a tension amounting to half of their RTS.

Table 7-14: Cable Tension in the Conducting spans of Towers 1 & 2. (Case 2.1)

Conductors	Tension (kN)	Use Factor	MF
OGW1	122.4	0.59	8.87
OGW2	61.09	0.29	4.42
CS +XT1	108.13	0.45	4.74
CS +XT2	94.72	0.40	4.15
CS +XM1	23.49	0.10	1.03
CS +XM2	24.07	0.10	1.05
CS +XB1	22.66	0.10	1.00
CS +XB2	23.05	0.10	1.01
CS -XT1	118.84	0.50	5.21
CS -XT2	93.45	0.39	4.09
CS -XM1	23.84	0.10	1.04
CS -XM2	24.65	0.10	1.08
CS -XB1	23.18	0.10	1.01
CS -XB2	23.34	0.10	1.02

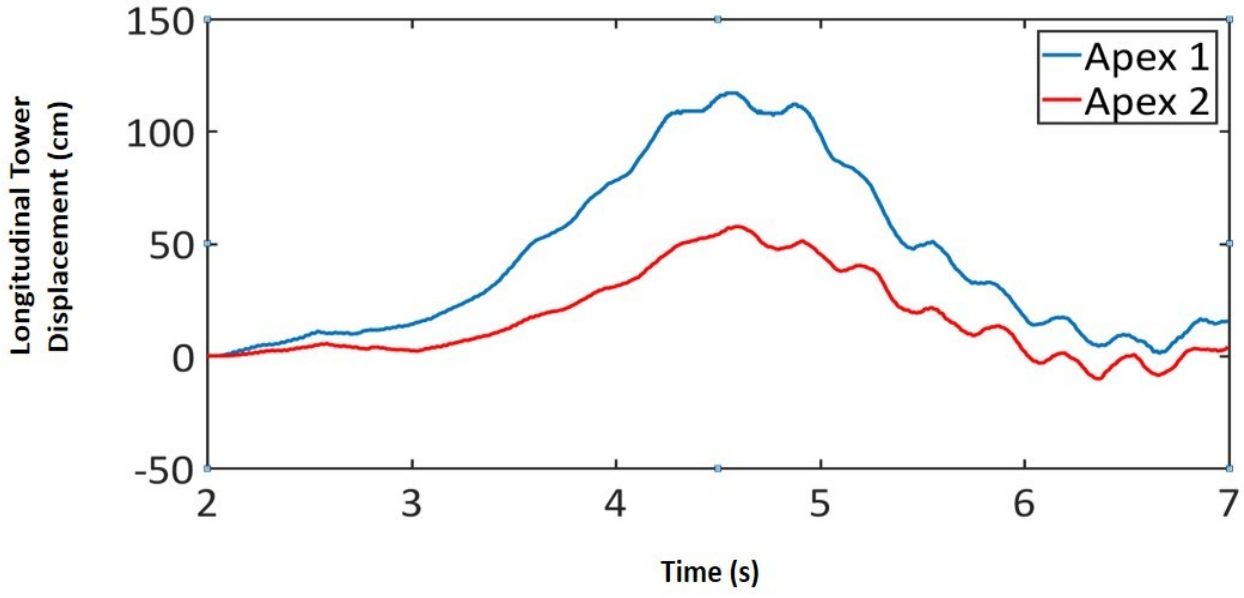

Figure 7-25: Longitudinal displacement at the apex of adjacent supports 1 & 2. (Case 2.1)

As the displacement at the node joining the cross-arms increases (Figure 7-25), the top section of the tower mast is subjected to combined axial compression and bending. The increase in the thickness of the section allows for larger straining until all the layers within the steel can undergo full plastification. The tower failure momentarily arrests the slow and monotonic increase in the effective span length of the ground wire and the free fall of the severed section of the support triggers a mechanical shock wave (force imbalance) that travels through the system. The conductors on reaching maximum sag for the super span continue to oscillate about this new position of equilibrium. The first peak in the tension is experienced when the conductors reach this position and it continues to decrease thereon. Any span rupture can only occur if this peak value exceeds its RTS.

Table 7-15: Longitudinal forces at all points of connection of Towers 1 & 2. (Case 2.1)

Point of Connection	Longitudinal Force (kN)	Use factor	MF
Apex 1	67.1	0.32	4.9
Apex 2	41.1	0.20	3.0
CR +XT1	22.5	0.10	1
CR +XT2	12.1	0.05	0.5
CR +XM1	9.4	0.04	0.4
CR +XM2	9.3	0.04	0.4
CR +XB1	11.4	0.05	0.5
CR +XB2	9.2	0.04	0.4
CR -XT1	34.2	0.15	1.5
CR -XT2	14.7	0.06	0.6
CR -XM1	8.8	0.03	0.4
CR -XM2	7.8	0.03	0.3
CR -XB1	15.4	0.07	0.7
CR -XB2	9.4	0.04	0.4

Table 7-15 lists the longitudinal unbalanced forces exerted on the points of connection of the lines to the supports. The strengthening of the support does not have much influence on the frequencies of the waves generated due to the shock, although their amplitudes are amplified, and the effects of the failure on adjacent supports is practically quasi-static.

7.2.2. Transverse failure at the middle cross-arm of a stiff support

The controlled rotation here is applied at the node connecting the middle longer cross-arms, and the response is more severe than in the previous case. The tensions in the conductors listed in Table 7-16 quantify the same.

Table 7-16: Cable tension in the spans adjacent to Towers 1 & 2. (Case 2.2)

Conductor	Tension (kN)	Use factor	MF
OGW 1	146.9	0.70	10.6
OGW 2	85.4	0.41	6.2
CS +XT1	93.8	0.39	4.1
CS +XT2	83.1	0.35	3.6
CS +XM1	171.7	0.72	7.5
CS +XM2	133.5	0.56	5.9
CS +XB1	32.9	0.14	1.4
CS +XB2	34.5	0.14	1.5
CS -XT1	90.2	0.38	4
CS -XT2	79.7	0.33	3.5
CS -XM1	190.5	0.80	8.4
CS -XM2	132.7	0.56	5.8
CS -XB1	35.2	0.15	1.5
CS -XB2	31.7	0.13	1.4

The tensions in the lines are large but still safe, within their RTS values. The peak tension reaching 0.8 RTS for the spans connected to the middle cross-arm are a cause of concern when taking into

consideration additional forces due to weather. As was reported prior to the results, the pipe-beam model underestimates the strength of the section. Thus, a prolonged failure in this case, may lead to a conductor rupture.

Table 7-17: Longitudinal forces at all points of connection to Towers 1 & 2. (Case 2.2)

Point of Connection	Longitudinal force (kN)	Use factor	MF
Apex 1	74.5	0.36	5.4
Apex 2	50.8	0.24	3.7
CR +XT1	33.0	0.14	1.4
CR +XT2	20.0	0.08	0.9
CR +XM1	33.2	0.14	1.5
CR +XM2	20.4	0.09	0.9
CR +XB1	15.6	0.07	0.7
CR +XB2	18.2	0.08	0.8
CR -XT1	23.7	0.10	1.1
CR -XT2	23.3	0.10	1.1
CR -XM1	36.3	0.15	1.6
CR -XM2	20.7	0.09	0.9
CR -XB1	13.1	0.05	0.6
CR -XB2	14.4	0.06	0.6

7.2.3. Transverse failure at the lowest cross-arm of a stiff support

The rotational displacement is applied at the node connecting the lowest cross-arm to the support. On application of the rotational displacement, it was found that the tension in the attached ground wire spans increased and reached its RTS, which implies an OGW failure. (See Figure 7-26)

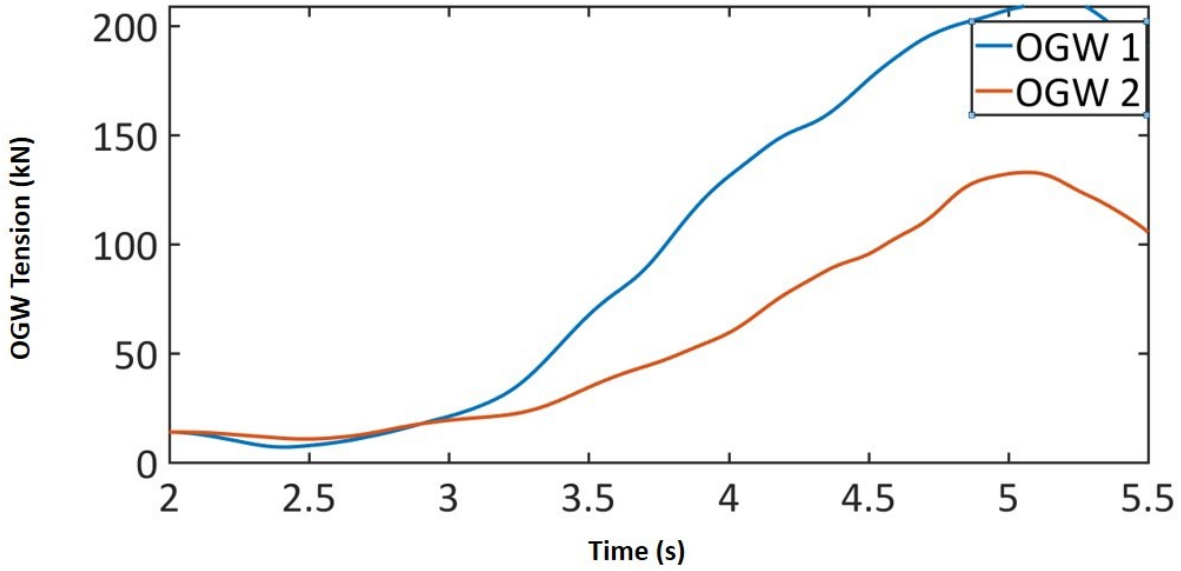

Figure 7-26: Ground wire tensions in end span elements of spans 1 and 2. (Case 2.3)

The analysis was stopped at the time step when the ground wire reaches its RTS value. Further analysis was not carried out as the main objective of the runs were to check for possibility of conductor or ground wire rupture. The results discussed further hold good until the ground wire ruptures as the failure shock induced by a sudden ground wire rupture can propagate through the line and trigger a longitudinal cascade in tower peaks if the capacity of the pole is exceeded locally. The conductors attached to the middle cross-arm reach a peak tension equal to 95% of their RTS, which signals a risk of conductor rupture. In the prior case of a flexible support, a rotational displacement at the bottom cross-arm lead to the tower failure into three parts.

The conductor tensions prior to the ground wire rupture have been listed in the Table 7-18.

Table 7-18: Cable tension in the spans adjacent to Towers 1 & 2. (Case 2.3)

Conductors	Tension (kN)	Use Factor	MF
CS +XT1	157	0.66	6.9
CS +XT2	135.1	0.57	6
CS +XM1	181.	0.76	8.0
CS +XM2	141.6	0.59	6.2
CS +XB1	114.6	0.48	5.0
CS +XB2	90.8	0.38	4.0
CS -XT1	133.6	0.56	5.9
CS -XT2	119.8	0.50	5.3
CS -XM1	158.3	0.67	7.0
CS -XB1	114.8	0.48	5.0
CS -XB2	87.7	0.37	3.8

Prior to the ground wire failure, the conductors are not much affected and the resulting longitudinal forces on the supports at the various points of connection are listed in the Table 7-19.

Table 7-19: Longitudinal forces at all points of connection to Towers 1 & 2. (Case 2.3)

Point of Connection	Longitudinal Force (kN)	Use Factor	MF
CR +XT1	30.1	0.13	2.2
CR +XT2	28.7	0.12	2.1
CR +XM1	36	0.16	1.6
CR +XM2	15.6	0.07	0.7
CR +XB1	23.7	0.10	1.1
CR +XB2	15.7	0.07	0.7
CR -XT1	29.7	0.13	1.3
CR -XT2	23	0.10	1.0
CR -XM1	29.5	0.13	1.3
CR -XM2	20.5	0.09	0.9
CR -XB1	37.1	0.16	1.6
CR -XB2	29.8	0.13	1.3

As was the case with the prior simulations, the majority of the longitudinal imbalance is absorbed by the conductors. The forces acting at the adjacent support are well within values corresponding to stress limit sates according to the calculated use factors.

The major outcome of this analysis is the shield wire rupture. A similar run with the displacement applied at the base also concluded with the same result, and the conducting spans were within allowable tensile limits. The insulators were subjected to forces well within their axial capacities. But, all of these hold good assuming the dynamic effects of the ground wire rupture do not trigger a failure in the spans. The dynamic effects associated with conductor rupture can cause a cascade

of multiple supports, a scenario which is further worsened with the presence of wind or icing. Siddam (May, 2014).

7.3 Observations

The transverse movement of a support at failure depends on its bearing capacity, mode of failure, and ductility. It was found in the study that the modelling of the support failure greatly influences the overall effects on adjacent spans and supports in terms of longitudinal load imbalances. The preliminary runs have established the criticality of longitudinal displacements over the transverse to trigger a cascade. The gradual transverse failure of the flexible support simulated in this study leads to a quasi-static response as it allows for distribution of the longitudinal imbalances within the system without important inertia effects. The seriousness of the consequences of a transverse failure is larger for failures occurring within a shorter time duration because of the inertia effects caused by the shock. Besides, the material and rupture modelling of the tower elements influences the overall calculated response of the system. The sacrificed tower when modelled elastically allows for larger transverse displacements thus leading to ground wire rupture and also failures of the apex and cross-arms of the adjacent supports. The 2-node Hermitian nonlinear pipe-beam elements, although they constitute an exhaustive formulation leading to detailed stress interpolations, have been shown to under-estimate the strength of the tower sections when compared to a full shell element model. This is because the pipe-beam material nonlinear material formulation comes with a rupture criterion that eliminates the element (hence the whole cross section) when the failure criterion is reached, while the nonlinear shell formulation allows for inelastic deformations to develop progressively at various elements on the cross section. However, in this study, modeling of each support with a detailed nonlinear shell finite element was deemed inappropriate because of excessive processing time.

The free-vibration analysis of the tower under different support conditions was conducted to understand how the support would react dynamically in the continuous line system. As expected, the frequency of vibration of the isolated support increased from the fixed-free condition to the fixed-pin condition. However, the overhead line system constitutes multiple components of varying flexibilities attached together and expected to behave interactively. A different way to illustrate this is to check the change in vibration modes of the tower only compared to that

attached to insulators and conductors first. The insulators swing about the pivot point, which in this case is the end node of the last beam element of the cross-arm. At the onset for a freely standing support, this node is free to move however with the addition of an insulator and attached conductors, the movement is now influenced by the swinging of the insulator. Further consideration of the attached conductors makes the response more complex. Thus, it is important to study and quantify the effects of the various line components on the natural frequencies of the support. As explained, for the six-span model, the fundamental frequency of the system was reduced to less than 1Hz.

The first set of runs using the tower configuration and properties as provided by Hydro Québec, yields a conservative approximation of the unbalanced loads exerted on the adjacent supports. Conductor tensions for each of the runs have been provided. Fourier frequency analysis shows that the frequencies of the disturbance created in the system range within 10Hz. The effective length of the span increases within a time duration of 2 seconds until the span 'bottoms up' under the combined action of its self-weight, the applied displacement and the weight of sections of the tower attached to it. The prescribed displacement was applied with the objective to replicate the effects of a localized failure in the support at four positions in four different scenarios: three at the mast junction of the three sets of cross-arms and the last one near the base. Amongst these simulations, only the two scenarios involving the imposed rotation at the lowest cross-arm connection (11m from the apex) and at the base suggested the possibility of conductor rupture as the calculated forces approached the theoretical RTS value. The calculated longitudinal force imbalance following the support failure at the various points of connection with the supports have been listed in terms of the RTS of the conductors attached to it, and they do not exceed 20% of the RTS. Of course, if the comparison is done with the initial static load (RSL) the ratios are considerably large because the denominator is small. The stress analysis of the components of the adjacent support most likely to fail confirms that they are not overloaded and the adjacent support remains well within its elastic range of response.

The second set of runs, although they represent a hypothetical case of a much stiffer and stronger support than in reality are important to understand the effect of support flexibility on the response of the system. The conductors and ground wires reach their maximum tension about

2.5 seconds from the initiation of failure in the sacrificed support. The frequency range of disturbance created lies within the range of 0-10Hz however, and intensity of the unbalanced forces is significantly larger than for a flexible and weaker support. Comparing case by case, on average the conductor tensions are 50% higher than for the line section on flexible supports. An important point of difference between the results of the two different supports is the lack of localized failures in the stiffer and stronger supports, which lead to the increase in tension in the ground wire which ruptured when the displacement was applied at the bottom cross-arm connection joint and the base. With respect to the localized failures, the mast of the support appears to be most likely to fail due to combined axial and bending stresses.

8. Conclusions

This study has successfully conducted analysis of the effects of the transverse failure of a flexible tubular support on the adjacent supports and spans. The analysis was carried out on a tubular support used by Hydro-Québec for double-circuit 230 kV lines. The material non-linearity of the support was included in the model. The material model used to define the pipe-beam elements follows an element death upon rupture criterion which under-estimates the strength of the entire section as the element ruptures as soon as any integration point within the section reaches the rupture criterion. This is an important limitation of this model. Several modelling options have been considered with a view to evaluate the possibility of transverse cascades as opposed to creating a genuine or realistic mode of failure for the sacrificed support. Also, the computational time needed to run the analysis for a more accurate nonlinear detailed shell was deemed impractical, considering also that several supports in the line section were to remain in their elastic range of response. It should be noted that experimental results of failure tests on the supports were not available for effective modelling calibration.

The preliminary simulations led to the conclusion that the mode of failure of the support, combined with the span length and available slack in the system through additional spans, and the support flexibility govern the response of the system. Thus, the most critical scenario with the shortest span length (200 m) was modelled and the failures were modelled in a manner to allow for maximum transverse displacement of the support to check for the longitudinal load imbalances created there on.

The results obtained show that the transverse failure within a flexible support under bare conditions will not propagate to a cascade. The effect of a transverse failure is predominantly longitudinal through the system. This transverse failure mode is governed by the material and geometric properties of the support sections. The higher the allowable ductility, the larger the tower transverse displacement at failure. The elongation of the span and whether it exceeds its rated tensile strength depend on the strength of the sacrificed flexible support, while the forces on the adjacent supports are well within their capacities. The cables of the failing span on the

other hand will face an increase in tension until the span attached to the failing support stabilizes. The transient effects of this failure propagate through the system of conductors but in the form of low intensity and high frequency disturbances hardly of significant importance when compared to the initial tension of the conductors not attached to the failing element.

Amongst the simulations of various failure location scenarios on the actual tubular tower, the higher conductor tensions were obtained for the scenarios where the point of failure is lower. The resultant longitudinal forces acting at the adjacent supports points of connections never exceeded 0.2 times the RTS of the conducting span. The apex, however, does undergo a significant amount of axial compression combined with the longitudinal forces because of its direct connection to the ground wire. If the forces at the cross-arm ends were to increase due to additional ambient forces (say high wind and/or ice) in addition to the failure of the support, these combined effects could trigger failure at the joints connecting the cross-arms to the mast of the tower: These failures would be primarily due to combined axial and bending stresses. However, such an occurrence due to a transverse failure is unlikely under bare conditions and a reasonably strong and flexible support.

An important limitation of the model relates to the nonlinear material model used to define the pipe-beam elements of the supports which is combined to an element death upon rupture criterion which under-estimates the strength of the entire section. The pipe-beam element ruptures as soon as any integration point within the section reaches the failure criterion.

The latter part of the study concentrated on a hypothetical case of a stringer and stiffer support to verify the effect of support rigidity on the response of the system. The additional rigidity (modeled using thicker tubular sections than in the real supports) caused the rupture of the shield wire when the rotational displacement was applied at the bottom cross arm connection joint and at the base. Although the tension in the conducting spans was significantly high, no localized failures within the adjacent supports were predicted by the model and the conducting spans did not fail.

The goal of this study was to ascertain if the transverse failure of a single flexible support can trigger a cascade. The case we have studied is a highly idealized failure assumption based on

imposed displacements of the sacrificed support. Yet, we have found that the failure mode of the support dictates the load distribution to adjacent supports. It would be important to perform analysis of multiple support failures by numerically modelling the conditions of cyclones and other high intensity wind events to reach a practical conclusion.

Accurate numerical modelling a tubular support at failure has proven difficult, especially in the absence of experimental validation in the post-elastic range of response. The majority of the line cascade studies conducted to date used overhead lines on latticed supports; it is understood that latticed supports are the most frequently used transmission supports over long distances. But in urban areas the use of tubular supports has increased in recent years because of their reduced visual impact.

Events such as conductor rupture due to line icing increase the severity of longitudinal cascades. The same needs to be checked for transverse failures too. An important criterion governing the response of a system to transverse failures is the span length: the shortest spans are more prone to large tension increases and possibly failure due to their limited slack available. Depending on the mechanism of the failure, the option of allowing for a slight increase in spans to counteract the effects of a transverse failure could also be investigated.

9. List of References

ADINA, R. (2012). ADINA theory and modeling guide, ADINA R & D.

Al-Bermani, F. G. and Kitipornchai, S. (1990). *Elasto-plastic large deformation analysis of thin-walled structures.* Engineering Structures 12(1): 28-36.

Albermani, F., Kitipornchai, S., & Chan, R. W. K. (2009). *Failure analysis of transmission towers.* Engineering Failure Analysis, 16(6), 1922-1928.

Alminhana, F., Mason, M., and Albermani, F. (2018). *A compact nonlinear dynamic analysis technique for transmission line cascades.* Engineering Structures, 158, 164-174.

American Society of Civil Engineers (1991). *Guidelines for Electrical Transmission Line Structural Loading.* New York. 345 East 47th Street. ISBN 0-87262-825-6

CIGRÉ (Technical Brochure 485) (2012). *Overhead Line Design Guidelines for Mitigation of Severe Wind Storm Damage.* International Council on Large Electrical Systems, 38 p. ISBN: 978-2-85873-177-0.

CIGRÉ (Technical Brochure 515) (2012). *Mechanical Security of Overhead Lines - Containing Cascading Failures and Mitigating Their Effects.* International Council on Large Electrical Systems, 80 p. ISBN: 978-2-85873-208-1.

Gupta, S., Wipf, T.J., Fanous, F., Baenziger, M. and Hahm, Y.H.(1994). *Structural failure analysis of 345 kV transmission line.* IEEE transactions on power delivery, 9(2), pp.894-903.

IEC. 2003. *Design criteria of overhead transmission lines.* International standard IEC-60826, International Electrotechnical Commission (IEC), Geneva, Switzerland.

Kalman, T., Farzaneh, M., and McClure, G. (2007). *Numerical analysis of the dynamic effects of shock-load-induced ice shedding on overhead ground wires.* Computers & structures, 85(7-8), 375-384.

Lapointe, M., and McClure, G. (2003). *Modeling the structural dynamic response of overhead transmission lines.* Computers & Structures 81(8): 825-834.

Lee, P.-S., and McClure, G. (2007). *Elastoplastic large deformation analysis of a lattice steel tower structure and comparison with full-scale tests.* Journal of Constructional Steel Research 63(5): 709-717.

Lindsey, K. E. (1978). *Mathematical Theory of Longitudinally Loaded Elastic-Plastic Transmission Lines--Statics.* IEEE Transactions on Power Apparatus and Systems (2): 574-582.

Lummis, J. and Fiss, R. (1969). *Effect of Conductor Imbalance on Flexible Transmission Structures.* IEEE Transactions on Power Apparatus and Systems (11): 1672-1678.

McClure, G. and Tinawi, R. (1987). *Mathematical modeling of the transient response of electric transmission lines due to conductor breakage.* Computers & Structures 26(1-2): 41-56.

Mirshafiei, F. (2010). *Modelling the dynamic response of overhead line conductors subjected to shock-induced ice shedding*, McGill University Library. M. Eng. Thesis

Mozer, J. D., Wood, W. A., & Hribar, J. A. (1981). *Broken wire tests on a model transmission line system.* IEEE transactions on power apparatus and systems, (3), 938-947.

Peabody, Alan B. (2004). Applying shock damping to the Problem of Transmission Line Cascades. Department of Civil Engineering. Montreal, McGill University. PhD. Thesis

Peyrot, A. H., Kluge, R. O., & Lee, J. W. (1980). *Longitudinal loads from broken conductors and broken insulators and their effect on transmission lines.* IEEE Transactions on Power Apparatus and Systems, (1), 222-234.

Richardson, A. (1987). *Longitudinal dynamic loading of a steel pole transmission line.* IEEE transactions on power delivery 2(2): 425-436.

Roshan Fekr, M. and McClure, G. (1998). *Numerical modelling of the dynamic response of ice-shedding on electrical transmission lines*. Atmospheric Research 46(1): 1-11.

Sediver (2015). Sediver toughened glass suspension insulators. Catalogue

Siddam, A. (2014). *Cascade Failure Analysis of Electrical Transmission Lines Using Adina*. Faculty of Engineering and Applied Sciences. St. John's Newfoundland and Labrador, Memorial University of Newfoundland. M.Eng. Thesis.

Taylor, H. T., Ward, B., Willis, M., & Zaleski, W. (2012) *The Saffir-Simpson Hurricane Wind Scale*. URL

Tucker, K. B. (2007). *Validation of full-scale and small-scale transmission line test results on dynamic loads with numerical modeling.* Faculty of Engineering. St. John's, Memorial University of Newfoundland. Master of Engineering.